Cloud Publications
International Journal of Advanced Civil Engineering and Architecture Research
2012, Volume 1, Issue 1, pp. 1-5, Article ID Tech-27

Research Article | Open Access

Variation of Moisture Content as a Parameter of Study by Induced Polarization Technique in Soil Sample of Coastal Andhra Pradesh

E.V. Raghava Rao[1], R.P. Das[2] and Madhu Chandra Popuri[3]

[1] Department of Civil Engineering, Visakha Technical Campus, Visakhapatnam, Andhra Pradesh, India
[2, 3] Department of Electrical and Electronics Engineering, Pydah College of Engineering and Technology, Visakhapatnam, Andhra Pradesh, India

Correspondence should be addressed to Madhu Chandra Popuri, madhuflo@yahoo.com

Publication Date: 13 December 2012

Article Link: http://technical.cloud-journals.com/index.php/IJACEAR/article/view/Tech-27

Abstract By using non-destructive methods such as induced polarization (IP) based on indigenous equipment; experimental data has been collected to find relations of chargeability/resistivity and moisture content. The same techniques are applicable to other parameters such as CEC and grain size. Induced polarization technique based upon time domain methods can be used for studying the parameters of soil mechanics. Moisture content is a common quality which cannot be properly studied by electrical resistivity techniques. Chargeability of soil is directly related to moisture content. The chargeability is expressed as $m = \frac{V_s}{V_p}\left(\frac{mV}{v}\right)$ where V_p is ON-time measured voltage and V_s is the OFF-time measured voltage. Measurements are made of the decay of V_s over a short time period (0.1s) after some discreet intervals of time. The value of m is calculated from the integration techniques.
Keywords *Induced Polarization, Chargeability, Resistivity, Four Probe Method*

1. Introduction

Induced polarization is an electromagnetic method that uses electrodes with time-varying currents and voltages to map the variation of electrical permittivity (dielectric constant) in the Earth at low frequencies. Induced polarization is observed when a steady current through two electrodes in the Earth is shut off: the voltage does not return to zero instantaneously, but rather decays slowly, indicating that charge has been stored in the rocks, Figure 1. This charge, which accumulates mainly at interfaces between clay minerals, is responsible for the IP effect, Figure 2. This effect can be measured in either the time domain by observing the rate of decay of voltage, or in the frequency domain by measuring phase shifts between sinusoidal currents and voltages. The IP method can probe to subsurface depths of thousands of meters.

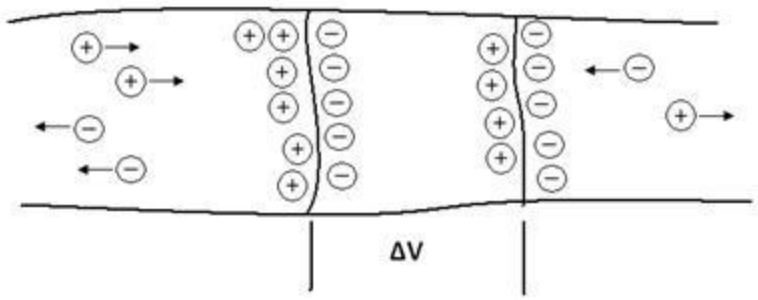

Figure 1: *Change in Voltage because of the Charged Particles in the Soil*

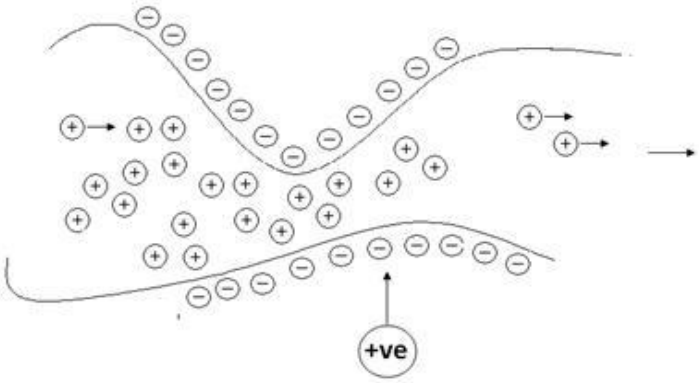

Figure 2: *Change in Voltage when the Rocks and Other Metallic Surfaces are Present*

In nature, the induced polarization (IP) effect is seen primarily with metallic sulfides, graphite, and clays. For this reason, IP surveys have been used extensively in mineral exploration. Recently, IP has been applied to hazardous waste landfill and groundwater investigations to identify clay zones. As with electrical resistivity surveys, vertical or horizontal profiles can be generated using IP. IP can also be used in borehole logging.

2. Instrumentation

The instrumentation for IP has been indigenously developed consists of a) transmitter b) receiver and c) display unit [1]. Using four probe methods, based on schlumberger, two electrodes are current electrodes and inner electrodes are used as voltage electrodes. With a timer, the applied voltage is given to the two current electrodes at intervals 2 or 4 or 8 seconds. The potential developed at the inner electrodes is measured by an accurate digital voltmeter. When the applied voltage is off, the induced voltage decays exponentially depending on the changeability of the soil. The decay is recorded and plotted in the electronic scope. The decay curve can be analyzed to give the exact value of m.

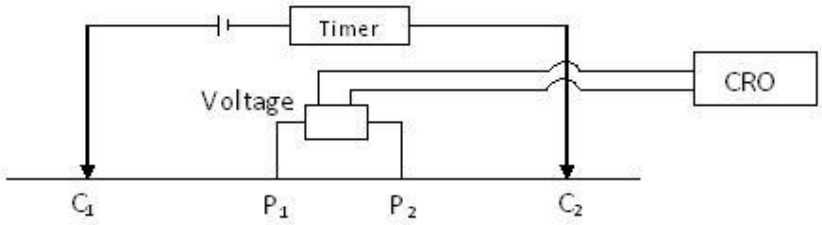

Figure 3: *Block Diagram of the IP Instrument*

When the current is forced through clay, the positive ions are displaced-the displacements in fact constitute the main part of the current. When the current is interrupted, positive charges redistribute themselves in their equilibrium pattern giving rise to decay in voltage.

Clay rich rock such as shall have comparatively less ability to polarize whereas siltstone has lower content of clay minerals have higher ability. This is because in rock having substantial current of clay, almost all the negative charges in exchange positions in the lattice so that no anion exists in the solution.

The transmitter generates a square pulse electric current a crystal controlled timer and relay drives have ON-OFF pulsing with 2-4-8 selection mechanism, Figure 4. Current rays are 30µA to 30mA. Receiver has log and arithmetic sampling modes of chargeability, Figure 5. The programmable mode has IP windows, Figure 3. It measures voltages between receiving electrodes and displays apparent resistivity and chargeability values.

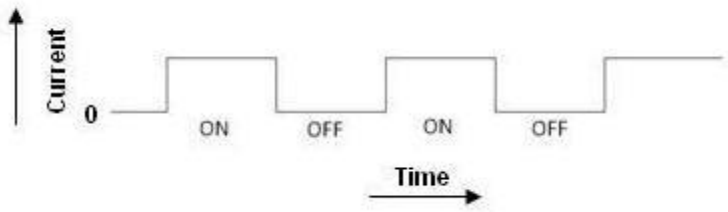

Figure 4: *Square Pulse Given to the IP Instrument*

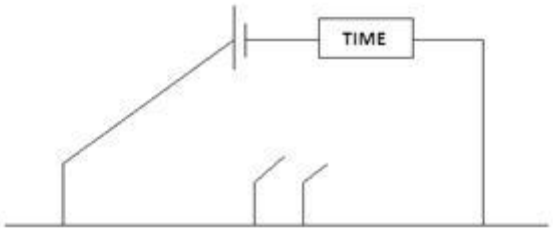

Figure 5: *Block Diagram of the Timer Circuit*

Main variable parameters of response obtained are chargeability and resistivity. These can be related to water content/clay content/grain size and CEC. Running readings displayed are average values of three last consecutive pulses, Figure 6. Cumulative readings shows values which are average of all pulses received from the beginning of measurement, Figure 7.

2.1. IP Effect

- Higher for disseminated than massive clay & metallic properties
- Depends on concentration of clay and metallic particles
- Increases if water in ground has a low conductivity
- Increases with decreasing porosity
- Varies with amount of water
- Depends on current input & current frequency

1. The presences of clay particles are filaments of fiber minerals both of these have negative charge. In the absence of conductive minerals IP over its origin to clay particles contain within pore structure of rock [3].
2. The surface of clay is negative and attracts positive ions from the electrolytes present in the capillaries of clay aggregate. Electrical double layers are formed, concentration of positive ions being greatest at the surface.

By constricting within a pore channel, the effects are:

- Net negative charge at the interface but most minerals and pore fluids
- Positive charges within pore fluid moving to rock surface for buildup positive charges (100µm)
- Pore channel diameter can be reduced by constriction which will block the flow of ions when charges are positive
- Negative charges will leave increasing the potential difference

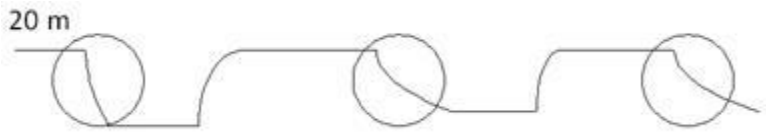

***Figure 6**: Change in the Chargeability from Pulse to Pulse*

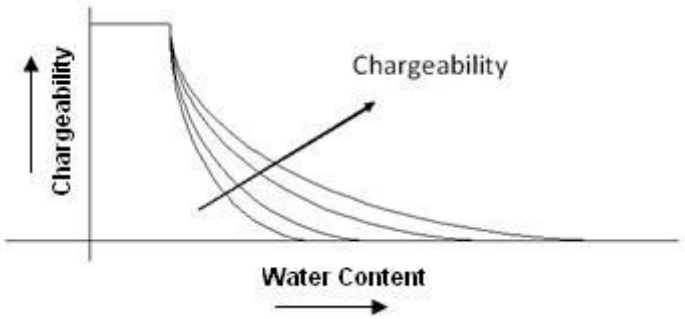

***Figure 7:** Variation in Chargeability with the Variation in Water Content*

3. Analysis of Experimental Results

A comparative analysis was made of chargeability and resistivity at different places. In the second phase, comparison of chargeability and water content was done. Generally it was found that chargeability values increases with water content up to a certain point [2]. After which there is decrease. For chargeability of 0-5 mv/v, resistivity variation was from 0-200 Ω-m. Table 1 records the comparison of water content and chargeability.

***Table 1:** Variations in Chargeability with Water Content and Type of Soil*

Chargeability	Water Content	Type of Soil
15 mV/V	Higher ≈ 30 %	Clay Silt Sand
8 mV/V	Lower ≈ 20 %	Clay Silt Sand
3 mV/V	Sandy ≈ 30 %	Sandy

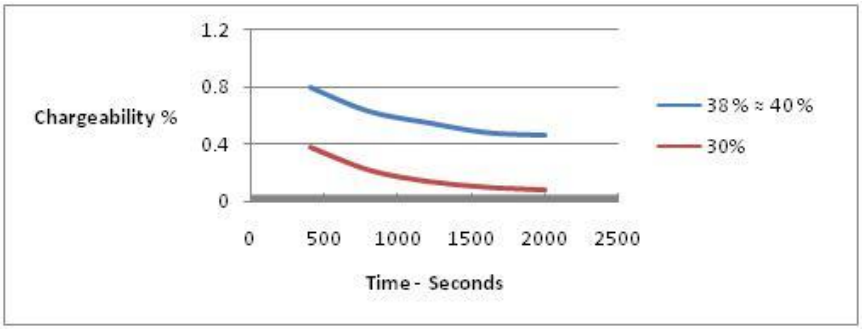

Figure 8: *Graph between the Chargeability and Time in Various Types of Soils*

Figure 8 gives the comparison of delay values for two types of soil.

4. Conclusion

Nondestructive methods such as IP can be used to correlate chargeability/resistivity and parameters such as water content. These techniques can be extended for CEC as well as grain size.

Acknowledgements

This paper is incomplete without the support of Prof. (Dr.) R.P. Das. His immense provision of vital aspects shaped the simple idea into a good work.

References

[1] Bharati Dass et al. *Soil Electrical Conductivity- a Tool for Precision Farming*. Journal of the Instrument Society of India. 2012. 42 (1) 21-22.

[2] Kotra Krishna Kumar. *Geomorphological Impact Assessment on Groundwater Quality and Fluoride Genesis along the Bay of Bengal of Visakhapatnam District, Andhra Pradesh, India.* CLEAN- Soil, Air, Water. 2011. 39 (10) 925-930.

[3] He Jishan. *Measuring Precision of Induced Polarization Method*. Trans. Nonferrous Met. Soc. China. 1994. 4 (4) 1-6.

Cloud Publications
International Journal of Advanced Civil Engineering and Architecture Research
2012, Volume 1, Issue 1, pp. 6-15, Article ID Tech-30

Research Article | Open Access

Active Force on Retaining Wall Supporting Φ Backfill Considering Curvilinear Rupture Surface

Sima Ghosh[1] and Chirabrata Debnath[2]

[1, 2] Civil Engineering Department, National Institute of Technology, Agartala, Tripura, India

Correspondence should be addressed to Sima Ghosh, sweekriti_100@yahoo.co.in and Chirabrata Debnath, chirabrata100@gmail.com

Publication Date: 31 December 2012

Article Link: http://technical.cloud-journals.com/index.php/IJACEAR/article/view/Tech-30

Abstract The evaluation of active earth pressure coefficient for safe design of retaining wall constructed to retain the supporting material at different elevation on two sides is one of the most important parameter. In this paper an effort has been made to provide an analytical expression for static active earth pressure acting on inclined rigid retaining wall considering non-linear failure surface by applying the horizontal slice method and limit equilibrium principle which gives more general solution compared to linear kind of failure surface. Considering curvilinear rupture surface the effect of wide range of parameters like angle of internal friction (Φ), angle of wall friction (δ), wall inclination angle (α), surcharge loading (q) are taken in to account to evaluate the static active earth pressure co-efficient. The results are presented in terms of static active earth pressure co-efficient and compared with the available solutions.

Keywords *Active Earth Pressure, Φ Backfill, Rigid Retaining Wall, Wall Inclination, Curvilinear Rupture Surface*

1. Introduction

Earth pressure theories constitute one of the most important parts in the civil engineering structures. Active earth pressure theories have been analyzed by our prominent researchers in the most accurate ways. Coulomb (1776) [1] was the first to establish the formulation for active and passive earth pressure for the retaining structures. Rankine's theory (1857) [2] has been a landmark for determination of active and passive earth pressure. Graphical methods have also been introduced by Culmann (1865) [3]. All these analyses have been conducted considering the Φ nature of backfill. In most of the cases, the determination of active earth pressure coefficient developed by several researchers based on the assumption that the failure surface is to be planner. In this analysis, considering non-linear failure surface and applying Horizontal Slice Method of analysis the optimum value of static active earth pressure coefficient is calculated.

2. Method of Analysis

A retaining wall of height, H inclined at an angle α with the vertical as shown in the figure 1 has been considered with the failure surface being curvilinear. The failure surface makes angles of θ_n and θ_1 with the vertical at bottom and top respectively. The failure wedge is split into 'n' number of thin slices of thickness ΔH. The rate of change of failure angle (θ_1 and $\theta_{n)}$ has been assumed as $\theta_R = \{(\theta_1 \sim \theta_n)/(n-1)\}$. Free Body Diagram of retaining wall-backfill system under active state of equilibrium is shown in figure 2.

The forces acting on the wall has been calculated by considering the following parameters:

- H_{i-1}, H_i = Horizontal shear acting on the top and bottom of the i^{th} slice
- W_i = Weight of the failure wedge of i^{th} slice
- V_{i-1}, V_i = Vertical load (UDL) on top and bottom of i^{th} slice
- Φ = the angle of internal friction of soil
- P_{ai} = Active earth pressure on i^{th} slice
- R_i = the reaction of the retained soil on i^{th} slice
- δ = the angle of wall friction

3. Derivation of Formulations Considering Active State of Equilibrium

Applying the force equilibrium conditions for i^{th} slice, we can solve the equations in the following pattern:

$$\sum H = 0$$

$$P_i \cos(\delta+\alpha) = R_i \cos(\phi+\theta_1+(i-1)\theta_r)$$

$$-\gamma(\Delta H)^2 \tan\phi\left\{\sum_{m=i}^{n-1}\left[\tan(\theta_1+m\theta_r)\right]+(n-i)\tan\alpha-(i-1)(\tan(\theta_1+(i-1)\theta_r)+\tan\alpha)\right\} \quad (1)$$

$$\sum V = 0$$

$$P_i \sin(\delta+\alpha) = -R_i \sin(\phi+\theta_1+(i-1)\theta_r)+(i-\frac{1}{2})\gamma(\Delta H)^2(\tan\alpha + \tan(\theta_1+(i-1)\theta_r)) \quad (2)$$

Solving the above equations, the generalized equation is derived as follows:

$$P_{ai} = \frac{\frac{\gamma}{2}(\Delta H)^2\left[\begin{array}{l}\{(2i-1)(\tan\alpha+\tan(\theta_1+(i-1)\theta_r))\cos(\phi+\theta_1+(i-1)\theta_r) \\ -2\tan\phi(\sum_{m=i}^{n-1}\left[\tan(\theta_1+m\theta_r)\right]+((n-i)\tan\alpha- \\ (i-1)(\tan(\theta_1+(i-1)\theta_r)+\tan\alpha)))\sin(\phi+\theta_1+(i-1)\theta_r)\}\end{array}\right]}{\sin(\phi+\delta+\alpha+\theta_1+(i-1)\theta_r)} \quad (3)$$

Where, $\tan(\theta_1+m\theta_r)=0$ for i = n

The active earth pressure coefficient can be simplified as,

$$K_a = \frac{\sum_{i=1}^{n} P_{ai}}{\frac{\gamma}{2} H^2} \quad (4)$$

Optimisation of the active earth pressure coefficient K_a is done for the variables θ_1 and θ_n satisfying the optimization criteria. The optimum value of K_a is given in table 1.

4. Parametric Study

A detailed Parametric study has been conducted considering non-linear failure surface to find the effect of variations of wide range of parameters like soil friction angle (Φ), wall inclination (α), wall friction angle (δ) on evaluation of static active earth pressure coefficient for Φ = 10^0, 20^0, 30^0 , 40^0 ; δ = 0, Φ/2, Φ and α = $+20^0$, 0, -20^0 . The details of these studies are presented below:

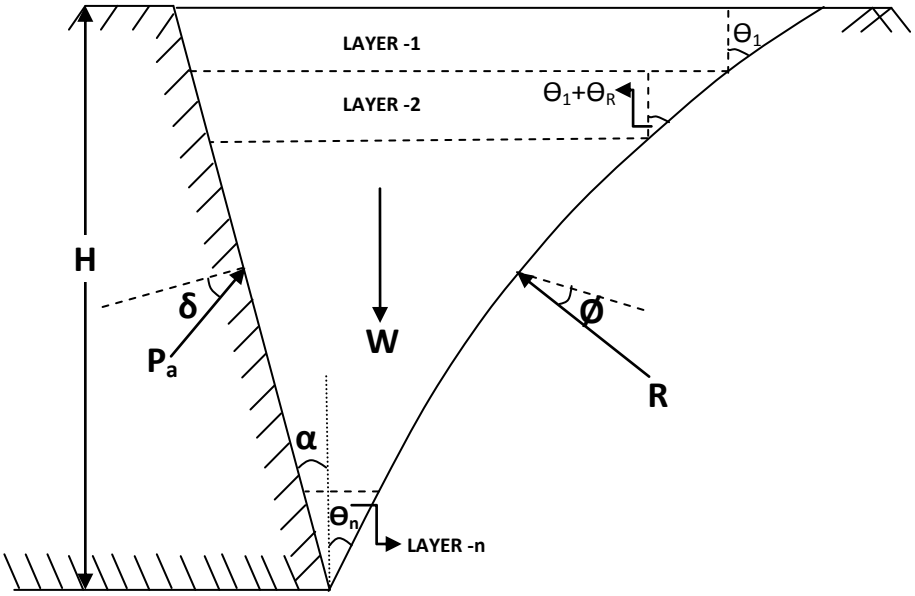

Figure 1: *Inclined Retaining Wall (Active state of equilibrium)*

4.1. Effect of Inclination of the Wall (α)

The effect of inclination of the wall on the evaluation of static active earth pressure for different value of wall inclination angle α is shown in figures 3 to 5. From these plots, it is seen that the magnitude of static active earth pressure increases with the increase in wall inclination angle α. The reason behind it is that when the inclination of the wall is positive with the vertical then it has to support more soil in comparison to the wall when it is inclined negative with the vertical. For example at Φ = 20° and δ =0°, the increase in K_a is 48% for α = +20° over α = 0 value, whereas the decrease in K_a is 21.2% over α = 0 value for α = -20. Again at Φ = 30° and δ = Φ/2, the increase in K_a is 89% for α = +20° over α = 0 value, whereas the decrease in K_a is 41.09% over α = 0 value for α = -20. Again at Φ = 20° and δ = Φ, the increase in K_a is 60% for α = +20° over α = 0 value, whereas the decrease in K_a is 28.9% over α = 0 value for α = -20. It is also observed that the value of K_a for α = +20° and δ = Φ, decreases with the increase in the value of Φ upto Φ = 20°, then the value suddenly increases with the increase in the value of Φ.

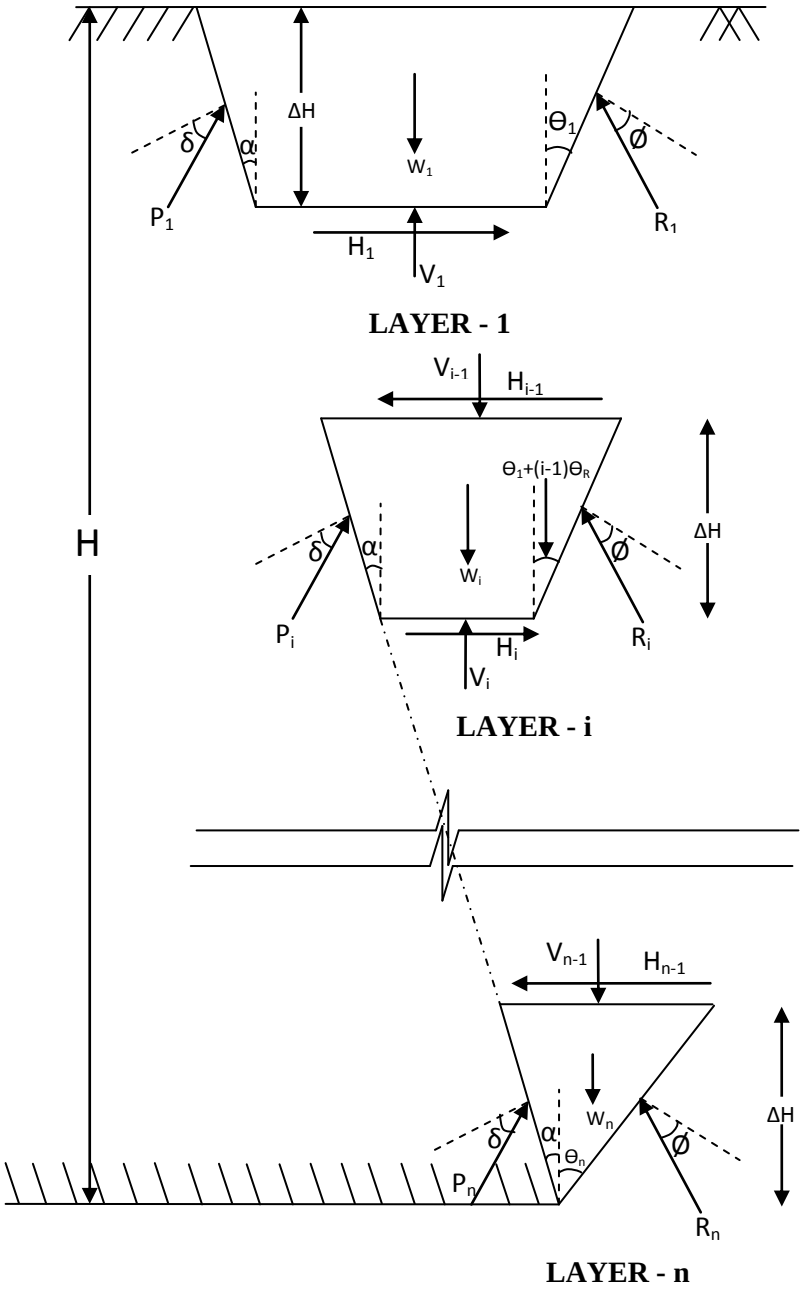

Figure 2: *Detailed drawing showing various components of the retaining wall along with slices (active state of equilibrium)*

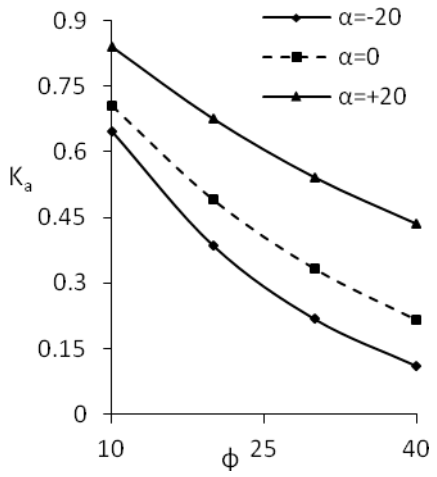

Figure 3: *Shows the variation of K_a with respect to soil friction angle (Φ) at different Wall inclination angles (α= -20, 0, 20) for δ = 0*

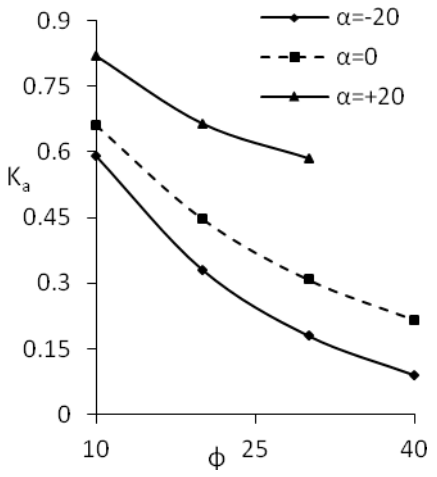

Figure 4: *Shows the variation of active earth pressure coefficient with respect to soil friction angle (Φ) at different Wall inclination angles (α= -20, 0, 20) for δ = Φ/2*

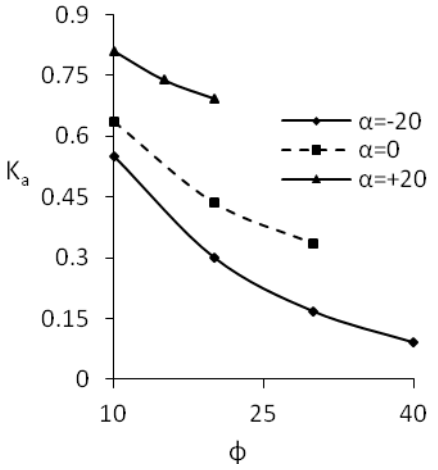

Figure 5: *Variation of active earth pressure coefficient with soil friction angle (Φ) at different Wall inclination angles (α= -20, 0, 20) for δ = Φ.*

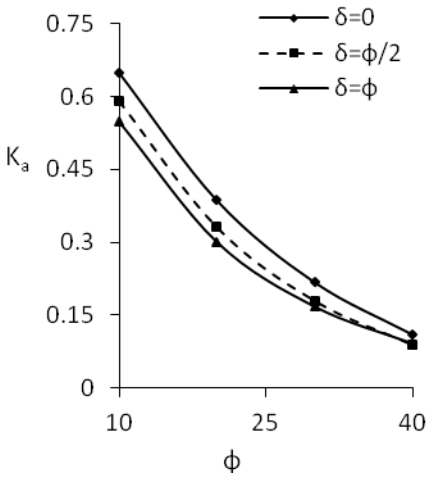

Figure 6: *Variations of active earth pressure coefficient with soil friction angle (Φ) at different Wall friction angles (δ= 0, Φ /2, Φ) for α = -20^0.*

4.2. Effect of Wall Friction Angle (δ)

The effect of wall friction angle on the evaluation of static active earth pressure coefficients for different value of wall friction angle δ is shown in figures 6 to 8. From these plots, it is seen that the magnitude of active earth pressure coefficient is going to be decreased due to increase in δ value. The reason behind it is that the frictional resistance of wall and soil is increasing with the increase in the value of δ. For example at Φ = 10° and α =20°, the decrease in K_a is 2.7% for δ = Φ/2 over δ = 0 value, whereas the decrease in K_a is 3.6% for δ = Φ over δ = 0. Again at Φ = 20° and α =0, the decrease in K_a is 8.5% for δ = Φ/2 over δ = 0 value, whereas the decrease in K_a is 11.6% for δ = Φ over δ = 0. Again at Φ = 30° and α =-20°, the decrease in K_a is 17.5% for δ = Φ/2 over δ = 0 value, whereas the decrease in K_a is 20.3% for δ = 2Φ/3 over δ = 0. It is also observed that the value of K_a for α = +20° and δ = Φ, decreases with the increase in the value of Φ upto Φ = 20°, then the value suddenly increases with the increase in the value of Φ.

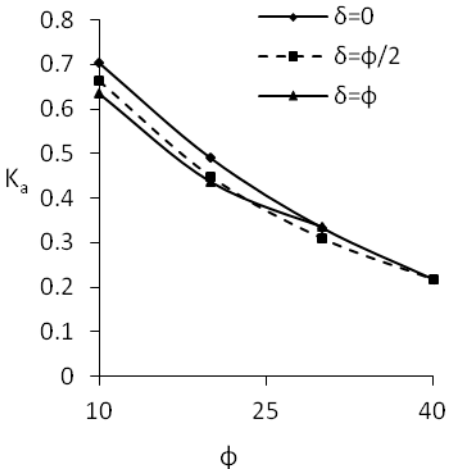

Figure 7: *Variations of active earth pressure coefficient with respect to soil friction angle (Φ) at different Wall friction angles (δ= 0, Φ /2, Φ) for α = 0^0*

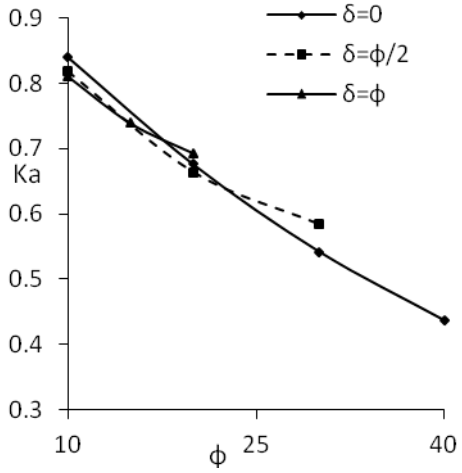

Figure 8: *Variations of active earth pressure coefficient with respect to soil friction angle (Φ) at different Wall friction angles (δ= 0, Φ /2, Φ) for α = 20^0*

4.3. Effect of Surcharge (q)

Figure 9 shows the variations of active earth pressure for inclusion of surcharge. It is seen that the value of active earth pressure increases gradually with the increase of surcharge. For Φ = 30^0, α = 20^0 and δ= Φ/2, the increment in K_a is 28% and 55% for q=10KN/m^2 and 20KN/m^2 respectively compared to q = 0 for a constant height. Also at Φ = 30^0, the value of active earth pressure decreases compared to other Φ values.

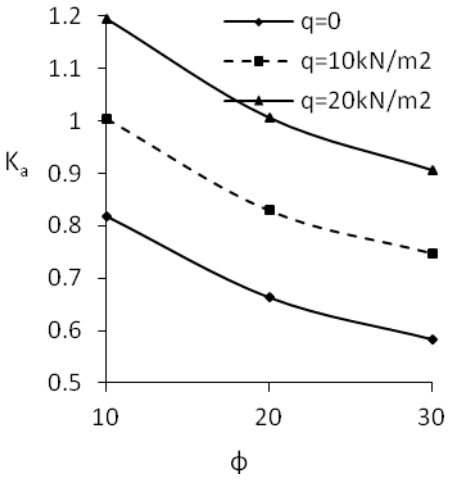

Figure 9: *Shows the variations of active earth pressure coefficient with respect to soil friction angle (Φ) for different surcharge loads (α = 20^0, δ= Φ/2*)

4.4. Wall Inclination and Nonlinearity of Failure Surface

Figure 10 shows the nonlinearity of failure surface of backfill (active case) for different values of wall inclinations (α = -20^0, 0^0, +20^0). The shape of the failure surface may be sagging or hogging in nature depending on the soil and wall properties. The shape of the failure surface is linear if the value of wall friction angle δ = 0 and the wall is vertical. With the increase in wall friction angle δ value the non-linearity of the failure surface is increases. For example, at Φ=30º, δ= Φ/2 and α = +20º, the value of failure angle at bottom is 54º whereas the value of failure angle at top is -41º. Also figures 11-12 show that the failure wedge is quite different as compared to the failure surface of the Ghosh and Sengupta (2012) [4] analysis. It is seen that the failure angle reduces with the increase in the wall inclination angles. The comparison shows that the value of failure angle is 26º in case of Ghosh and Sengupta (2012) [4] for the aforesaid conditions.

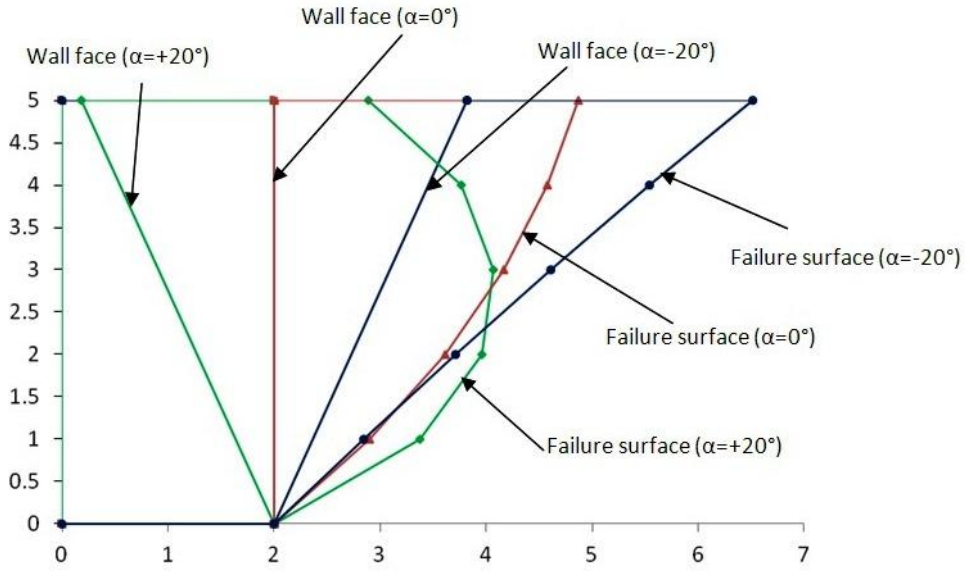

Figure 10: *Shows the nonlinearity of failure surface of backfill (active case) for different values of wall inclinations, α = -20^0 ,0^0, +20^0) at Φ = 30^0, δ= Φ/2*

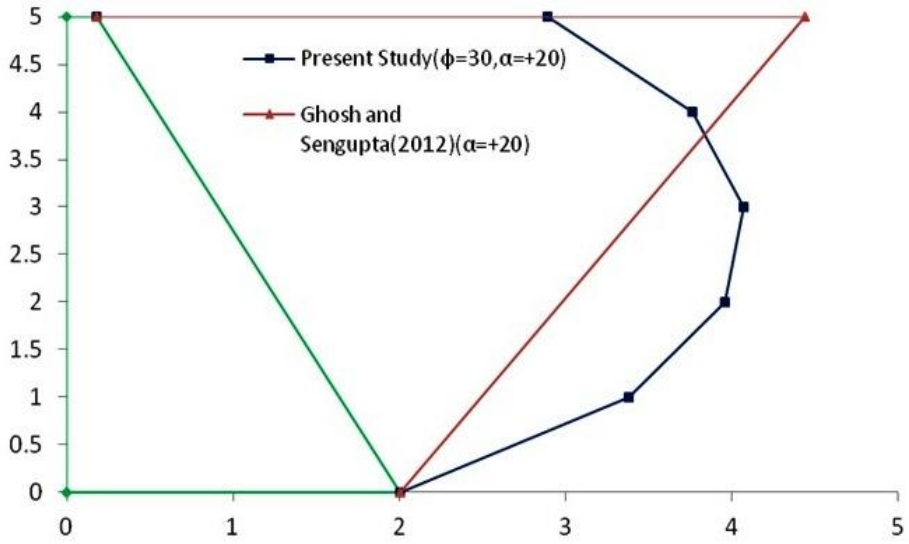

Figure 11: *Shows the comparison between failure surface of backfill (active case) for wall inclination, α = +20^0 at Φ = 30^0, δ= Φ/2*

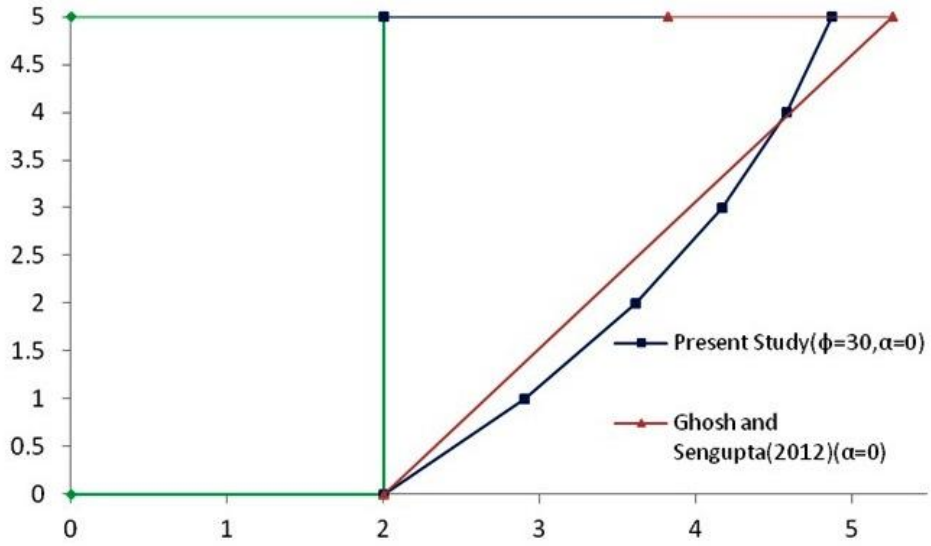

Figure 12: *Shows the comparison between failure surface of backfill (active case) for wall inclination, α = 0^0 at Φ = 30^0, δ= Φ/2*

4.5. Comparison of Results

Figure 13 shows the variations of active earth pressure coefficient with respect to soil friction angle (Φ) at Wall friction angles δ= Φ/2 for α = 20^0. K_a decreases uniformly with the increase in the value of soil friction angle (Φ). It can also be observed from table 2 that the value of $K_{a,}$ is around 5-15% higher than the values of Classical Coulomb (1776) theory.

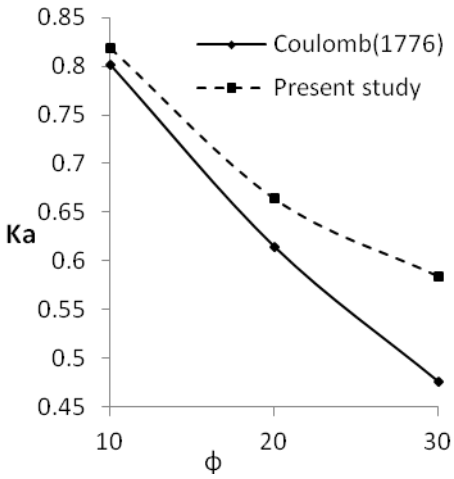

Figure 13: *Shows the variations of active earth pressure coefficient with respect to soil friction angle (Φ) at Wall friction angles δ= Φ/2 for α = 20^0*

Table 1: *Active Earth Pressure Coefficients (Static Case)*

φ	δ	Co-efficient of Active Earth Pressure, (K_a)		
		α = 20	α = 0	α = -20
10	0	0.841	0.7040	0.6487
	φ/2	0.819	0.6626	0.5907
	φ	0.811	0.6358	0.5499
20	0	0.676	0.4902	0.3862
	φ/2	0.664	0.4486	0.3314
	φ	0.693	0.4333	0.3018
30	0	0.542	0.3333	0.2187
	φ/2	0.584	0.3090	0.1805
	2φ/3	0.765	0.3172	0.1742
	φ	0.773	0.336	0.1686
40	0	0.436	0.2173	0.1117
	φ/2	0.638	0.5487	0.0904
	φ	--	0.2894	0.0926

Table 2: *Shows the comparison of results: -Active case*

φ	δ	α	Present Study	Coulomb (1776)
10	5	20	0.819	0.8013
20	10	20	0.664	0.6147
30	15	20	0.584	0.4762
40	20	20	0.638	0.3694

5. Conclusion

In this paper, an analytical solution has been developed to obtain active earth pressure coefficients using horizontal slice method. The analysis develops curvilinear rupture surface, may be sagging or hogging in nature depending upon the soil-wall parameters. The results obtained from the present solution are compared with the available solution like Coulomb (1776) method and it is concluded that the present solution gives higher value of active earth pressure co-efficient. The active force decreases with the increase in Φ and δ whereas; it is also observed that the negative inclination of wall (α) and surcharge (q) reduces the value of active earth pressure coefficient. The present analysis gives higher value of coefficient of active earth pressure in comparison to linear failure surface analysis. The present study can be further extended for determination of seismic active and passive earth pressure co-efficient considering non-linear nature of failure surface using both pseudo-static and pseudo-dynamic methods.

Notations

- θ_1 =Failure surface angle with vertical for top slice
- θ_n =Failure surface angle with vertical for bottom slice
- θ_R =Rate of change of failure surface angle
- Φ = Soil friction angle
- δ = Wall friction angle
- α = Wall inclination angle with the vertical
- P_a = active earth pressure
- H_1, H_2 = horizontal shear
- ΔH = height of each slice
- W_i = weight of i^{th} slice
- R = soil reaction force
- V_1 = vertical load (UDL) acting on the bottom surface of the 1^{st} layer
- V_2 = vertical load (UDL) acting on the top surface of the 1^{st} layer
- γ = unit weight of soil

References

[1] Coulomb C.A. 1773: *Essai Sur Une Application Des Regles Des Maximis et Minimis a Quelque Problems Des Statique Relatifs a1 Architecture*. Memoires d, Academie Roy. Pres. Diverssavants, 7.

[2] Rankine W.J.M. *On the Stability of Loose Earth*. Philosophical Transactions of the Royal Society of London. 1857. 147; 9-27.

[3] Culmann K., 1866: *Die Graphische Statik*. Mayer and Zeller, Zurich, 633.

[4] Ghosh S., et al. *Extension of Mononobe-Okabe Theory to Evaluate Active Earth Pressure Supporting c-Φ Backfill*. EJGE. 2012. 17 (2012) 495-504.

[5] Azad A., et al. *Seismic Active Pressure Distribution History behind Rigid Retaining Walls*. Soil Dynamics and Earthquake Engineering. 2008. 28; 365-375.

[6] Ghanbari A., et al. *Pseudo-Dynamic Active Earth Pressure Analysis of Inclined Retaining Walls Using Horizontal Slices Method.* SCIENTIA IRANICA- Transaction A: Civil Engineering. 2010. 17 (2) 118-130.

Cloud Publications
International Journal of Advanced Civil Engineering and Architecture Research
2012, Volume 1, Issue 1, pp. 16-24, Article ID Tech-49

Research Article | Open Access

Soil Characteristics and Its Behavior in the Lower Flood Plain of River Daya in Odisha, India

T.K. Lohani[1] and K.P.Dash[2]

[1, 2] Department of Civil Engineering, Orissa Engineering College, Bhubaneswar, Odisha, India

Correspondence should be addressed to Lohani T.K., tklohani@gmail.com

Publication Date: 19 February 2013

Article Link: http://technical.cloud-journals.com/index.php/IJACEAR/article/view/Tech-49

Abstract The river bank of Daya in the S-E of the state of Odisha is presently mushrooming with constructions and infrastructural developments. Since the region is devoid of solid and hard rock basement, it has become a matter of concern for the technocrats and architects to provide suitable and stabilized foundations for those upcoming massive structures. The present study reflects the complex behavior of the soil parameters whose index and engineering properties have been determined strictly based on Indian Standard codes. The lithological variation of the land shows the entire region is spread by a thick blanket of clayey soil having high porosity with less permeability generating a swampy land throughout the year. But fortunately at a shallow to deep the stratum is defined by a compact, hard and impervious lateritic bed that gives ample support for a safe and stable foundation. Due to this, selection of foundation for construction purpose has become a challenging job. In the present research two nos. of boreholes were drilled up to 10m NGL, laboratory experiments were conducted and soil parameters were determined. From the various studies of soil it was found that clayey sand, sandy clay and thick blanket of clay pre-dominates the study area. Load bearing structures are completely unfavorable on such type of soil. Due to expansive nature of soil, deep foundation/pile foundation is suggested.
Keywords *SPT, UDS, Borehole Logs, Shear Strength, Safe Bearing Capacity*

1. Introduction

The coastal alluvium forms unconsolidated material of which the study area is a part of that. These formations composed of sand, gravel, silt, clay and laterite. It has extensive unconfined and confined zone down to 150m - 300m. This zone is underlain by the Mahanadi graben extending in a NW-SE direction. The physical and index parameters of soil under the study area with an aerial extension of around 120km2 are completely dependent on the percolation and penetration of surface and groundwater. As the water of Daya is comparatively sweeter it may be assessed that impact of saline environment is too negligible on the soil characters. The spectacular hydrogeological set up of the study area owes to the varied geomorphic and geological set up which controls the physical and chemical behavior of the soil strata. Geotechnical parameters at various depths of soil strata along the

river Daya is alarming. The primary reason behind the variation is the impact of coastal environment, rapid growth of population, abandonment of agricultural lands and conversion of cultivable lands to infrastructural projects. Stratigraphic, lithologic and geomorphic set ups partially control the performance of soil. The annual rainfall in the area also varies considerably from year to year which affects the physico-chemical characteristic of soil and its strength parameters. Large number of central and state level organizations has been setup to investigate the soil strength in district and block level to meet the requirement for infrastructural development but still remarkable work is lacking.

The study area which extends from Sundarpada under Bhubaneswar Municipal Corporation to Harirajpur block of Khurda district a stretch of 12.3km locates between the latitude of 2008′ to 20029′ and longitude 85044′ to 85073′ constituting the part of Khurda district has its own importance due to massive infrastructural growth, mushrooming educational institutes and high rise apartments. The scope of work comprises of conducting detail soil investigation, laboratory testing, conducting and estimation of safe bearing capacity for the proposed work on drilling two nos. of boreholes.

2. Methodology

The methods of investigation consist of visual reconnaissance, drilling of boreholes, laboratory experiments and determination of soil parameters and analysis of the results. The field borehole drillings are extended up to 10m below Natural Ground Level (NGL) or refusal. This is followed by collection of UDS samples as per [4] and finally the soil samples are transported to the Civil engineering laboratory of Orissa Engineering College. The bulk density, moisture content, grain size analysis, shear strength, liquid limit, plastic limit, specific gravity, DFS, water absorption, porosity and density of the samples are determined in the laboratory [11]. For detailed laboratory investigation SPT is conducted at 1.5m intervals or at change of soil strata in different boreholes. Disturbed soil samples from both the boreholes were collected at 1.5m SPT tests were conducted as [2] and [3] respectively in different levels at the boreholes in a continuous manner using spilt-spoon samplers. The SPT sampler was lowered inside the borehole after drilling the required level and is driven by a 63.50kg hammer with a free fall of 750mm driving 450mm in three stages 150mm each and the number of blows for each 150mm penetration for 2nd and 3rd 150mm drive recorded as “N”. Refusal is considered for N>100. In the course of drilling groundwater was encountered at a depth of 1.20m to 1.50m NGL.

3. Results and Discussion

Table 1: *Result of different properties from different boreholes*

Sl. No	Borehole reference	Sample Depth (in m.)	Bulk density (gm/cc)	Natural Moisture Content	Dry Density	Cohesion (Kg/Cm2)	Angle of Internal Friction (in degrees)	Attenberg's Limit (in %)			Specific Gravity [6]	Void ratio	DFS (in %)
								LL	PL	PI			
1	BH-1, SPT-1	1.5	1.81	18.2	1.53	xxxxx	xxxxx	35	21	14	2.69	0.757	20
2	BH-1, SPT-2	3	1.81	18.5	1.53	xxxxx	xxxxx	34	21	13	2.69	0.761	20
3	BH-1, SPT-3	4.5	1.81	18.7	1.52	xxxxx	xxxxx	34	21	13	2.69	0.764	20
4	BH-1, UDS-1	6	1.82	19.6	1.52	0.41	7	45	24	21	2.69	0.768	35
5	BH-1, SPT-4	7.5	1.82	19.4	1.52	xxxxx	xxxxx	44	24	20	2.69	0.765	35
6	BH-1, UDS-2	9	1.83	19.1	1.54	0.37	9	45	24	21	2.69	0.751	32
7	BH-1, SPT-5	10	1.83	19.2	1.54	xxxxx	xxxxx	45	24	21	2.69	0.752	32
8	BH-2, SPT-1	1.5	1.8	18.3	1.52	xxxxx	xxxxx	36	22	14	2.69	0.768	20
9	BH-2, SPT-2	3	1.8	18.7	1.52	xxxxx	xxxxx	35	21	14	2.69	0.774	20
10	BH-2, SPT-3	4.5	1.81	18.9	1.52	xxxxx	xxxxx	35	21	14	2.69	0.767	20

11	BH-2, UDS-1	6	1.82	19.7	1.52	0.39	7	45	24	21	2.69	0.769	35
12	BH-2, SPT-4	7.5	1.82	19.6	1.52	xxxxx	xxxxx	44	24	20	2.69	0.768	35
13	BH-2, UDS-1	9	1.82	19.5	1.52	0.41	8	45	24	21	2.69	0.766	35
14	BH-2, SPT-5	10	1.83	19.3	1.53	xxxxx	xxxxx	45	24	21	2.69	0.754	32

The result of different properties of soil samples in the study area in shown in Table 1.

A. Calculation of Safe Bearing Capacity from Strength Parameters (SPT Values)

(At 1.50m)	**Borehole No-1**
Square Footing	
Field SPT Value N =	6
Overburden Pressure	0.271 kg/cm^2 [3]
Dilaitancy Factor, the corrected SPT Value N$'$	6 [3]
Taken corresponding C=	0.00 kg/cm^2
Angle of shearing resistance value Φ for zone =	28 degrees
Size of Footing = 2m. X 2m.	
Cohesion C =	0.00 kg/cm^2 [7]
Angle of Shearing resistance Φ =	28 degree [8]
Φ$'$ =	19 degree [9]
Specific Gravity Gs =	2.69 (IS: 2720-1980, Part III)
Void ratio e =	0.757 [7]
Bulk density γ =	1.810 g/cc [5]
Depth of foundation Df =	1.50 m
Assuming width of footing B =	2.00 m
Q = [Df X (γ)]/10	0.271 kg/cm^2
Bγ = (Bxγ)/10	0.3620 kg/cm^2

Bearing Capacity Factors [1]

Φ & Φ′	**Nc & Nc′**	**Nq & Nc′**	**Nγ & Nγ′**
28	26.372	15.304	17.792
19	14.06	5.908	4.842

Shape Factors [1]

Sc = 1.3 Sq = 1.2 Sγ = 0.8

Depth Factors & Inclination Factors [1]

$d_c = 1 + 0.2 \times (Df/B) \times \tan(45 + \Phi/2) = 1.25$

$d_p = d_\gamma = 1.125$ $i_c = i_q = i_\gamma = 1$

Effect of Water Tables [1]

w′ = 0.5

In Case of Local Shear Failure for Circular Footing [1]

$Qd' = q(Nq' - 1)S_q d_q i_q + 0.5 B_\gamma N_{\gamma N\gamma S\gamma d\gamma i\gamma} W$

= 1.796 + 0.394

= 2.190 kg/cm^2

Ultimate Bearing Capacity Obtained from Interpolation = Qd [1]

Qd = 2.190 kg/cm^2

Net Safe Bearing Capacity Considering Factor of Safety of 3 = 0.730 kg/cm^2

=> NSBC= 7.30T/m^2

B. Calculation of Safe Bearing Capacity from Strength Parameters (SPT Values)

(At 3.00m)	**Borehole No. 1**
Square Footing	Depth of foundation = 3.00m
Field SPT Value N =	8
Overburden Pressure	0.542 kg/cm^2 [3]
Dilaitancy Factor, the corrected SPT Value N'	8 [3]
Taken corresponding C=	0.00 kg/cm^2
Angle of shearing resistance value Φ for zone =	28 degrees
Size of Footing = 2m X 2m	
Cohesion C =	0.00 kg/cm^2
Angle of Shearing resistance Φ =	28 degree
Φ′ =	19 degree
Specific Gravity Gs=	2.69
Void ratio e =	0.761
Bulk density γ=	1.810 g/cc
Depth of foundation D_f=	3.00 m
Assuming width of footing B=	2.00 m
Q = [D_f X (γ)]/10	0.542 kg/cm^2
Bγ = (Bxγ)/10	0.3620 kg/cm^2

Bearing Capacity Factors [1]

Φ & Φ′	**Nc & Nc′**	**Nq & Nc′**	**Nγ & Nγ′**
28	6.372	15.304	17.792
19	4.06	5.908	4.842

Shape Factors [1]

$S_c = 1.3$ $S_q = 1.2$ $S_\gamma = 0.8$

Depth Factors & Inclination Factors [1]

$d_c = 1 + 0.2 \times (Df/B) \times \tan(45 + \Phi/2) = 1.499$

$d_p = d_\gamma = 1.25$ $i_c = i_q = i_\gamma = 1$

Effect of Water Tables [1]

w′ = 0.5

In case of Local Shear Failure for Circular Footing [1]

$Qd' = q (Nq' - 1) S_q d_q i_q + 0.5 B_\gamma N_{\gamma N \gamma S \gamma d \gamma i \gamma} W$

= 3.99 + 0.438

= 4.428 kg/cm^2

Ultimate Bearing Capacity Obtained from Interpolation = Qd [1]

Qd = 4.428 kg/cm^2

Net Safe Bearing Capacity Considering Factor of Safety of 3 = 1.476 kg/cm^2

=>SBC=14.76 T/m^2

C. Calculation of Safe Bearing Capacity from Strength Parameters (SPT Values)

(At 1.50m)	**Borehole No-2**
Square Footing	Depth of Foundation = 1.50m
Field SPT Value N =	2

Overburden Pressure		0.270 kg/cm^2 [3]
Dilaitancy Factor, the corrected SPT Value N'		2 [3]
Taken corresponding C=		0.00 kg/cm^2
Angle of shearing resistance value Φ for zone =		28 degrees
Size of Footing = 2m. X 2m.		
Cohesion C =		0.00 kg/cm^2
Angle of Shearing resistance	Φ =	28 degree
	Φ′ =	19 degree
Specific Gravity Gs =		2.69
Void ratio e =		0.768
Bulk density γ =		1.80 g/cc
Depth of foundation Df =		1.50 m
Assuming width of footing B =		2.00 m
Q = [Df X (γ)]/10		0.270 kg/cm^2
Bγ = (Bxγ)/10		0.360 kg/cm^2

Bearing Capacity Factors [1]

Φ & Φ′	Nc & Nc′	Nq & Nc′	Nγ & Nγ′
28	26.372	15.304	17.792
19	14.06	5.908	4.842

Shape Factors [1]

Sc = 1.3 Sq = 1.2 Sγ = 0.8

Depth Factors & Inclination Factors [1]

$d_c = 1 + 0.2 \times (Df/B) \times \tan(45 + \Phi/2) = 1.25$

$d_p = d_\gamma = 1.125$ $i_c = i_q = i_\gamma = 1$

Effect of Water Tables [1]

w′ = 0.5

In Case of Local Shear Failure for Circular Footing [1]

$Qd' = q(Nq' - 1)S_q d_q i_q + 0.5\, B_\gamma N_{\gamma N \gamma S \gamma d \gamma i \gamma} W$

= 1.789 + 0.392

= 2.181 kg/cm^2

Ultimate Bearing Capacity Obtained from Interpolation = Qd [1]

Qd = 2,181 kg/cm^2

Net Safe Bearing Capacity Considering Factor of Safety of 3 = 0.727 kg/cm^2

=> NSBC = 7.27 T/m^2

D. Calculation of Safe Bearing Capacity from Strength Parameters (SPT Values)

(At 3.00m)		**Borehole No-2**
Square Footing		Depth of Foundation = 3.0m
Field SPT Value N =		4
Overburden Pressure		0.540 kg/cm^2 IS: 2131-1981, Clause 3.6.1
Dilaitancy Factor, the corrected SPT Value N′	2	IS: 2131-1981, Clause 3.6.1
Taken corresponding C=		0.00 kg/cm^2
Angle of shearing resistance value Φ for zone =		28 degrees

Size of Footing = 2m X 2m

Cohesion C =	0.00 kg/cm^2
Angle of Shearing resistance Φ =	28 degree
Φ′ =	19 degree
Specific Gravity Gs =	2.70
Void ratio e =	0.774
Bulk density γ =	1.80 g/cc
Depth of foundation Df =	3.00 m
Assuming width of footing B =	2.00 m
Q = [Df X (γ)]/10	0.540 kg/cm^2
Bγ = (Bxγ)/10	0.360 kg/cm^2

Bearing Capacity Factors [1]

Φ & Φ′	**Nc & Nc′**	**Nq & Nc′**	**Nγ & Nγ′**
28	26.372	15.304	17.792
19	14.06	5.908	4.842

Shape Factors [1]

Sc =1.3 Sq =1.2 Sγ = 0.8

Depth Factors & Inclination Factors [1]

$d_c = 1 + 0.2 \text{ X } (Df/B) \text{ X } \tan(45 + \Phi/2) =$ 1.499

$d_p = d_\gamma =$ 1.25 $i_c = i_q = i_\gamma = 1$

Effect of Water Tables [1]

w′ = 0.5

In Case of Local Shear Failure for Circular Footing [1]

$qd' = q (Nq' - 1)S_q d_q i_q + 0.5 B_\gamma N_{\gamma N \gamma S \gamma d \gamma i \gamma} W$

= 3.975 + 0.436

= 4.411 kg/cm^2

Ultimate Bearing Capacity Obtained from Interpolation = Qd [1]

Qd = 4.411kg/cm^2

Net Safe Bearing Capacity Considering Factor of Safety of 3 = 1.47 kg/cm^2

=> NSBC = 14.70 T/m^2

Design of Pile Foundation

D = Diameter of Pile	= 30.00 cm
L = Length of Pile	= 10 m
DU = Diameter of Under ream	= 75.00 m
Grade of Concrete	= M-20

For Sandy Zone

Thickness Layer = 500 cm

$Qu = Ap (1/2 \text{ D } \lambda N_1 + \lambda d_f N_q) + A_2 (1/2 D_u n \lambda N_2 + \lambda d_f N_q) + 1/2\pi \text{ D } \lambda \text{ K } \tan\sigma D_f^2$

Aa = (π/4) X ($Du_2 – D_2$) is the under reamed bulb diameter	= 3709.13 cm^2
A_p = Cross section area of pile stem at toe level	= 706.50 cm^2
N = Number of the under reamed bulbs	= 1.00
Λ = Average submerged unit weight of soil	= 0.871 X 10^{-3}gm/cc

N_λ = Bearing Capacity factors depending upon the angle of internal friction = 17.79
N_q = Bearing Capacity factors depending upon the angle of internal friction = 15.30
d_f = Total Depth of pile in sandy strata = 500.00 cm
K = Earth pressure co-efficient = 1.00
σ = Angle of wall friction = 28
Qu = Ultimate Bearing Capacity of Pile
$Qu = Ap(1/2\ D\ \lambda\ N_1 + \lambda\ d_f N_q) + A_2(1/2\ D_u\ n\ \lambda\ N_2 + \lambda\ d_f N_{q)} + 1/2\pi\ D\ \lambda\ K\ Tan\sigma\ D_f^2$
Qu = 36744.064 KG
= 36.7441 MT

For Clay Zone (Screen Friction)
Thickness Layer =500 cm
Qu = AaNcC′a + C′aA′a + αCsAs
Nc = Bearing Capacity Factor Usually taken As 9 = 9.00
Aa = π/4 (Du_2-D_2), Where Du & D are the diameters of under ream & pile stem in cm = 3709.125 cm^2
C′a = Average Cohesion of Soil along the pile stem in (kgf/cm^2) = 0.39 kgf/cm^2
A′a = Surface area of the Cylinder Circumscribing the under reamed bulb in cm^2 = 2943.75 cm^2
α = Reduction Factor Usually 0.5 = 0.50
Average Cohesion of Soil around under reamer =0.33 kgf/cm^2
Cs = Bulb in (kgf/cm^2)
As = Surface area of stem in cm^2 = 47115.00 cm^2
Q_u = Ultimate Bearing Capacity of pile
Qu = For Clay Zone = 21.941 MT
Qu = For Sandy Zone = 36.74 MT
Total Load Carrying = 58.685 MT
Safe Load Carrying Capacity of Pile (Assuming F O S: 3.0) = 19.56 MT
Say = 20.00 MT
N.B: The load carrying capacity of the pile may be confirmed by conducting pile load test [10]

Design of Pile Foundation
D = Diameter of Pile = 37.80 cm
L = Length of Pile = 10.00 m
DU = Diameter of Under ream = 23.75 m
Grade of Concrete = M-20

For Sandy Zone
Thickness Layer = 500 cm
$Qu = Ap(1/2\ D\ \lambda\ N_1 + \lambda\ d_f N_q) + A_2(1/2\ D_u\ n\ \lambda\ N_2 + \lambda\ d_f N_{q)} + 1/2\pi\ D\ \lambda\ K\ Tan\sigma\ D_f^2$
Aa = (π/4) X (Du_2 – D_2) is the under reamed bulb diameter = 5795.51 cm^2
A_p = Cross section area of pile stem at toe level = 1103.91 cm^2
N = Number of the under reamed bulbs = 1.00
Λ = Average submerged unit weight of soil = 0.871 X 10^{-3}gm/cc
N_λ = Bearing Capacity factors depending upon the angle of internal friction = 17.79
N_q = Bearing Capacity factors depending upon the angle of internal friction = 15.30
d_f = Total Depth of pile in sandy strata = 500.00 cm
K = Earth pressure co-efficient = 1.00

σ = Angle of wall friction = 28
Qu = Ultimate Bearing Capacity of Pile
$Qu = Ap(1/2\ D\ \lambda\ N_1 + \lambda\ d_f N_q) + A_2(1/2\ D_u\ n\ \lambda\ N_2 + \lambda\ d_f N_{q)} + 1/2\pi\ D\ \lambda\ K\ Tan\sigma\ D_f^2$
Qu = 56757.90 KG
= 56.7579 MT

For Clay Zone (Screen Friction)
Thickness Layer = 500 cm
Qu = AaNcC′a + C′aA′a + αCsAs
Nc = Bearing Capacity Factor Usually taken as 9 = 9.00
Aa = π/4 (Du_2-D_2), Where Du & D are the diameters of under ream & pile stem in cm = 5795.508 cm^2
C′a = Average Cohesion of Soil along the pile stem in (kgf/cm^2) = 0.39 kgf/cm^2
A′a = Surface area of the Cylinder Circumscribing the under reamed bulb in cm^2 = 2943.75 cm^2
α = Reduction Factor Usually 0.5 = 0.50
Average Cohesion of Soil around under reamer = 0.33 kgf/cm^2
Cs = Bulb in (kgf/cm^2)
As = Surface area of stem in cm^2 = 58893.75 cm^2
Q_u = Ultimate Bearing Capacity of pile
Qu = AaNcC′a + C′aA′a + αCsAs
Qu = 31207.764 Kg
31.206 MT
Total Load Carrying Capacity is deduced as
Qu = For Clay Zone = 31.208 MT
Qu = For Sandy Zone = 56.76 MT
Total Load Carrying = 87.968 MT
Safe Load Carrying Capacity of Pile (Assuming F O S: 3.0) = 29.32 MT
Say = 29.00 MT

4. Conclusion

The study area is that zone where the importance of residential apartments and buildings are increasing day by day. Considering the importance of utility based on the present scenario the investigated results has been reviewed to ascertain the suitable type of foundation depending on stability and economy. The foundation may be shallow or deep but the most suitable type will be deep foundation for the following setbacks.

1. Soil bearing capacity is suitable to some extent for shallow foundation at a depth of 3m.
2. If shallow foundation of any suitable geometrical shape is suggested then the size of foundation will become too large as the SBC is very less and simultaneously gives un-economical foundation.
3. The soil characteristics below 3m depth show a drastic increase in differential free swell (DFS) and Plasticity Index Value (PIV).
4. This character indicates the soil is highly expansive in nature.
5. The pressure bulb lies in the soil which exhibits high compressibility, shrinkage and extremely high swelling characteristics under very little load. The permeability is extremely low.
6. Considering the above constraints in providing shallow foundation the alternative i.e. deep foundation/pile foundation is suggested.

References

[1] Bureau of Indian Standards, 1981: *Indian Standard Code of Practice for Determination of Breaking Capacity of Shallow Foundations (First Revision) Sixth Reprint February 1998*, IS: 6403-1981, 15.

[2] Bureau of Indian Standards, 1980: *Indian Standard Code of Practice for Split Spoon Sampler: ZI 3089*, IS 9640-1980, 8.

[3] Bureau of Indian Standards, 1982: *Indian Standard Code of Practice for Standard Penetration for Soil (First Revision) Third Reprint March 1997,* IS: 2131-1981.

[4] Bureau of Indian Standards, 1979: *Indian Standard Code of Practice for Subsurface Investigation for Foundations (First Revision), Second Reprint, November 1985*, IS: 1892-1979.

[5] Bureau of Indian Standards, 1973: *Indian Standard Code of Practice for Preparation of Dry Soil a sample for Various Tests, IS*: 2720-1973, Part-II (Revision 2).

[6] Bureau of Indian Standards, 1980*: Indian Standard Code of Practice for Determination of Specific Gravity of Soil,* IS: 2720-1980, Part-XIII.

[7] Bureau of Indian Standards, 1973: *Indian Standard Code of Practice for Determination of Unconfined Compressive Strength,* IS: 2720-1973, Part-X.

[8] Bureau of Indian Standards, 1978: *Indian Standard Code of Practice for Determination of Shear Strength Parameters of a Specimen Tested In Unconsolidated Undrained Triaxial Compression without the Measurement of Pore Water Pressure*, IS: 2720-1978, Part-XI.

[9] Bureau of Indian Standards, 1978: *Indian Standard Code of Practice for Determination of Shear Strength Parameters of a Specimen Tested In Unconsolidated Undrained Triaxial Compression with the Measurement of Pore Water Pressure*, IS: 2720-1978, Part-XII.

[10] *Bureau of Indian Standards, 1985: Indian standard code of practice for Design and construction of Pile foundations, load test on piles, are: 2911-1985, part-4.*

[11] Mishra A. K., et al. *A New Technology of Marble Slurry Waste Utilization in Roads*. Journal of Scientific and Industrial Research. 2010. 69; 67-72.

Cloud Publications
International Journal of Advanced Civil Engineering and Architecture Research
2013, Volume 2, Issue 1, pp. 25-31, Article ID Tech-57

Research Article | Open Access

Geohydrological Investigation at Pullampet, Cuddapah District, Andhra Pradesh, India

S. Siddiraju

Department of Civil Engineering, Siddharth Institute of Engineering and Technology, Narayanavanam Road, Puttur, Chittoor District, Andhra Pradesh, India

Correspondence should be addressed to S. Siddiraju, ssiddiraju@gmail.com

Publication Date: 8 May 2013

Article Link: http://technical.cloud-journals.com/index.php/IJACEAR/article/view/Tech-57

Abstract The area of investigation located at Pullampet mandal, Cuddapah district, Andhra Pradesh, India. Vertical Electrical Soundings (VES) were carried out at 30 locations using schlumberger configuration for the investigation of ground water resources in the drought prone area. The data were interpreted by partial curve matching and more sophisticated techniques based on inversion schemes. The curves are prominently at A, K&H type. Interpretations reveal the number of sub-surface layers, their thickness and their water bearing capacity within the study area. This will greatly help to understand the sub-surface geology and in identifying bore wells and digging of wells in negative areas will be avoided.
Keywords *VES, Schlumberger Electrode, Curve Matching and Sub-Surface Area*

1. Introduction

The area of investigation, located Pullampet mandal, Cuddapah district, Andhra Pradesh. (Lat, $13^0 58^1 00^{11}$ to $14^0 13^1$ Long, $79^0 03^1$ to $79^0 17^1$) is about 406.63 square kilometers. The climate of the study area is hot and semi-arid. The area receiving an annual rainfall of 795 mm, out of which 45 to 65 % of the total rainfall received during the north-east monsoon period. The ground water level has been declined in recent times. The rapid urban development in Pullampet, Cuddapah (DIST), demands excesses utilization of ground water, because of over exploitation of ground water, the warrants ground water assessments for sustainable methods provide indirect information about sub-surface formations by measuring the various physical parameters of the earth crust electrical resistivity survey by far is most suitable methods for ground water investigation.

Geophysical techniques are the highly useful one for the identification of ground water potential zones. Among various geophysical studies, we have selected vertical electrical sounding (VES) to carry out ground water potential zones identification in the present study area. The true resistivity values and thickness of layers are obtained by interpretation of the sounding curves [1]. Using this method, depth and thickness of various sub-surface layers and their water yielding capabilities can be

inferred [2]. The main objective of the present study is to apply electrical resistivity method (VES) to identify the ground water condition and the nature of sub-surface layers within the study area [7].

2. Geology of the Study Area

The rock formations of the study area represent a suite of sedimentary and metamorphic rocks formed during pre-cambrian times. Lithologically the Cuddapah formations are predominantly argillaceous and arenaceous sequence with sub ordinate calcareous sediments. Characteristically each group starts with quartzite and ends with dolomite or shale/phyllite. Structurally, the rocks have general trend of NNW-SSE with dips of formations in generally varying from 10^0 -40^0. The Nagari Quartzites exposed mainly in the southern part of the basin. This is dominantly an arenaceous consisting of conglomerate quartzite, quart ride with shale intercalations.

The Pullampet formations rest over the Nagari quartzite conformably in the southern part of the basin with purple shale, carbonaceous shale and calcareous shale with prominent intercalations of dolamitic limestones. The basal part of the Pullampet is marked by ferruginous chart and jasper with lensoid dolomite and patches. Large out crops are quartzite are seen in the southern and western portion of the area as hills and ridges. Dolomitic limestone occurs at places as discontinuous interbands and lenses. The shale occurs mostly in low lying lands and strike in a NNW direction with variable dips. The shale is interspersed by bands with quartzite, which sometimes occurs as low-lying elongated hill locks. Aluminum of recent age is composed mostly of sand and subordinately of silty or clayey sand and is combined all along and on either side of the Pulang River.

3. Materials and Methods

In this study, vertical electrical sounding (VES) method has been adopted VES survey was carried out in 30 locations (Figure 1) using schlumberger electrode configuration [3]. For resistivity sounding schlumberger array was adopted, for which the current electrodes are spaced much further apart than potential electrodes [8]. Various electrode arrangements for A, B and M, N have been suggested for this purpose. One of the most commonly used for resistivity sounding is symmetrical arrangement in which the points. A, M, N, B are taken on a straight line such that points M and N are symmetrically placed about center ‘O’ of the spread. (Figure 2)

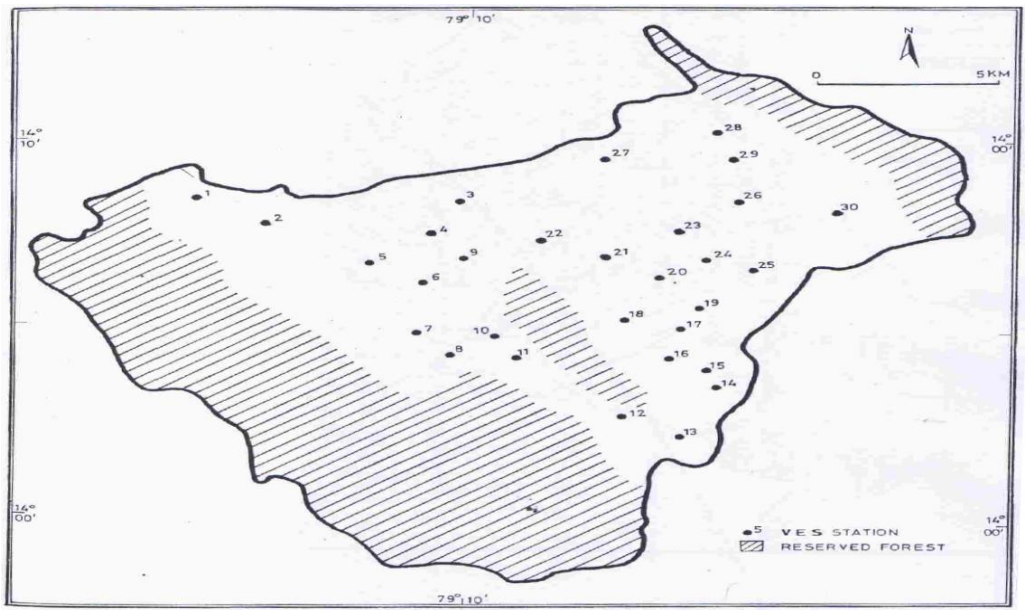

Figure 1: *The Location of Vertical Electrical Resistivity Soundings*

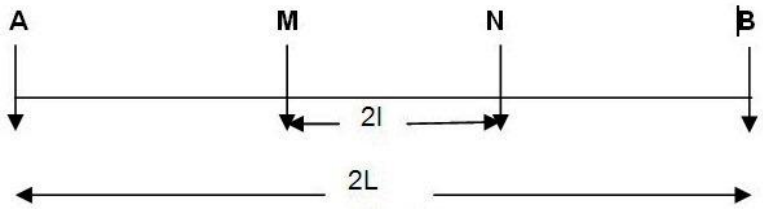

Figure 2: *Schlumberger Electrode Arrangement*

The distance between two current electrodes A and B is 2L and the distance between the two potential electrodes is 2l. Now the relation between potential drop (ΔV) and current flow I, resistivity (ρ) and the distance between current electrode and potential electrodes is given by

$$P=\frac{\Pi}{2}\frac{(L^2-l^2)}{l}\left(\frac{\Delta V}{I}\right)=K\left(\frac{\Delta V}{I}\right) \quad \text{where } K=\frac{\Pi}{2}\frac{(L^2-l^2)}{l}$$

In case of schlumberger sounding the above mathematical equation is used but in the sounding method the distance between the current electrodes AB (2L) is always five times greater than the distance between the potential electrodes MN (2l) [6].

This procedure which is adopted in case of schlumberger sounding is observed as a function of electrode separation and therefore of depth by fixing central point, i.e. sounding point and progressively increasing electrode separation.

4. Results and Discussion

Based on the resistivity interpretations it is known that the resistivity sounding data are interpreted with the help of two layer master curves and auxiliary points' charts [4]. Detailed study of evaluated layer parameter has reveal fluctuations in resistivity values of the top layer due to the variations of moisture content and also due to change in surface conditions from place to place [5]. The results of interpretations are shown in Table 1 and geological sections are drawn on the basis of resistivity sounding data (x & y) (Figures 3.1, 3.2 & 3.3).

Table 1: *Field Interpretation Results*

Sounding Point	P_1 Ohm-metres	P_2 Ohm-metres	P_3 Ohm-metres	h_1 (metres)	h_2 (metres)	H (h1+h2) metres
SP1	120	80.4	480	2.5	5.0	7.5
SP2	100	33.3	1000	2.1	10.5	12.6
SP3	60	180.0	α	1.6	12.8	14.4
SP4	85	28	α	1.8	14.4	16.2
SP5	68	45.0	680	1.5	12.0	13.5
SP6	56	28.0	280	1.6	25.6	27.2
SP7	160	80.0	α	1.8	36.0	37.8
SP8	98	49	196	1.8	10.8	12.6
SP9	110	22.0	240	2.5	20.0	22.5
SP10	70	5.0	270	1.5	12.0	13.5
SP11	15	1.0	375	2.6	31.2	33.8
SP12	95	190.0	570	1.8	7.2	9.0

SP13	100	66.7	400	1.5	12.0	13.5
SP14	75	50.0	300	1.6	6.4	8.0
SP15	170	17.0	350	2.5	20.0	22.5
SP16	25	16.6	α	2.0	4.0	6.0
SP17	52	3.4	α	1.6	3.2	4.8
SP18	32	21.0	α	2.0	6.2	8.0
SP19	32	11.0	192	1.5	21.0	22.5
SP20	23	1.5	α	1.9	3.8	5.7
SP21	70	46.6	1750	2.0	6.0	8.0
SP22	220	8.8	α	2.6	10.4	13.0
SP23	42	84.0	252	1.6	12.8	14.4
SP24	46	15.3	276	2.5	1.3	11.5
SP25	32	16.0	320	1.6	19.2	20.8
SP26	130	26.0	260	1.5	18.0	19.5
SP27	65	2.6	650	1.8	21.6	23.4
SP28	28	14.0	700	1.7	20.4	22.1
SP29	105	10.5	315	1.6	4.8	6.4
SP30	100	50.0	500	1.5	18.0	19.5

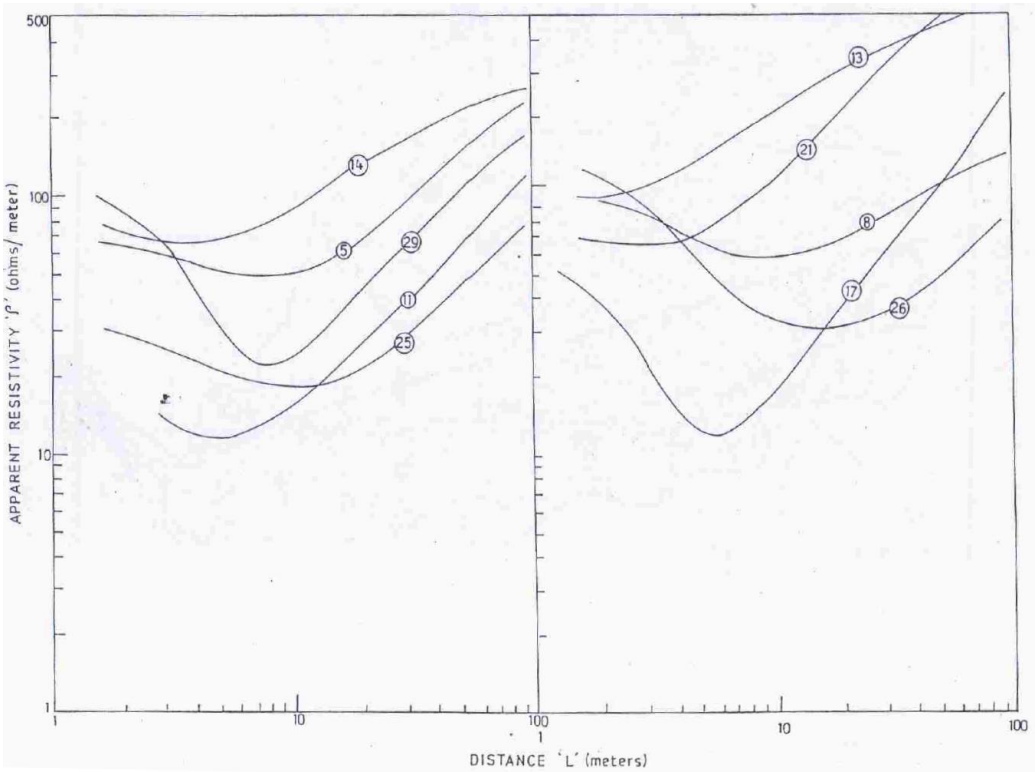

Figure 3.1: *Schlumberger's Resistivity Depth Field Curves*

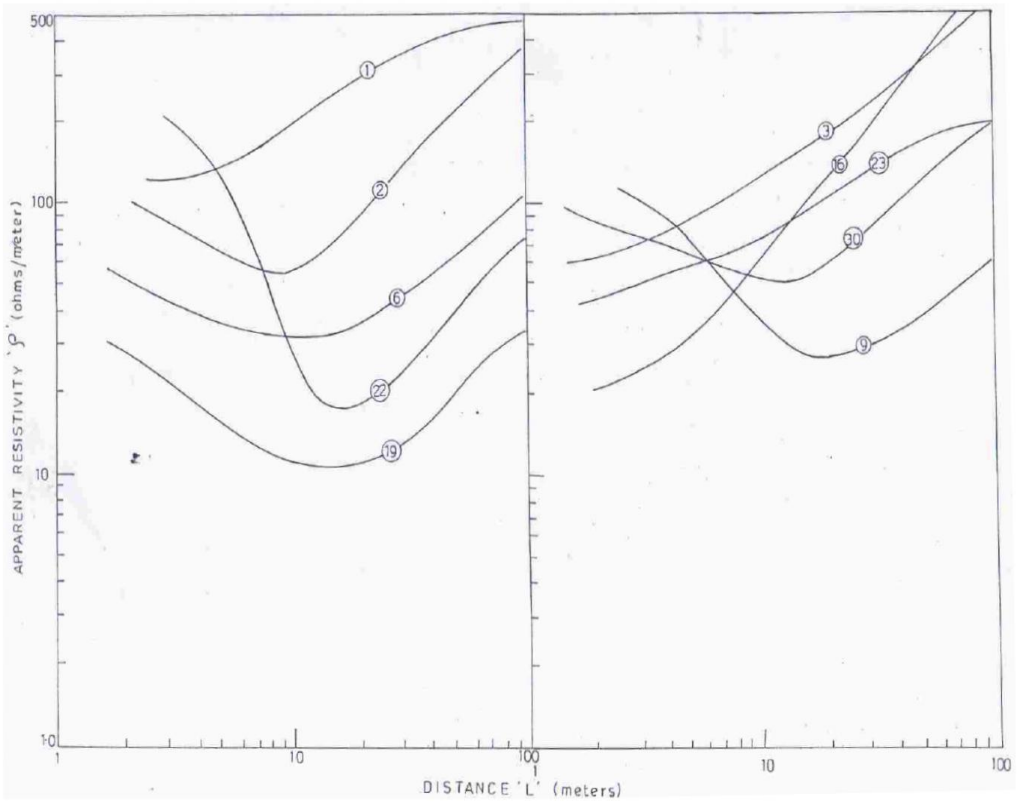

Figure 3.2: *Schlumberger's Resistivity Depth Field Curves*

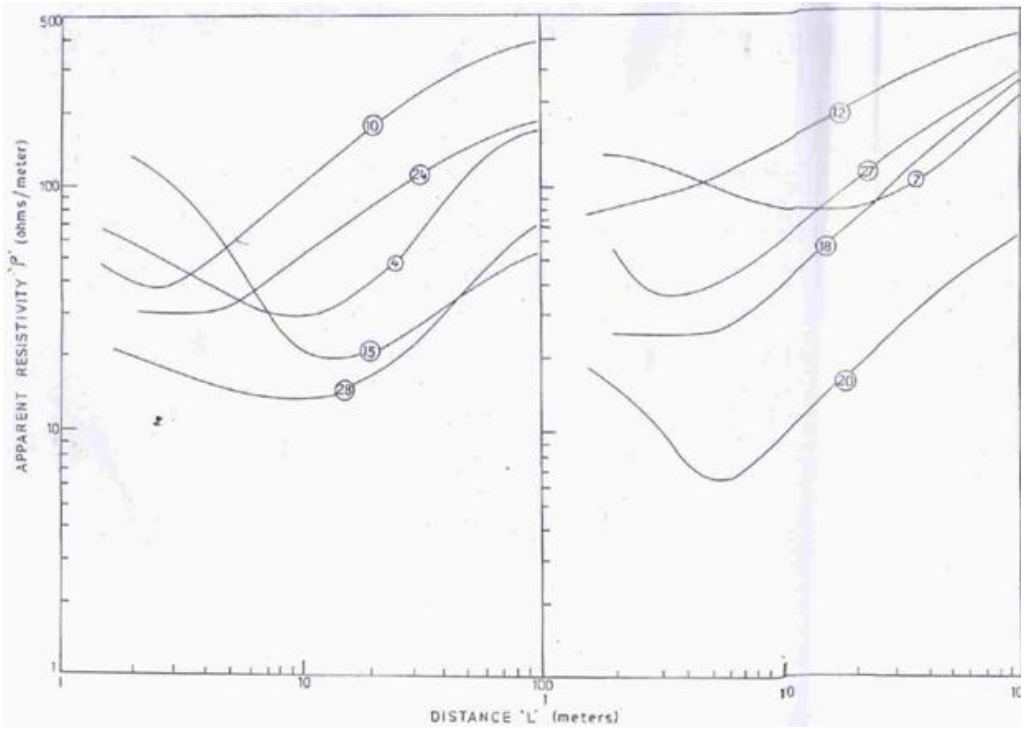

Figure 3.3: *Schlumberger's Resistivity Depth Field Curves*

The main features arising out of this resistivity investigation can be summarized as follows:-
The sequence of resistivity curves obtained were mostly three layered that are generally divided into H-type, A-type & K-type.

H-type: high – low – high
A-type: low – low – high
K-type: low – high – low

The top most layers has resistivity values ranging from 15.0 to 220.0 ohm meter and an average thickness of about 2.4 meters this corresponds to the surface soil layer. This fluctuation in the resistivity values is due to the local conditions mainly the moisture content the resistivity of the second layer varies from 1 to 190 ohm meter and its thickness ranges from 1.3 to 36 meters.

This layer corresponds to the weathered layer. The third layer has resistivity ranges from 192 to α, which generally represents the hard sub-stratum extending to infinity below the second layer. The high resistivity is noticed in areas of hard sub-stratum. Depth to bed rock in the study area varies from 4.8 to 37.8 meters. Figure 4 is the bed rock contour map of the study area.

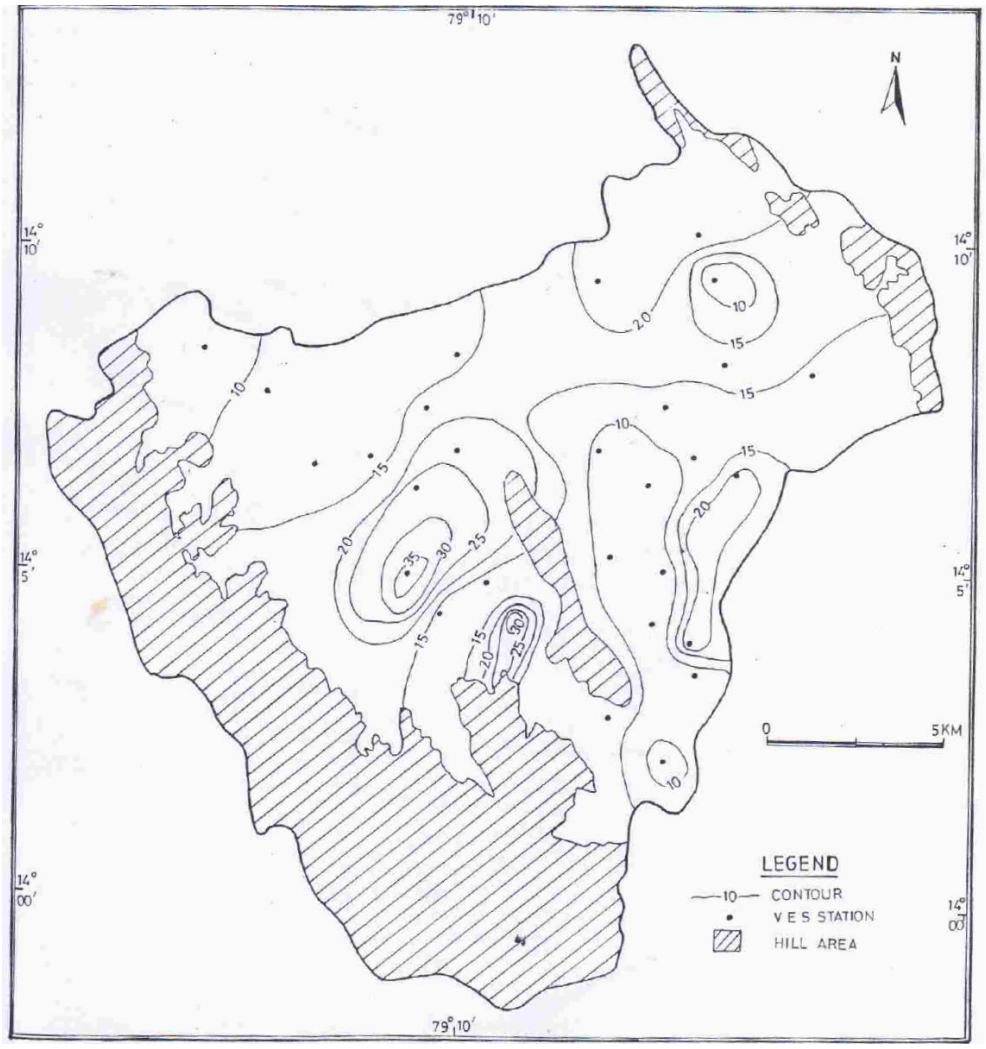

Figure 4: *Contour Map of Depth to Bedrock*

Based on the interpretations of the curves it is observed high apparent resistivity values in the areas of northern and northeastern parts of the mandal due to the presence of hard formations at shallow depths and in turn the absence of water bearing zones. The rest of the mandal area has low to moderate apparent resistivity containing the favorable ground water zones for exploitation. It is established with the results obtained through electrical resistivity surveys that different types of wells namely dug-wells, deep bore-wells and dug-cum-borewells are possible to exploit to the possible extent in the central, western and southeastern areas of the mandal in addition to this it is of immense help to the already existing wells for further development by way of deepening and sinking of bores.

5. Conclusion

The present work reveals that the vertical electrical soundings (VES) has proved to be very reliable for shallow and deep ground water studies and therefore the method can excellently be used for shallow and deep underground water geo physical resistivity investigation. It is observed light and apparent resistivity values in the areas of northern and north eastern parts of the study area. Due to the presence of hard formations at shallow depth, the study reveals that ground water table occurs approximately at 23 m depth equally or more water potential zones are identified in pockets of deep sandy alluvial regions all along the river course. From the work done and the ground water assessment made both laterally and depth wise it is quite possible to suggest the probable well locations and the type of wells. In addition to this, it is of immense help to already existing wells for further development by way of deepening the dug wells and by way of sinking bores at such well bottoms based on the prevailing favourable hydro geological conditions. This will further go a long way in avoiding well locations in barren areas which often adversely affect the economy of the farmers in the study area.

References

[1] Bhattacharya P.K., et al., 1968. *Direct Current Geoelectric Sounding Principles and Interpretation*. 1st Ed. Methods in Geochemistry and Geophysics. Elsevier Pub. Co, New York. 135.

[2] Murthuraj D., et al., 2010. *Delineation of Ground Water Potential Areas- A Case Study from Tirunalveli District, Tamil Nadu, India.* International Journal of Applied Environmental Sciences. 5; 49-56.

[3] Patra H.P., et al., 1999. *Schlumberger Geoelectric Sounding in Ground Water: Principles, Interpretation and Applications*. Oxford & IBH Publishing Company Pvt. Ltd., New Delhi. 153.

[4] Rijkswaterstaat, 1969: Standards Graphs for Resistivity Prospecting. European Association of Exploration Geophysicists, The Hague, the Netherlands.125-140.

[5] Selvam S., et al. 2010. *Groundwater Investigation Using Geo Electrical Survey: A Case Study from Kanukunta Village,* Andhra Pradesh. India Journal of Outreach. 4; 147-158.

[6] Todd D.K., 1980: *Groundwater Hydrology*. John Willey Sons. Inc., New York. 535.

[7] Yadav G.S., et al. 1985. *New Sets of Direct and Inverse Schlumberger Filters Fore Resistivity Sounding Interpolation.* Bolletino di Geofisica teorica ed Applicata. 1985. 27 (108) 251-262.

[8] Zohdy A.A.R., et al. 1969. *Application of Deep Electrical Soundings for Ground Water Exploration In Hawaii.* Geophysics. 34; 584-600.

Cloud Publications
International Journal of Advanced Civil Engineering and Architecture Research
2013, Volume 2, Issue 1, pp. 42-52, Article ID Tech-106

Research Article | Open Access

Passive Pressure on Retaining Wall supporting c-Φ Backfill using Horizontal Slices Method

Sima Ghosh and Sumen Deb

Civil Engineering Department, National Institute of Technology, Agartala, Tripura, India

Correspondence should be addressed to Sima Ghosh, sima.civil@nita.ac.in

Publication Date: 30 August 2013

Article Link: http://technical.cloud-journals.com/index.php/IJACEAR/article/view/Tech-106

Abstract An attempt is made to evaluate the passive earth pressure on rigid retaining wall under static loading condition. The analysis is based on Horizontal Slices Method using c-Φ nature of backfill and the analysis generates non-linear failure surface. The effects of variation of all the parameters have been studied in detail and it is seen that the shape of the rupture surface may be hogging or sagging in nature. The results have been given both tabular as well as graphical representations.

Keywords *Passive Earth Pressure, Horizontal Slices Method, c-Φ Backfill, Rigid Retaining Wall, Wall Inclination, Curvilinear Rupture Surface*

1. Introduction

The pioneering theories for the determination of lateral earth pressure behind retaining walls were developed by Coulomb (1776) and Rankine (1857). Culmann (1865) introduced a graphical method for the solution of lateral earth pressure behind rigid retaining walls. These analyses are mainly based on cohesion-less backfill and linear failure surface. Bell's (1915) equation gives the solution of lateral earth pressure considering the effect of cohesion. The non-linearity of the backfill failure surface is taken into account by Terzaghi (1943) considering a log spiral sliding surface. A combination of log spiral and straight line has been considered by Kumar (2001) to show the non-linearity of failure surface in the determination of seismic lateral earth pressure. Azad et al. (2008) and Ghanbari and Ahmadabadi (2010) have adopted Horizontal Slices Method (HSM) to calculate the seismic earth pressure with the assumption of linear failure surface. In the present study, the Horizontal Slices Method has been used in such a way that the failure wedge itself generates a non-linear rupture surface. The values of passive earth pressure coefficients have been optimized considering the simultaneous effects of unit weight, surcharge, cohesion and adhesion.

2. Method of Analysis

Let us consider a battered face rigid retaining wall of height H (in the passive zone) supporting a c-Φ nature of backfill as shown in Figure 1. The wall on the passive zone is inclined at an angle, α with the vertical. The rupture surface is non-linear having different values of inclinations of failure surface with the vertical at bottom and top. The inclination of failure surface with the vertical at the bottom slice is considered as θ_n, whereas; the inclination of the failure surface at the bottom of the top slice is θ_1 with the vertical. If we consider the number of horizontal slices (of thickness ΔH) as n, then the forces acting on the individual slices under passive state of equilibrium is shown in Figure 2.

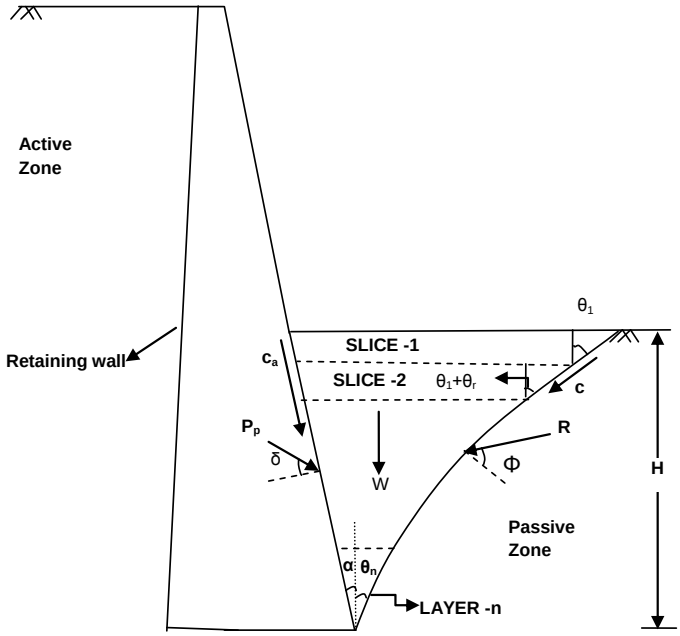

Fig. 1 Shows the forces acting battered face retaining wall under passive state of equilibrium

Free body diagram of retaining wall-backfill system under passive state of equilibrium is elaborated in Figure 2. The forces acting on the wall has been calculated by considering the followings:

H_{i-1}, H_i = Horizontal shear acting on the top and bottom of the i^{th} slice
W_i = Weight of the failure wedge of i^{th} slice
V_{i-1}, V_i = Vertical load (UDL) on top and bottom of i^{th} slice
Φ = the angle of internal friction of soil
P_i = Passive earth pressure on i^{th} slice
R_i = the reaction of the retained soil on i^{th} slice
δ = the angle of wall friction
α = the angle of wall inclination
c = Cohesion acting between the failure surface
c_a = Adhesion acting between the wall and soil surface

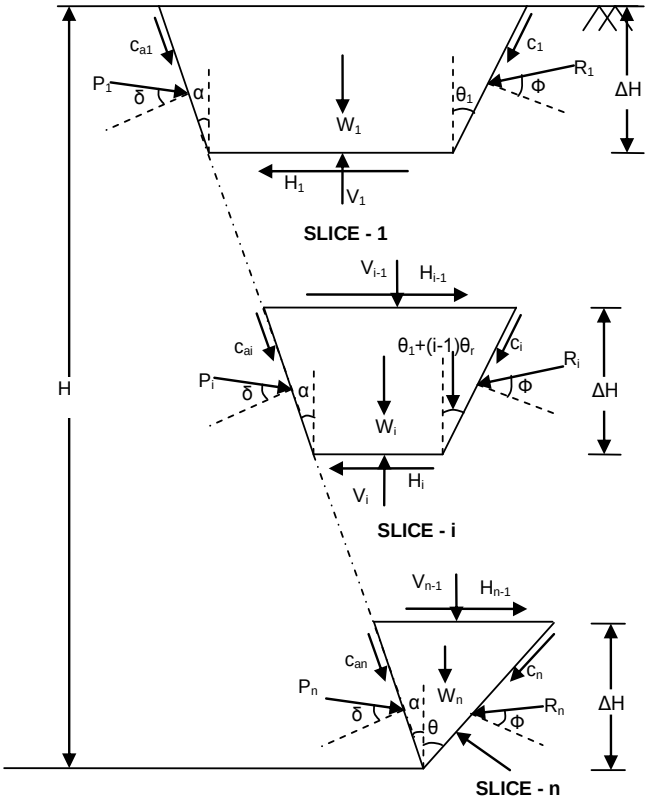

Fig. 2 Shows force components acting on the wedge slices under passive state of equilibrium

3. Derivation of Various Formulations during the Passive Case of Equilibrium

Applying the pressure equilibrium condition, we can solve the equations in the following pattern,

$$\sum H = 0$$

$$P_i \cos(\delta - \alpha) = R_i \cos\{\Phi - \theta_1 - (i-1)\theta_r\} + \frac{c\Delta H \sin\{\theta_1 + (i-1)\theta_r\}}{\cos\{\theta_1 + (i-1)\theta_r\}} - \frac{c_a \Delta H \sin\alpha}{\cos\alpha} + [\gamma \Delta H^2\{(\Delta H_s)_i\}] \quad (1)$$

Where,

$$(\Delta H_s)_i = \left\{ \begin{matrix} (n-i)\tan\alpha - (i-1)(\tan(\theta_1 + (i-1)\theta_r) \\ + \tan\alpha)) + \sum_{m=i}^{n-1}\{\tan(\theta_1 + m\theta_r)\} \end{matrix} \right\}$$

$$\sum V = 0$$

$$P_i \sin(\delta - \alpha) = -R_i \sin(\Phi - \theta_1 - (i-1)\theta_r) - (i - \frac{1}{2})\gamma \Delta H^2(\tan\alpha + \tan(\theta_1 + (i-1)\theta_r)) - \frac{c\Delta H \cos(\theta_1 + (i-1)\theta_r)}{\cos(\theta_1 + (i-1)\theta_r)} - \frac{c_a \Delta H \cos\alpha}{\cos\alpha} \quad (2)$$

Solving these two equations, we find the value of generalized equation for Passive earth pressure for i^{th} slice as follows:

$$P_{p_i} = \frac{\frac{\gamma}{2}\left[\begin{matrix} (\Delta H)^2\{(2i-1)(\tan\alpha + \tan(\theta_1 + (i-1)\theta_r))(-\cos(\Phi - \theta_1 - (i-1)\theta_r)) \\ - \frac{N_s \cos\Phi}{\cos(\theta_1 + (i-1)\theta_r)} - \frac{M_s \cos(\Phi - \alpha - \theta_1 - (i-1)\theta_r)}{\cos\alpha} - (\Delta H_s)_i \sin(\Phi - \theta_1 - (i-1)\theta_r)\} \end{matrix} \right]}{\sin(\Phi + \delta - \alpha - \theta_1 - (i-1)\theta_r)} \quad (3)$$

Where,

$$(\Delta H_s)_i = \gamma(\Delta H)^2 \left\{ \begin{array}{l} (n-i)\tan\alpha - (i-1)(\tan(\theta_1 + (i-1)\theta_r) \\ + \tan\alpha)) + \sum_{m=i}^{n-1} \{\tan(\theta_1 + m\theta_r)\} N_s (\tan\alpha + \tan(\theta_1 + (i-1)\theta_r)) \end{array} \right\} \quad (4)$$

Where, $\tan(\theta_1 + m\theta_r) = 0$ for i = n (5)

The passive earth pressure coefficient can be simplified as,

$$kp = \frac{\sum_{i=1}^{n} P_{pi}}{\frac{\gamma}{2} H^2} \quad (6)$$

The values of N_s and M_s in Eqn 6 are given by

$$N_s = \frac{N_c H}{\Delta H} \quad (7)$$

$$M_s = \frac{M_c H}{\Delta H} \quad (8)$$

Where,

$$N_c = \frac{2c}{\gamma H} \quad (9)$$

$$M_c = \frac{2c_a}{\gamma H} \quad (10)$$

4. Discussion on Results

The optimized values of passive earth pressure coefficient (K_p) have been evaluated for the variation of different parameters. The results are given tabular form and a detailed parametric study is given in graphical form. The various parameters considered for the purpose are as follows:

Φ = 10°, 20°, 30° and 40°; δ = 0, Φ/2, Φ; N_c = 0.1, 0.2; M_c = 0, $N_c/2$, N_c and α = +20°, 0°, -20°.

Optimization of the passive earth pressure co-efficient, k_p is done for the variables θ_1 and θ_n satisfying the optimization criteria. The optimum value denoted as K_p is given in Table 1.

Table 1: *Passive Earth Pressure Co-Efficient (K_p)*

Φ	Δ	M_c	N_c=0.1			N_c=0.2		
			α=-20°	α=0°	α= +20°	α=-20°	α=0°	α=+20°
10°	0	0	1.906	1.524	1.434	2.506	1.612	1.496
		$N_c/2$	1.98	1.57	1.467	2.186	1.691	1.544
		N_c	2.051	1.612	1.496	2.315	1.763	1.584
	Φ/2	0	2.177	1.66	1.514	2.321	1.741	1.564
		$N_c/2$	2.25	1.702	1.54	2.458	1.813	1.605
		N_c	2.321	1.741	1.564	2.589	1.885	1.639
	Φ	0	2.506	1.812	1.596	2.654	1.889	1.638
		$N_c/2$	2.581	1.851	1.618	2.795	1.961	1.673

		N_c	2.654	1.889	1.638	2.932	2.029	1.703
20°	0	0	3.141	2.173	1.814	3.338	2.295	1.925
		$N_c/2$	3.241	2.235	1.867	3.528	2.409	2.013
		N_c	3.338	2.295	1.925	3.71	2.516	2.088
	Φ/2	0	4.559	2.749	2.155	4.781	2.866	2.233
		$N_c/2$	4.671	2.808	2.195	4.996	2.979	2.304
		N_c	4.781	2.866	2.233	5.207	3.087	2.369
	Φ	0	7.325	3.607	2.565	7.599	3.728	2.631
		$N_c/2$	7.462	3.668	2.598	7.84	3.847	2.693
		N_c	7.599	3.728	2.631	8.132	3.962	2.751
30°	0	0	5.476	3.167	2.377	5.739	3.324	2.46
		$N_c/2$	5.608	3.246	2.415	5.996	3.473	2.573
		N_c	5.739	3.324	2.46	6.247	3.617	2.7
	Φ/2	0	12.495	5.083	3.27	12.874	5.253	3.377
		$N_c/2$	12.682	5.169	3.325	13.253	5.419	3.479
		N_c	12.874	5.253	3.377	13.626	5.582	3.575
	Φ	0	--	9.868	4.837	--	10.093	4.939
		$N_c/2$	--	9.98	4.888	--	10.317	5.038
		N_c	--	10.093	4.939	--	10.535	5.136
40°	0	0	10.62	4.809	3.246	10.985	5.01	3.303
		$N_c/2$	10.804	4.91	3.258	11.345	5.204	3.398
		N_c	10.985	5.01	3.303	11.705	5.392	3.475
	Φ/2	0	--	11.628	5.492	--	11.9	5.64
		$N_c/2$	--	11.764	5.566	--	12.172	5.783
		N_c	--	11.9	5.64	--	12.44	5.922
	Φ	0	--	--	12.58	--	--	12.77
		$N_c/2$	--	--	12.675	--	--	12.96
		N_c	--	--	12.77	--	--	13.141

4.1. Effect of Inclination of the Wall (α)

Figures 3 to 5 represents the effect of inclination of the wall on the passive earth pressure for different values of δ.

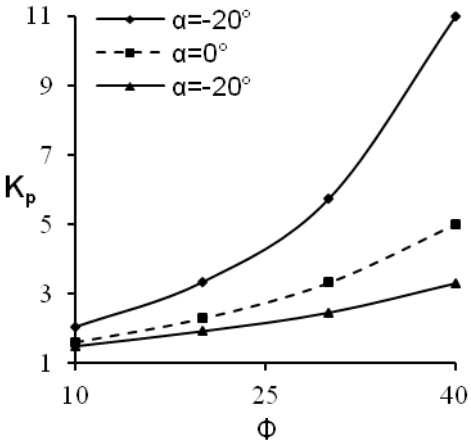

Fig. 3 Shows the variation of Passive earth pressure coefficient with respect to soil friction angle (Φ) at different Wall inclination angles (α= -20°, 0°, 20°), N_c=0.1, M_c=N_c for δ = 0

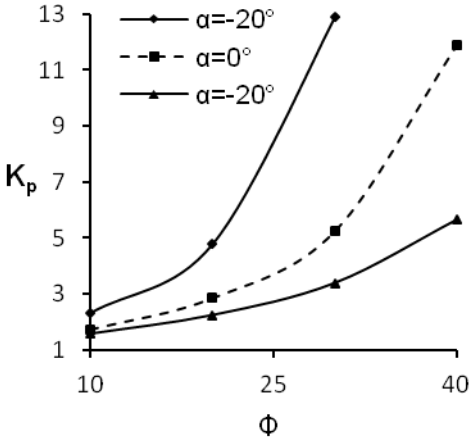

Fig. 4 Shows the variation of Passive earth pressure coefficient with respect to soil friction angle (Φ) at different Wall inclination angles (α= -20°, 0°, 20°), N_c=0.1, M_c=N_c for δ = Φ/2

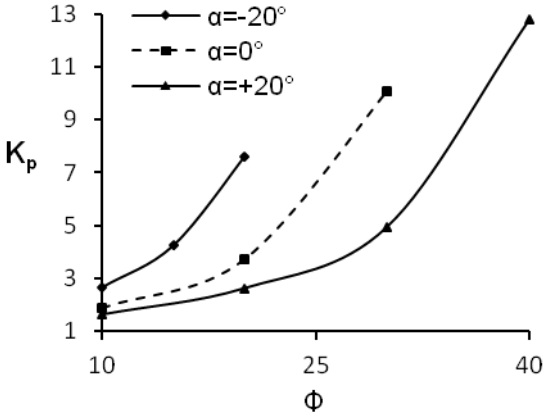

Fig. 5 Shows the variation of passive earth pressure coefficient with respect to soil friction angle (Φ) at different Wall inclination angles (α= -20°, 0°, 20°), N_c=0.1, M_c=N_c for δ = Φ

From these figures, it is seen that due to decrease in α, the passive resistance increases. For example, at Φ = 20°, N_c=0.1, M_c= N_c and α = -20°, the values are found 3.338, 4.781 and 7.599 for δ = 0, Φ/2 and Φ respectively, whereas; with the above conditions the values are1.925, 2.233 and 2.631 at Φ=20° and α = +20°. When the inclination of wall goes away from the backfill, then the wall is in a position to support more load from the backfill material. Thus, the active earth pressure increases and due to this, the passive resistance is decreased.

4.2. Effect of Wall Friction Angle (δ)

Figure 6 to 8 represents the effect of wall friction angle on the passive earth pressure for different values of α. From the plots, it is seen that due to the increase in the value of δ, the passive resistance increases. The reason behind this is the frictional resistance between wall and soil, which increases with the increase in the value of δ.

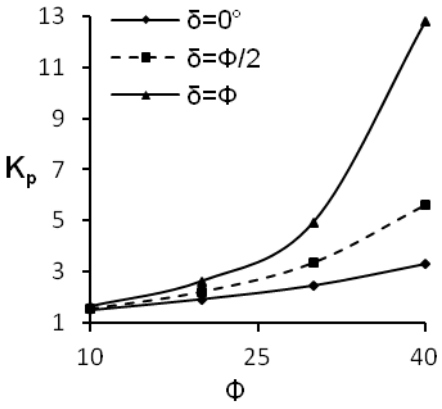

Fig. 6 Shows the variations of passive earth pressure coefficient with respect to soil friction angle (Φ) at different Wall friction angles (δ= 0, Φ/2, Φ), N_c=0.1, M_c=N_c for α = +20°

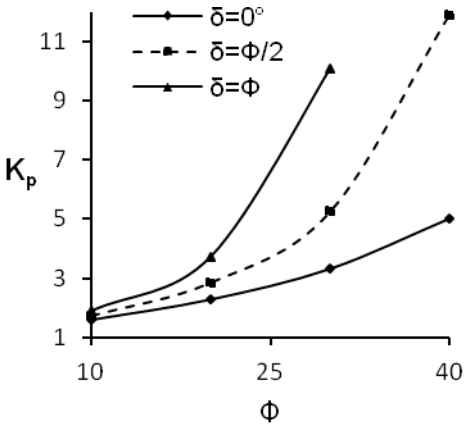

Fig. 7 Shows the variations of passive earth pressure coefficient with respect to soil friction angle (Φ) at different Wall friction angles (δ= 0, Φ/2, Φ), N_c=0.1, M_c=N_c for α = 0^0

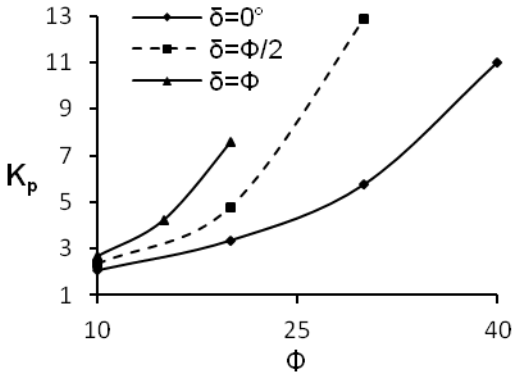

Fig. 8 Shows the variations of passive earth pressure coefficient with respect to soil friction angle (Φ) at different Wall friction angles (δ= 0, Φ/2, Φ), N_c=0.1, M_c=N_c for α =

For example, at Φ = 20°, N_c = 0.1, M_c = N_c and δ = Φ/2, the values are 4.781, 2.866 and 2.233 for α= -20°, 0° and +20° respectively, whereas; the values are found 7.599, 3.728 and 2.631 for α= -20°, 0° and +20° respectively for δ = Φ and all above conditions remaining unchanged. Thus, it is found that the increase in δ is increasing the increment in the passive earth pressure coefficient. The increase in wall friction angle increases the frictional resistance of soil-wall system, so the passive resistance increases.

4.3. Effect of Cohesion and Adhesion

Figure 9 shows the variations of passive earth pressure coefficient (K_p) with respect to soil friction angle (Φ) at M_c= 0, N_c/2, N_c for N_c=0.1, δ=Φ/2 and α=20°.

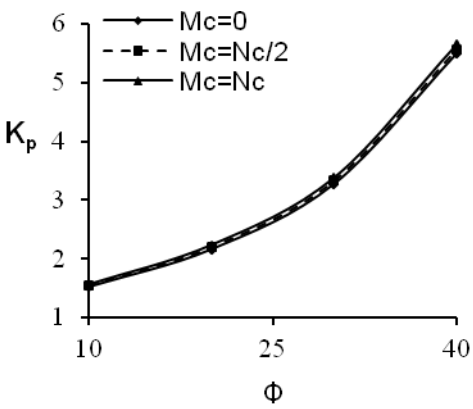

Fig. 9 Shows the variations of passive earth pressure coefficient with respect to soil friction angle (Φ) at M_c= 0, N_c/2, N_c for N_c = 0.1, δ= Φ/2 and α = 20°

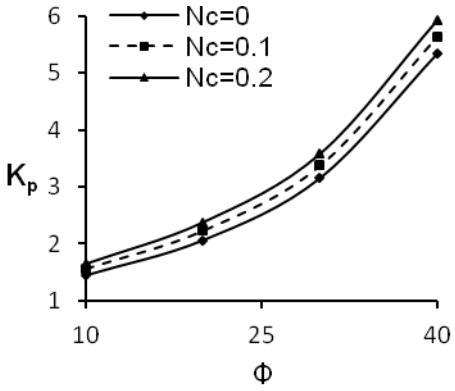

Fig. 10 Shows the variations of passive earth pressure coefficient with respect to soil friction angle (Φ) at N_c= 0, 0.1, 0.2 for M_c=N_c, δ= Φ/2 and α = 20°

For example, at Φ=30°, δ=Φ/2, α=20° and M_c= N_c/2, the values of K_p are 3.325, and 3.479 respectively for N_c=0.1 and 0.2. Whereas the value increases up to 3.377 and 3.757 for M_c=N_c with all other conditions remaining unchanged. Again, from Figure 10, it is also found that the value of K_p increases with the increase of N_c value. For example, at Φ=20°, δ=Φ/2, α=20° and N_c=0.1, the values of K_p are 2.155, 2.195 and 2.233 respectively for M_c=0, N_c/2 and N_c. whereas; the value increases up to 2.233, 2.304 and 2.369 for N_c=0.2 with all other conditions remaining unchanged.

4.4. Effect of Height (H)

Figure 11 shows the variations of passive earth pressure for different heights of retaining wall (5m, 7.5m and 10m). It is observed that the passive resistance gradually decreases with the increase in height of retaining wall. For higher values of soil friction angle (Φ), the passive resistance increases for the same height. For Φ=20° , α=20°, N_c=0.1, M_c=N_c and δ=Φ /2, the decrease in K_p is 10.2% and 15.3% for 7.5m and 10m high retaining walls respectively compared to 5m high retaining walls.

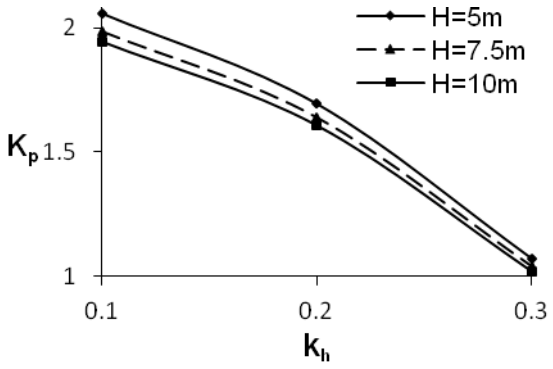

Fig. 11 Shows the variation of Passive earth pressure coefficient (K_p) with respect to soil friction angle (k_h) for different heights at N_c=0.1, M_c=N_c, δ = Φ/2, α = 20°

Also, for Φ=40° , α=20°, N_c=0.1, M_c=N_c and δ=Φ/2, the decrement in K_p is again 5.8% and 12.1% for 7.5m and 10m high retaining walls respectively compared to 5m high retaining walls. With the increase in height, the values of (2c/γH) and ($2c_a$/γH) decreases, so the passive resistance gets decreased.

4.5. Wall Inclination and Nonlinearity of Failure Surface

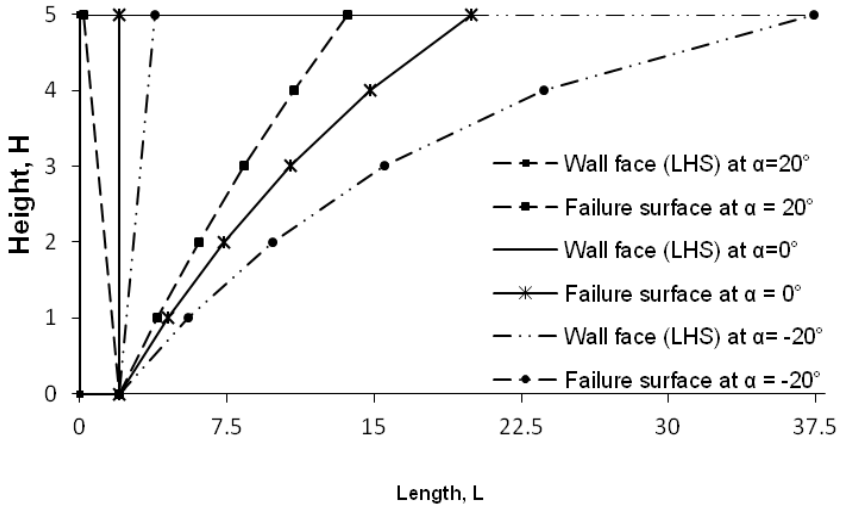

Fig. 12 Shows the failure surface of backfill generated for different values of wall inclinations, α = +20°, 0°,-20° at Φ = 30°, δ= Φ/2, N_c=0.1 and M_c=N_c

Figure 12 shows the nonlinearity of failure surface of backfill for different values of wall inclinations (α = -20°, 0°, +20°). It is seen that the inclination of failure surface with the vertical (α) increases with the increase in the wall inclination (α) angles. For example, at Φ=30º, δ=Φ/2, N_c=0.1, M_c=N_c and α= -20º, the value of angle, α at bottom is 75º whereas the value of angle, α at top is 84º.

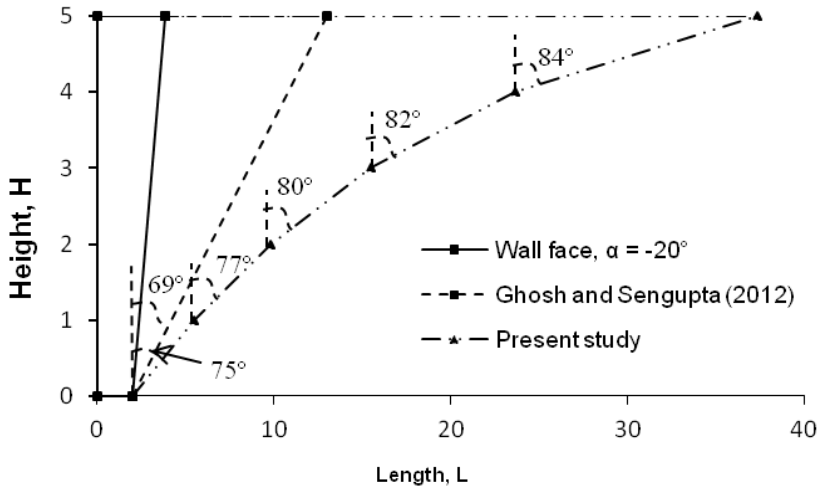

Fig. 13 Shows the comparison of failure surface of backfill generated for different values of wall inclinations, α = -20° at Φ = 30°, δ= Φ/2, N_c=0.1 and M_c=N_c

Figure 13 shows the variation of failure surface with respect to height of the retaining wall. From the plot it is seen that present study represents non-linear failure surface, whereas, Ghosh and Sengupta represents linear failure surface. The comparison shows that the value of inclination of failure surface with the vertical (θ) is 69º in case of Ghosh and Sengupta (2012) for the previously mentioned conditions. Whereas; in the present study, the angle is 77° at bottom and 84° at top of the failure surface. Thus, it shows a curvilinear shape as it progresses upward. Also, on the basis of present study, it is seen that due to the non-linearity, the present study represents participation of more backfill soil in comparison to Ghosh and Sengupta (2012) analysis.

4.6. Comparison of Results

Figure 14 shows the variations of passive earth pressure coefficient with respect to soil friction angle (Φ) at δ=Φ/2, N_c =0.1, M_c =N_c for α =20°. K_p increases uniformly with the increase in the value of soil friction angle (Φ).

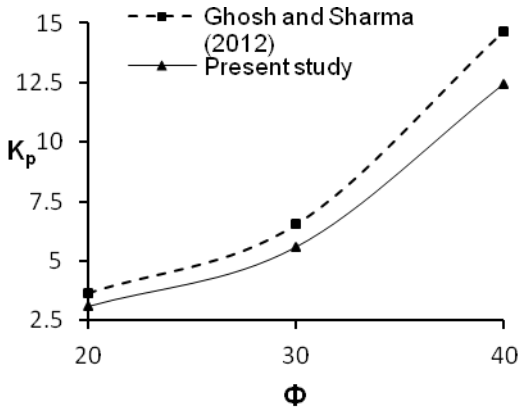

Fig. 14 shows the variations of passive earth pressure coefficient with respect to soil friction angle (Φ) at Wall friction angles δ=Φ/2, N_c=0.1, M_c=N_c for α = 0^0

The comparison in tabular form is presented in Table 2. The comparison shows that the value of K_p obtained from the present study is 15% lesser than the values obtained from the analysis of Ghosh and Sharma (2012).

Table 2: *Shows the Comparison of Results for N_c = 0.1, M_c = N_c*

Φ	δ	α	K_p, Present study	K_p, Ghosh and Sharma (2012)
20°	10°	0	3.087	3.66
30°	15°	0	5.582	6.54
40°	20°	0	12.44	14.66

5. Conclusion

Considering the curvilinear rupture surface and using the horizontal slices method, an analysis has been developed for the determination passive force on the back of a retaining wall supporting c-Φ backfill. Very interestingly, it is seen that the shape of the rupture surface may be sagging or hogging in nature. The above study of c-Φ soil gives a general solution for passive earth pressure. The passive resistance increases with the increase in the value of Φ, δ, c and c_a. Generally, the passive resistance is in an average 15% lower in comparison to Ghosh and Sharma (2012). This fact suggests the acceptability of the model which may be extended for the analysis of retaining wall under seismic loading condition.

Notations

Φ = soil friction angle
δ = wall friction angle
α = wall inclination angle with the vertical
C = cohesion
C_a = adhesion
P_p = passive earth pressure
W_i = weight of i^{th} slice

R = soil reaction
γ = unit weight of soil
$N_s = (H/\Delta H)*N_c$
$M_s = (H/\Delta H)*M_c$

References

Azad A., et al. *Active Pressure Distribution History behind Rigid Retaining Walls.* Soil Dynamics and Earthquake Engineering. 2008. 28 (5) 365-375.

Bell A.L., 1915: *Lateral Pressure and Resistance of Clay and the Supporting Power of Clay Foundations, Minutes.* Proceedings of the Institution of Civil Engineers, London, 199.

Coulomb C.A., 1776: *Essai Sur Une Application Des Regles Des Maximis et Minimis a Queques Problems De Statique Relatifs a1'Architecture, Memoires d'Academie Roy Pres*. Diverssavants. 7.

Culmann K. 1866: *Die Graphische Statik*. Mayer and Zeller, Zurich.

Ghanbari A., et al. *Pseudo-Dynamic Active Earth Pressure Analysis of Inclined Retaining Walls Using Horizontal Slices Method*. Transaction A: Civil Engineering. 2010. 17 (2) 118-130.

Ghosh S., et al. *Formulation of Passive Resistance on Non Vertical Retaining Wall Backfilled with c-Φ Soil*. Civil and Environmental Research. 2012. 2 (1).

Ghosh S., et al. *Pseudo-Dynamic Evaluation of Passive Response on the Back of A Retaining Wall Supporting c-Φ Backfill*. Geo-mechanics and Geo-engineering: An International Journal. 2012. 115-121.

Kumar J. *Seismic Passive Earth Pressure Coefficients for Sands.* Can. Geotech. J., Ottawa. 2001. 38; 876-881.

Rankine W.J.M., 1857: *On the Stability of Loose Earth*. Phil. Tras. Royal Society, London.

Sharma R.P., et al. *Pseudostatic Seismic Active Response of Retaining Wall Supporting c-Φ Backfill*. EJGE. 2010. 15.

Terzaghi K., 1943: *Theoretical Soil Mechanics*. John Wiley & Sons, New York, 510.

Cloud Publications
International Journal of Advanced Civil Engineering and Architecture Research
2013, Volume 2, Issue 1, pp. 32-41, Article ID Tech-131

Research Article

Open Access

Computation of Passive Earth Pressure Coefficients for a Horizontal Cohesionless Backfill Using the Method of Slices

N. Sarath Chandra Reddy[1], D.M. Dewaikar[1] and Gopal Mohapatra[2]

[1]Department of Civil Engineering, Indian Institute of Technology, Mumbai, Maharashtra, India
[2]Department of Civil Engineering, KIIT, Bhubaneswar, Orissa, India

Correspondence should be addressed to N. Sarath Chandra Reddy, sarath4321iitb@gmail.com

Publication Date: 29 August 2013

Article Link: http://technical.cloud-journals.com/index.php/IJACEAR/article/view/Tech-131

Abstract An approximate and acceptable solution for a retaining wall problem is developed using the method of slices. The failure surface consisting of log spiral followed by a tangent is considered in the analysis. To make the analysis statically determinate, the effect of wall friction is assumed to decrease linearly away from the wall. Static equilibrium conditions are used for the analysis of forces acting on the slices. The passive pressure coefficients for a vertical retaining wall with different wall friction and internal friction angles are computed. The results show a close agreement with some of the available solutions.

Keywords *Cohesionless Soil, Horizontal Backfill, Log-Spiral, Method of Slices, Passive Earth Pressure Coefficient*

1. Introduction

Coulomb (1776) and Rankine (1857) assumed planar failure surface and proposed methods for the estimation of earth pressure on the retaining walls. Later Terzaghi (1943) proposed a failure mechanism in which, the failure surface consisted of a log spiral originating from the wall base, followed by a tangent, which met the ground surface at an angle corresponding to Rankine's (1857) passive state. Several research workers have adopted this mechanism.

Caquot & Kerisel (1948) and Kerisel & Absi (1990) proposed a log spiral mechanism and presented their results in the form of charts. Janbu (1957), Sheilds & Tolunay (1973), Basudhar & Madhav (1980), and Kumar & Subba Rao (1997) used the method of slices for computing passive pressure coefficients in respect to cohesion-less soil by considering soil mass in the state of limit equilibrium. Soubra & Macuh (2002) proposed a method based on rotational log-spiral failure mechanism with the upper-bound theorem of limit analysis for the computation of passive earth pressure coefficients. Lancellotta (2002) provided an analytical solution for the passive earth pressure coefficients based on the lower bound theorem of plasticity. Shiau et al., (2008) used an approach based on upper and

lower bound theorems of limit analysis coupled with finite element formulation and nonlinear programming techniques for the analysis of passive earth pressures.

In the proposed analysis, the method of slices is employed for the computation of passive thrust for a vertical wall retaining horizontal cohesion-less backfill, using the failure mechanism suggested by Terzaghi (1943), i.e., a log spiral and its tangent.

2. Proposed Method

In the proposed method, the effect of wall fiction is assumed to decrease linearly away from the wall. The unique failure surface is fixed using the procedure suggested by Shield and Tolunay (1973). Static equilibrium equations are used for the analysis of forces acting on the slices. Figure 1 shows a vertical retaining wall AB, with a horizontal cohesion-less backfill. The failure surface consists of log spiral BC, that originates from the wall base, with tangent, CD meeting the backfill surface at an angle, (45^o - $\phi/2$), where ϕ is the angle of soil internal friction. At C, there is a conjugate failure plane CA, passing through the wall top. Thus, as seen from Figure 1, the pole of the log spiral lies on the line CA. The resultant of the normal and shear forces acting on the failure surface will pass through the pole, O, of the logarithmic spiral creating no unbalanced moments. Considering the fact that, the direction of the failure surface at the wall is dependent on the roughness angle δ, of the wall, Sheilds & Tolunay (1973) have developed an equation for α_w in terms of ϕ and δ, which represents the angle between the horizontal and the failure surface at the wall. It is considered positive when it is above horizontal and negative when it is below the horizontal.

$$\alpha_w = \frac{1}{2}\left[arc\cos\left[\cos(\phi-\delta) - \frac{\sin(\phi-\delta)}{\tan\phi}\right] - \phi - \delta\right] \quad (1)$$

Equation 1 can also be used to find inclination α_n for different values of ϕ and δ for the linear decrease of δ away from the wall.

From Figure 1, the following information is generated:

θ = maximum spiral angle
r_o = initial radius of log spiral at the wall base
r_1 = radius corresponding to the maximum spiral angle θ
B_R = width of the conjugate Rankine's failure wedge, AE
δ = wall friction angle
ϕ = soil internal friction angle
α_w = angle between the horizontal and the failure surface at the wall

Figure 1- Failure mechanism adopted in the proposed analysis
Figure 2 - Proposed Method of Slices

From Figure 2, the following information is generated:

H = height of the retaining wall, AB
H_R = height of the Rankine's wall, CE
x_i = distance of the left edge of i^{th} slice from point E
P_R = passive thrust acting on the Rankine wall, CE
P_p = passive thrust acting on the wall of height, AB=H

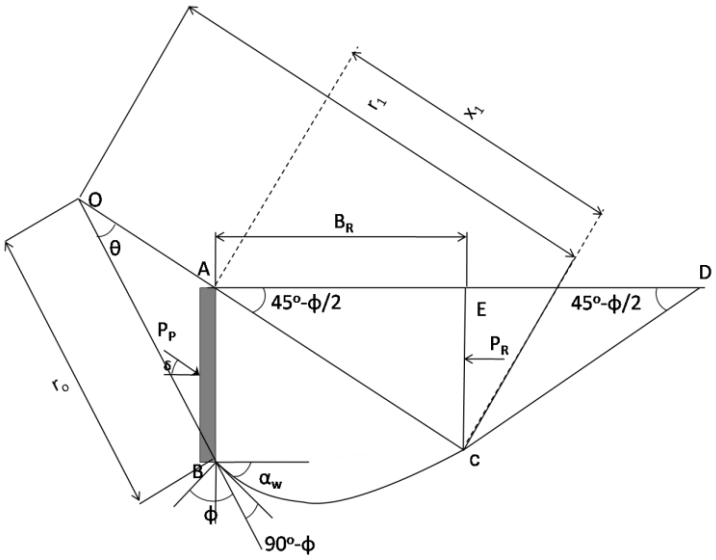

***Figure 1**: Failure Mechanism Adopted in the Proposed Analysis*

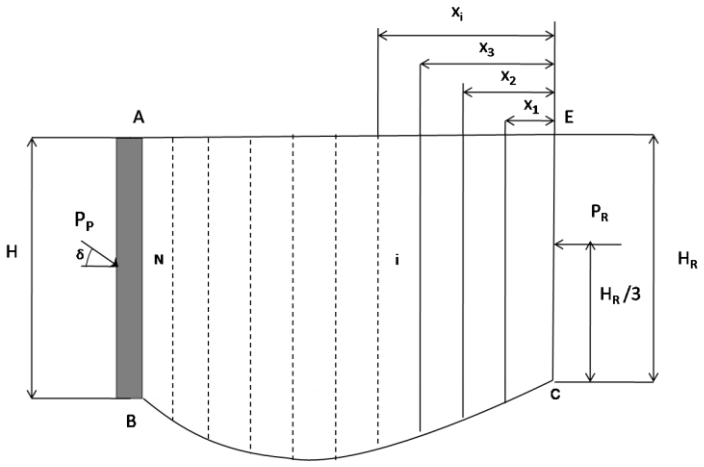

***Figure 2**: Proposed Method of Slices*

2.1. Geometry of the Failure Surface

Geometry of the failure surface is dependent on the values of soil internal friction ϕ and wall friction angle δ.

Referring to the Figure 1 and considering triangle, OAB,

$$\theta + \phi + \alpha_w + 180 - \left(45 + \frac{\phi}{2}\right) = 180 \quad (2)$$

In the above equation, θ is given as

$$\theta = 45 - \alpha_w - \frac{\phi}{2}$$

and

$$\frac{r_o}{\sin\left(180-\left(45+\frac{\phi}{2}\right)\right)}=\frac{x_1}{\sin(\phi-\alpha_w)}=\frac{H}{\sin\theta} \quad (3)$$

Also from the equation of log spiral,

$$OC = r_1 = r_o.e^{\theta.\tan\phi}$$

and

$$CA = x_2 = r_1 - x_1 \quad (4)$$

Now considering triangle, CAE,

$$\frac{x_2}{\sin 90}=\frac{H_R}{\sin(45-\frac{\phi}{2})}=\frac{B_R}{\sin(45+\frac{\phi}{2})} \quad (5)$$

Considering N number of slices, the slice width b is calculated as

$$b=\frac{B_R}{N}$$

In order to make the analysis statically determinate, the variation of direction of the inter slice force P_{p_i} (Figure 3) is required to be assumed. With the assumption of linear variation of the inter slice force, δ_i (Figure 3) is expressed as,

$$\delta_i=\frac{x_i}{B_R}\delta, \text{where } x_i = ib$$

From the Rankine's (1857) mechanism,

$$P_R=\frac{1}{2}\gamma {H_R}^2\tan^2(45+\frac{\phi}{2}) \quad (6)$$

Figure 3: (a) Free body diagram of slice for i=1. (b) Free body diagram of the slices for i=1 to N

From Figure 3 (a) and Figure 3 (b) the following information is generated:

P_{p_1} = passive thrust acting on the first slice
b = width of the slice
W_1 = weight of the first slice
R_1 = resultant reaction acting at the base of the first slice
δ_1 = direction of the inter slice force for the first slice
α_1 = angle of inclination of the normal with the vertical on the base of the first slice
P_{p_i} = passive thrust acting on the i^{th} slice
W_i = weight of the i^{th} slice
R_i = resultant reaction acting at the base of the i^{th} slice
δ_i = direction of the inter slice force for the i^{th} slice
α_i = angle of inclination of the normal with the vertical on the base of the i^{th} slice

2.1.1. For the First Slice (i=1)

Referring to the Figure 3 (a) and considering the equilibrium of all the forces acting on the slice,

Horizontal force equilibrium

$$P_{p_1} \cos \delta_1 - P_R - R \sin(\phi + \alpha_1) = 0 \tag{7}$$

Vertical force equilibrium

$$\mathrm{R} \cos(\phi + \alpha_1) - \mathrm{P}_{p_1} \sin \delta_1 - \mathrm{W}_1 = 0 \tag{8}$$

Where,

$$\mathrm{W}_1 = \mathrm{bH_R} + \frac{1}{2}\mathrm{b}^2 \tan \alpha_1$$

From Equations 7 and 8,

$$\mathrm{P}_{p_1} = \frac{\mathrm{P_R} + \left(\mathrm{bH_R} + \frac{1}{2}\mathrm{b}^2 \tan \alpha_1 \right) \tan(\phi + \alpha_1)}{[\cos \delta_1 - \sin \delta_1 \tan(\phi + \alpha_1)} \tag{9}$$

2.1.2. For Slices i=2 to N

Referring to the Figure 3 (b) and considering the equilibrium of all the forces acting on the slice,

Horizontal force equilibrium

$$\mathrm{P}_{p_i} \cos \mathrm{P}_{p_{i-1}} \cos \delta_{i-1} - \mathrm{R}_i \sin(\phi + \alpha_i) = 0 \tag{10}$$

Vertical force equilibrium

$$\mathrm{R}_i \cos (\phi + \alpha_i) - \mathrm{P}_i \sin \delta_i + \mathrm{P}_{p_{i-1}} \sin \delta_{i-1} - \mathrm{W}_i = 0 \tag{11}$$

Where,

$$\mathrm{W}_i = \mathrm{b}\left[\mathrm{H_R} + \mathrm{b}\left[\sum_{i=1}^{N} \tan \alpha_i\right]\right] + \frac{1}{2}\mathrm{b}^2 \tan \alpha_i$$

From Equations 10 and 11

$$\mathrm{P}_{p_i} = \frac{\mathrm{P}_{p_{i-1}} \cos \delta_{i-1} - \mathrm{P}_{p_{i-1}} \sin \delta_{i-1} \tan(\phi + \alpha_i) + \mathrm{W}_i \tan (\phi + \alpha_i)}{\cos \delta_i - \sin \delta_i \tan (\phi + \alpha_i)} \tag{12}$$

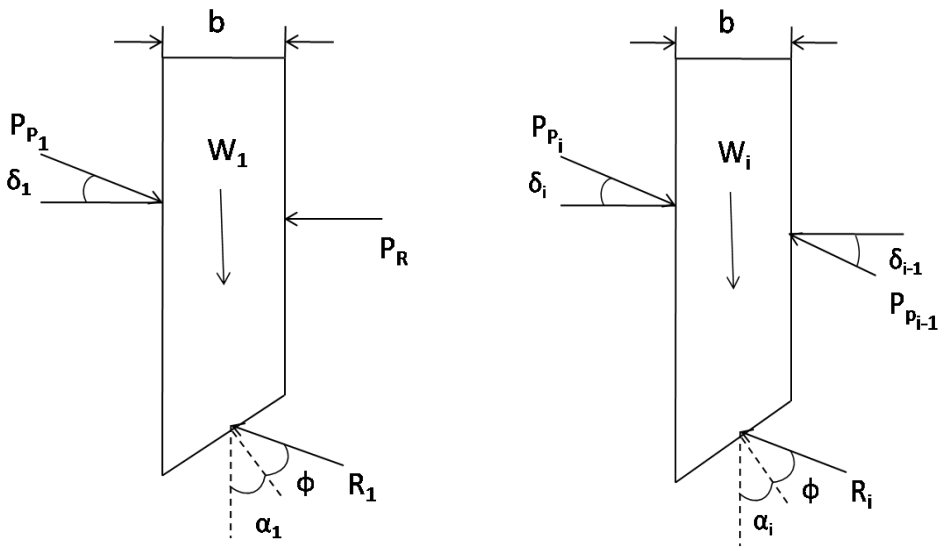

***Figure 3**: (a) Free Body Diagram of Slice for i=1. (b) Free Body Diagram of the Slices for i=1 to N*

2.2. Determination of Passive Earth Pressure Coefficient K_P

The soil wedge CDE (Figure 1), is in a passive Rankine (1857) state of equilibrium and the magnitude of passive force P_R acting on the wall CE is computed using Equation 6. In order to compute P_P, the soil wedge ABCE is divided in to N number of slices of width b and the analysis is carried out by considering all the forces acting on each slice as shown in the Figures 3(a) and (b). The passive thrusts are computed using equations 6, 9 and 12 for values of δ/ϕ from 0.1 to 1.0.

The passive earth pressure coefficient; K_P is then expressed as

$$K_P = \frac{2P_{pN}}{\gamma H^2} = \frac{2P_P}{\gamma H^2}$$

3. Results and Discussion

The basic purpose of this analysis was to compute passive earth pressure coefficient, K_P and study its variation with respect to the parameters involved in the analysis. It was found convenient to express the value wall friction angle δ in terms of its ratio with respect to soil internal friction, ϕ of the soil, in a non-dimensional form (δ/ϕ).

***Table 1**: Passive Earth Pressure Coefficients for Different Combinations of ϕ andδ/ϕ*

δ/ϕ	K_P Values for the Corresponding ϕ Values				
	20	25	30	35	40
0	2.04	2.46	3.00	3.69	4.60
0.1	2.14	2.64	3.28	4.15	5.34
0.2	2.25	2.82	3.60	4.67	6.22
0.3	2.36	3.02	3.93	5.25	7.26
0.4	2.48	3.23	4.31	5.93	8.50
0.5	2.61	3.46	4.73	6.71	10.00
0.6	2.75	3.72	5.21	7.62	11.82
0.7	2.91	4.01	5.77	8.72	14.10
0.8	3.06	4.30	6.31	9.79	16.29

0.9	3.22	4.61	6.92	11.01	18.84
1	3.40	4.95	7.58	12.33	21.64

In Table 1, the values of passive earth pressure coefficient, K_P are shown for various combinations of non-dimensional ratio, δ/ϕ and soil internal frictional angle ϕ.

3.1. Comparison with other Solutions

In Table 2, computed values of K_P for $\phi = 20^o$, 30^o and 40^o and $\delta = \phi$ and $\phi/2$ are compared with other available solutions and in Table 3, percentage variations in the results obtained by the proposed method in comparison with other solutions are reported.

The values computed by Coulomb's (1776) theory are higher than the values obtained by the proposed method. For $\phi \leq 30^o$ and $\delta \leq \phi/2$, they are in the range 0 to 5.29%, and for values $\phi \geq 40^o$ and $\delta > \phi/2$, the variation is very high.

***Table 2**: Comparison of K_P Values*

Parameters	Passive Earth Pressure Coefficient, K_P					
Angle of soil friction, ϕ (degrees)	20		30		40	
Angle of wall friction, δ (degrees)	½ ϕ	ϕ	½ ϕ	ϕ	½ ϕ	ϕ
Proposed Method	2.61	3.4	4.73	7.58	10.00	21.64
Coulomb (1776)	2.89	3.53	4.98	10.1	11.77	92.57
Caquot & Kerisel (1948)	2.60	3.01	4.50	6.42	10.36	17.5
Janbu (1957)	2.60	3.00	4.50	6.00	9.00	14.0
Sokolovski (1965)	2.55	3.04	4.62	6.55	9.69	18.2
Shield & Tolunay (1974)	2.43	2.70	4.13	5.02	7.86	11.00
Chen (1975)	2.58	3.14	4.71	7.11	10.07	20.90
Basudhar & Madhav (1980)	2.56	3.12	4.64	6.93	9.56	19.35
Kumar & Subba Rao (1997)	2.5	3.07	4.6	6.68	9.8	18.86
William Powarie (1997)	2.52	2.87	4.4	5.8	8.92	14.32
Soubra & Macuh (2002)	2.57	3.13	4.65	6.93	9.81	20.1
Lancellotta (2002)	2.48	2.70	4.29	5.03	8.38	11.03
Shiau et al. (2008) lower bound	2.50	3.02	4.38	6.58	8.79	18.64
Shiau et al. (2008) upper bound	2.62	3.21	4.46	7.14	10.03	20.10
Kame et al. (2011) Kötter's Equation	2.97	3.29	5.13	6.57	10.1	16.46

The values reported by Chen (1975) are based on the limit analysis. These values are lower than the proposed values in the range 0 to 3.42%.

The values reported by Caquot & Kerisel (1948) are based on the limit equilibrium of a log spiral mechanism. For $\phi = 20^0$ to 40^0 and the $\delta = 0$ to ϕ, values of K_P as computed by them are lesser than the proposed values in the range 0 to 19.13%.

The values reported by Kumar & Subba Rao (1997) are based on the method of slices and are lesser than the proposed values. For $\phi = 20^0$ to 40^0 and $\delta = 0$ to $\phi/2$ the difference is very less and is in the range 0 to 2.0%. For $\delta > \phi/2$ the difference is relatively higher and is in the range 2.0 to 12.85%. Soubra & Macuh (2002) used the rotational log spiral failure mechanism with an upper-bound theorem of limit analysis. The values obtained from their analysis are lower than the proposed values in the range 0 to 7.12%.

With the analytical solution based on the lower bound theorem of plasticity, the K_P values as reported by Lancellotta (2002) are lower than the proposed values in the range 0 to 47.78%.

The K_P values reported by Shiau et al (2008) using lower bound theorem coupled with finite element formulations of limit analysis and nonlinear programming techniques are lower than the proposed values in the range 4.21 to 13.86%. The values obtained using upper bound theorem as compared to the proposed values are in the range +0.38 to -7.12%.

Kame et al., (2011) used Kötter's equation and the values obtained by them are higher than the proposed value initially for lower values of δ and for higher values of δ the values reported by them are lesser than the proposed values. They are in the range +27.45 to -23.94%.

The values of K_P reported by Janbu (1957) based on the limit equilibrium analysis. These values when compared with the proposed values are in the range 7.85 to -35.3%.

Similarly, the K_P value reported by Shields and Tolunay (1973) based on the limit equilibrium analysis are lower than the proposed values in the range, 0 to 49.17%.

***Table 3**: Comparison K_P Values*

Angle of Friction (degrees)		**Passive Earth Pressure Coefficient K_P**										
		Coulomb (1776)		Caquot & Kerisel (1948)		Kumar & Subba Rao (1997)		Soubra & Macuh (2002)		Lancellotta (2002)		Proposed method
Soil ϕ	Wall δ	K_P	% diff.	K_P	% diff.	K_P	% diff.	K_P	% diff.	K_P	% diff.	K_P
20		2.04	0	2.04	0	2.04	0	2.04	0	2.04	0	2.04
25		2.46	0	2.46	0	2.46	0	2.46	0	2.46	0	2.46
30	0	3.00	0	3.03	0	3.00	0	3.00	0	3.00	0	3.00
35		3.69	0	3.69	0	3.69	0	3.69	0	3.69	0	3.69
40		4.6	0	4.59	0	4.6	0	4.6	0	4.6	0	4.60
20		2.41	0.42	2.35	-2.08	2.38	-0.83	2.39	-0.42	2.35	-2.08	2.40
25		3.12	1.3	3.03	-1.62	3.06	-0.65	3.07	-0.32	3.07	-0.32	3.08
30	1/3 ϕ	4.14	2.22	4.00	-1.23	4.02	-0.74	4.03	-0.49	4.03	-0.49	4.05
35		5.68	4.03	5.28	-3.3	5.42	-0.73	5.44	-0.37	5.44	-0.37	5.46
40		8.15	6.96	7.25	-4.86	7.58	-0.52	7.62	0	7.62	0	7.62
20		2.64	1.15	2.6	-0.38	2.5	-4.21	2.57	-1.53	2.48	-4.98	2.61
25		3.55	2.6	3.4	-1.73	3.4	-1.73	3.41	-1.45	3.22	-6.94	3.46
30	1/2 ϕ	4.98	5.29	4.5	-4.86	4.6	-2.75	4.65	-1.69	4.29	-9.3	4.73
35		7.36	9.69	6.0	-10.58	6.6	-1.64	6.59	-1.79	5.88	-12.37	6.71
40		11.8	18	9.0	-10	9.8	-2.00	9.81	-1.9	8.38	-16.2	10.00
20		2.89	1.4	2.65	-7.02	2.73	-4.21	2.75	-3.51	2.58	-9.47	2.85
25		4.08	4.35	3.56	-8.95	3.72	-4.86	3.76	-3.84	3.41	-12.79	3.91
30	2/3 ϕ	6.11	9.69	5.00	-10.23	5.26	-5.57	5.34	-4.13	4.63	-16.88	5.57
35		9.96	19.71	7.1	-14.66	7.78	-6.49	7.95	-4.45	6.51	-21.75	8.32
40		18.7	40.92	10.7	-19.37	12.24	-8.06	12.6	-5.05	9.57	-27.88	13.27

20		3.53	3.82	3.01	-11.47	3.07	-9.71	3.13	-7.94	2.7	-20.59	3.4
25		5.6	13.13	4.29	-13.33	4.42	-10.71	4.54	-8.28	3.63	-26.67	4.95
30	ϕ	10.1	33.25	6.42	-15.3	6.68	-11.87	6.93	-8.58	5.03	-33.64	7.58
35		22.9	85.73	10.2	-17.27	10.76	-13.22	11.3	-8.35	7.25	-41.2	12.33
40		92.6	327.91	17.5	-19.13	18.86	-12.85	20.1	-7.12	11.03	-47.78	21.64

4. Conclusion

The proposed analysis demonstrates the application of method of slices in which, the only assumption that is required to make the analysis statically determinate is on the variation of direction of inter slice forces. The unique failure surface is fixed using the method suggested by Shields and Tolunay (1973). With the linear variation of the direction of inter slice forces considered in the analysis, computed values of K_P show a reasonably good agreement with some of the available solutions.

References

Basudhar P.K., et al. *Simplified Passive Earth Pressure Analysis*. Journal of the Geotechnical Engineering Division, ASCE. 1980. 10 (4) 470-474.

Caquot A.I., et al. *Table for the Calculation of Passive Pressure, Active Pressure, and Bearing Capacity of Foundations*. Libraire du Bureau des Longitudes, de L'ecole Polytachnique. Gauthier-Villars, Paris. 1948. 120.

Chen W.F. *Limit Analysis and Soil Plasticity*. Elsevier Science Publishers, BV, Amsterdam, the Netherlands. 1975. 111-146.

Coulomb C.A. *Essais Sur Une Application Des Regles Des Maximis Et Minimis A Quelques Problems Statique Relatits A Architecture*. Mem. Acad. Roy. Pres. Divers, Sav., Paris. 1776. 7 343-382.

Dewaikar D.M. et al. *Computation of Bearing Capacity Factor N_γ–Terzaghi's Mechanism*. International Journal of Geomechanics. ASCE. 2003. 3 (1) 123-128.

Janbu N. *Earth Pressure and Bearing Capacity Calculations by Generalized Procedures of Slices*. Proc. 4th Int. Conf. on Soil Mechanics and Foundation Engineering, London. 1957. 2; 207-212.

Kumar J., et al. *Passive Pressure Coefficients, Critical Failure Surface and its Kinematics Admissibility*. Geotechnique. 1997. 47 (1) 185-192.

Kerisel J., et al. *Active and Passive Earth Pressure Tables*. Balkema, Rotterdam. 1990. 220.

Kame G.S., et al. *Passive Earth Pressure on a Vertical Retaining Wall with Horizontal Cohesionless Backfill. Soils and Rocks.* Associacao Brasileira de Mecanica dos Solos, Brazil. 2011. 34 (3) 237-248.

Lancellotta R. *Analytical Solution of Passive Earth Pressure.* Geotechnique. 2002. 52 (8) 617-619.

Rankine W. *On The Stability of Loose Earth*. Philosophical Transactions of the Royal Society of London. 1857. 147; 9-27.

Shiau J.S., et al. *Finite Element Limit Analysis of Passive Earth Resistance in Cohesionless Soils*. Japanese Geotechnical Society, Soils and Foundations. 2008. 48 (6) 843-850.

Shields D.H., et al. *Passive Pressure Coefficients by Method of Slices*. Journal of the Soil Mechanics and Foundations Division, ASCE. 1973. 99 (12) 1043-1053.

Sokolovski V.V., 1965: *Statics of Granular Media*. Pergamon Press, Oxford, 270.

Soubra A.H. *Active and Passive Earth Pressure Coefficients by a Kinematical Approach.* Proc. of the Institute of Civil Engineers and Geotechnical Engineering. 2002. 155 (2) 119-131.

Terzaghi K., 1943: *Theoretical Soil Mechanics*. Wiley and Sons, New York, 510.

Cloud Publications
International Journal of Advanced Civil Engineering and Architecture Research
2013, Volume 2, Issue 1, pp. 53-64, Article ID Tech-145

Research Article

Open Access

Durability Index Test Performance of Recycled Concrete Aggregate Mixed with Natural Aggregate

Suvash Chandra Paul and Gideon P.A.G. Van Zijl

Department of Civil Engineering, University of Stellenbosch, Stellenbosch, South Africa

Correspondence should be addressed to Suvash Chandra Paul, suvashpl@sun.ac.za

Publication Date: 18 September 2013

Article Link: http://technical.cloud-journals.com/index.php/IJACEAR/article/view/Tech-145

Abstract Recycling of old concrete is an efficient way of minimizing environmental hazards caused by construction and demolition waste (C&DW). The quality of recycled concrete aggregate (RCA) may sometimes cause major problems in structures which need to be resolved before being used. Damage caused to concrete by hostile agents can be a reason for the rapid deterioration of materials, and which can even cause permanent failure of the structure. Factors which negatively affect the durability of concrete are corrosion of steel due to depassivation by carbonation, insufficient concrete cover (some cases too small cover of concrete helps early corrosion of reinforcement), chloride penetration, freezing and thawing, presence of salt and the action by chemicals in the mixing water. This paper describes the durability performance of 100% natural aggregate (NA) and 30% replacement of RCA with it. It was found that there are no major changes in durability properties when 30% RCA was replaced to NA.

Keywords *Recycled Concrete Aggregate (RCA), Durability Index Test*

1. Introduction

The trend towards urbanization world-wide has provided, and probably will continue to provide, a strong demand for high-volume, low-cost aggregate material for the repair and development of additional infrastructure. The total demand for aggregates, driven by demographics, urbanization and the economy, is expected to remain strong in the short term. Recycling of construction materials has grown along with the demand for aggregates [1]. Recycled concrete aggregate (RCA) competes favourably with natural aggregate (NA) in many local markets as a non-structural and structural material. Recycling has the potential to reduce the amount of waste disposed of in landfills, to preserve natural resources, and to provide savings in cost while limiting environmental disturbance [2]. Potential sources for recycled material increase as maintenance or replacement of the nation's infrastructure continues. Because of the finite life of infrastructure, this "urban deposit" may be considered as a renewable resource.

Many countries are currently using RCA because in some applications this aggregate can be better than NA. The physical properties of coarse aggregates made from crushed demolition concrete make it the preferred material for applications such as road base and sub-base. This is because RCA often has better compaction properties (extra mortar breaks up during compaction) and requires less cement for sub-base uses. Furthermore, it is generally cheaper to obtain than NA. This material is becoming the aggregate base of choice in the USA, Japan, and China etc. Nationally and internationally much research has been done on different replacement levels of RCA [3, 4]. Up till now mostly 30% and in some cases up to 50% of RCA replacement is used with confidence in structural concrete without any noticeable change in properties [5-7]. Some positive results on different durability index test for 30% RCA replacement in new concrete are discussed in this paper.

2. Durability Index Tests of Concrete

Generally, concrete is a very durable material but environmental factors such as weathering action, chemical attack, abrasion and other deterioration processes may change the properties of concrete over time [8]. Corrosion of steel reinforcement is one of the major challenges for reinforced concrete structures. Presence of chloride ion at the steel position in concrete is a major cause of reinforcement corrosion. The chloride ion destroys the natural passivity of the surface of reinforcing steel and this leads to the corrosion of the steel which in turn causes cracking and spalling of concrete. The resistance of steel to corrosion is good when the thickness of the concrete cover is large, but too much cover could result in larger and more cracks which would allow direct access of aggressive agents to the steel reinforcement [9].

Many research studies are carried out on the use of RCA in new concrete in an attempt to understand the properties of RCA concrete; however, most of the studies are focused on the mechanical properties of the resulting concrete. Limited work has been carried out to understand the durability aspects of RCA as new construction material compared to concrete that is made with NA. Today, engineers are beginning to accept that many of the problems experienced in structures made with concrete are due to lack of adequate knowledge concerning the factors affecting the durability of RCA concrete as a material and the inability to apply effectively, the knowledge already gained. The reasons for the widespread lack of durability in concrete structures can be attributed to poor understanding of the deterioration processes by designers, the inadequate acceptance criteria of concrete on construction sites and the changes in materials properties and construction practices [10].

The use of RCA in the production of structural concrete may decrease its performance with respect to durability, due to the high water absorption of this type of aggregate. Research was carried out with the aim of understanding the essential properties of concrete in order to be able to predict the behaviour of concrete produced with RCA during the service life of the concrete. The objective was to obtain a better understanding of the durability of concrete prepared with 30% RCA. This paper shows analysis of the influence of 30% RCA on the durability of concrete. In an attempt to contribute to the existing pool of knowledge in this regard, three durability index tests were performed in order to characterize fluid and ion transport mechanisms in concrete. Details on these three durability tests are discussed in next section.

Table 1: *Concrete Mix Designs: Materials Used in Concrete*

Materials (kg/m^3)	NA mixes		RCA Mixes
	70%	100%	30%
CEM I 42.5	350		
Water	175		
*Sand	469	670	201
Aggregates	868	1240	372

*Note that small correcting adjustments to the sand content were made to accommodate the different densities of NA and RCA in the different mixes.

3. Experimental Design

CEM I 42.5 as a main binder, maximum 19 mm coarse aggregate (from both NA and RCA) size and fine sand with fineness modulus 2.64 were used in this research work. To characterize the durability performance of concrete, cubes (100 mm^3) containing 0% and 30% RCA were prepared and cured in submersed water at temperature 21 ± 2^o C until 23 days. For all three tests, a total four concrete disk samples of 28 ± 2 mm thickness and 70 ± 2 mm diameter were collected from each after this curing period. The samples were obtained by drilling into the exposed surface of 100 mm concrete cubes, and then by cutting the cylinders into the 28 mm slice. The samples were thereafter placed in an oven that was maintained at a temperature of 50 ± 20^o C and at a relative humidity of less than 20% for a minimum of 7 days ± 4 hrs. prior to testing. For all these three tests, procedures have been followed according to the University of Cape Town durability index testing procedure manual, 2009, version 1. The ranges of index values for durability classification of concrete were also followed by the suggestion made of in [11, 12]. Table 1 shows the materials mix design was used in this research study.

3.1. Oxygen Permeability Test

D'arcy's law is used to model the flow of fluid through a permeable body. This law may also be used for gas flow through a permeable medium. The permeability of the concrete is considered to be an internal property, but it also depends on the properties of the penetrating gas or fluid. The movement of fluids through a porous structure under an externally-applied pressure can be determined from the permeability test. Therefore, permeability refers to the capacity of concrete to transport gasses or fluids by permeation and is dependent on the concrete microstructure, the moisture condition of the material and the characteristics of the permeating gas or fluid. The oxygen permeability is presented as a permeability coefficient obtained from the measured flow of oxygen at different pressures through the specimen, expressed in terms of the Darcy coefficient of permeability. Esq. (1) to (3) was used to calculate oxygen permeability index (OPI) value of both concrete.

$$k = \frac{\omega v g dz}{RA\theta} \qquad (1)$$

where k is the coefficient of permeability of test specimen (in length per unit time), ω is the molecular mass of oxygen (32 g/mol), v is the volume of oxygen, g is the acceleration due to gravity (9.81 m/s^2), R is the universal gas constant (8.313 *Nm/K* mol), θ is the absolute temperature (K) and z is the slope of the linear regression line is given by:

$$z = \frac{\sum_i [\ln(P_o / P_i)]^2}{\sum_i [\ln(P_o / P_i) t_i]^2} \qquad (2)$$

Where P_0 is the initial pressure at time t_0, the start of the test, and P_i are the subsequent readings in pressure at times t_i, measured from t_0.

OPI is given as the negative log of the average of the coefficients of permeability of the specimens. For *n* specimen this is:

$$OPI = -\log_{10}\left(\frac{\sum_i^n k_i}{n}\right) \qquad (3)$$

D'Arcy coefficient of permeability was determined and converted into OPI by taking the negative log of the D'Arcy coefficient. Oxygen was used as the permeating medium and a constant pressure head of 115 kPa ± 5 kPa to the test specimen was used at the beginning of the test. This pressure was decreased with time. From the start of the test to the end of test the time elapsed was 6 hrs. The test procedure entailed measuring the flow of gas through a concrete specimen at a steady rate under the pressure head. This allows the permeability coefficient of the tested concrete to be determined. Figure 1 shows the OPI test set up used in this study at concrete lab in University of Cape Town, South Africa.

3.2. Chloride Conductivity Test

Chloride diffusion characteristics of concrete can be obtained from chloride conductivity (CC) test. Diffusion is defined as the process by which liquid, gas or ions move through a porous material under the action of a gradient. It may occur in partially- or fully-saturated concrete and is an important transport mechanism for most concrete structures that are exposed to salts [11, 12]. There are many ways of calculating chloride diffusivity in the concrete specimen like using Darcy law, however in this experiment it was calculated using the Eq. (4) given below.

$$CC = \frac{id}{VA} \qquad (4)$$

Where i is the electric current, V is the voltage difference, d is the average thickness and A is the cross-sectional area of the specimen.

Chloride conductivity test is based on the ionic flux that occurs by conduction due to voltage potential difference. The apparatus showing in Figure 2 consists of a two-cell conduction rig in which concrete core samples are exposed on both faces to sodium chloride solution. Chloride conductivity is determined by measuring the current that flows through the concrete specimen. The current is accelerated by the application of a voltage potential difference.

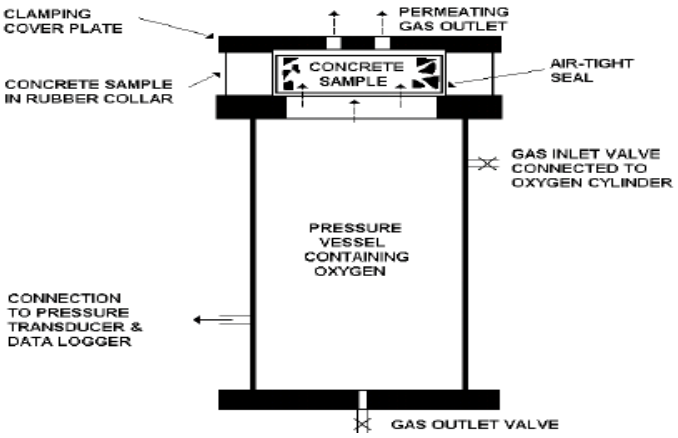

Figure 1: *Oxygen Permeability Test Set Up [13]*

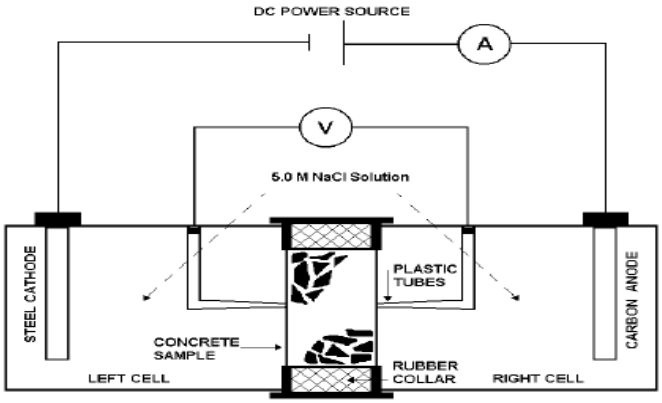

Figure 2: *Chloride Conductivity Test Set Up [13]*

3.3. Water Sorptivity Test

The rate of water movement into the concrete specimens under the action of capillary forces can be obtained from the water sorptivity (WS) test. Typically weight gain of the specimen with time (see Figure 3) of exposure of the lower surface to water is determined from this test. The water sorptivity of the specimen (*S*) is then calculated as follows:

$$S = \frac{md}{M_{sv} - M_{so}} \qquad (5)$$

Where *m* is the slope of the best fit line to the graph of measured mass gain versus square root of time which the specimen is exposed to capillary suction, M_{sv} is the vacuum saturated mass and M_{so} is the mass of the specimen at the initial time (t_0).

The porosity of each specimen can also be determined as follows:

$$\rho = \frac{M_{sv} - M_{so}}{Ad\rho_w} \qquad (6)$$

With ρ_w the density of water, and A is the specimen surface area exposed to the water.

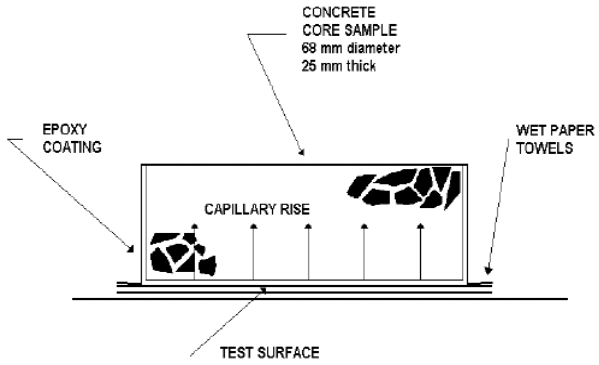

Figure 3: *Water Sorptivity Test Set Up [13]*

Sorptivity is the gradient of the line of water volume absorbed with the square root of time. The bottom face of the specimen is kept in contact with water and mass of water absorbed by this face of the specimen measured the sorptivity of the concrete specimen. Eqs. 5 and 6 were used to calculate sorptivity and porosity of both concrete specimens. The details specimen preparation and calculation procedure of these three tests can be found in [11]. Table 2 shows the suggested ranges of these three durability index test vales.

4. Experimental Outcome

Despite the fact that this paper is limited to the durability performance of both natural aggregate concrete (NAC) and recycle aggregate concrete (RAC), however this section of the paper also provides a brief overview on other tests which were also done in this research work. Physical properties of aggregates, slump of concrete, air content, strengths, E-modulus, shrinkage and creep strain results of both concrete were also determined and brief results are shown in Table 3. For details experimental procedures, results etc. readers are referred to references [14-16].

Almost similar range of relative density and a bit higher water absorption capacity was found in RCA than NA. Due to higher water absorption, relatively lower slump value and almost 8% higher air content was also found in concrete with RCA. In terms of strength and E-modulus, no major difference was observed in both types of concrete. Similar shrinkage strain was found in both concrete but RAC showed more than 65% higher creep strain than NAC.

Table 2: *Suggested Ranges of Durability Index Value [11]*

Acceptance Criteria		OPI (log Scale)	WS (mm/ $h^{1/2}$)	CC (mS/cm)
Laboratory Concrete		>10	<6	<0.75
As Built Structure	Full Acceptance	>9.4	<9	<1
	Conditional Acceptance	9 to 9.4	9 to 12	1 to 1.5
	Remedial Acceptance	8.75 to 9	12 to 15	1.5 to 2.5
	Rejection	<8.5	>15	>2.5

Table 3: *Summary of NAC100% and RAC30% Test Results*

Type of Test	NAC100%	RAC30%
Relative density	2.74	2.68
Water absorption	0.65	2.64
Slump (mm)	65	50
% of Air	2.2	2.4
Cylinder strength (MPa)	30.50	30.87
Cube strength (MPa)	46.57	47.21
E-modulus (GPa)	31.75	33.2
Splitting strength (MPa)	5.55	5.48
Flexural strength (MPa)	3.46	3.15
Shrinkage strain (µm/m)	822	839
Creep strain (µm/m)	571	954

Note that, these are 28 days strength and E-modulus values, 90 days creep and shrinkage values.

Table 4: *Durability Index Results Obtained from the Test*

Type		OPI (log scale)	CC (mS/cm)	WS ($mm/h^{1/2}$)
NAC100%	Ave value	9.61	1.65	7.1
	CoV (%)	44.9	3.28	20.2
RAC30%	Ave value	9.78	1.34	8.1
	CoV (%)	19	6.58	32.4

4.1. OPI Test Results

The results of oxygen permeability tests for both NAC100% and RAC30% are shown in Table 4. These are the average values of four specimens of the same mix sample. The oxygen permeability is presented as a permeability coefficient obtained from the measured flow of oxygen at different pressures through the specimen. It was expected, higher oxygen permeability value of concrete with RCA. Because of adhered mortar in dry RCA absorbs water during the mixing of concrete. Later when water evaporates from concrete, voids are created inside the concrete structure. As a result concrete becomes more permeable. However, almost similar OPI results for both NAC100% and RAC30% were found in this research. Figures 4 and 5 show samples response (time vs. pressure) during testing. Both concrete satisfy the good quality and durability of the class range suggested in Table 2. Good quality RCA with lower amount of adhered mortar may be the reason of improved response of RAC in OPI test. Note that in Figure 4 one invisible line (Sp-02) is hidden by the green line (Sp-03). It is because of the similar oxygen pressure values of both specimens. Similar situation had occurred in Figure 5 where the purple line (Sp-04) and the blue line (Sp-01) stay together because of the same oxygen pressure values to both specimens.

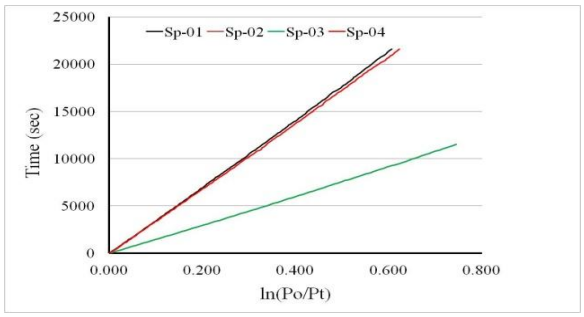

Figure 4: *Oxygen Pressure through Specimens with Time for NAC100%*

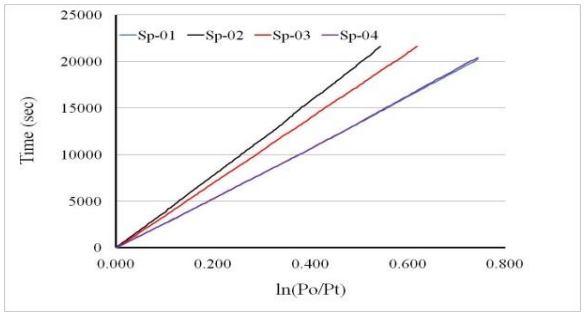

Figure 5: *Oxygen Pressure through Specimens with Time for RAC30%*

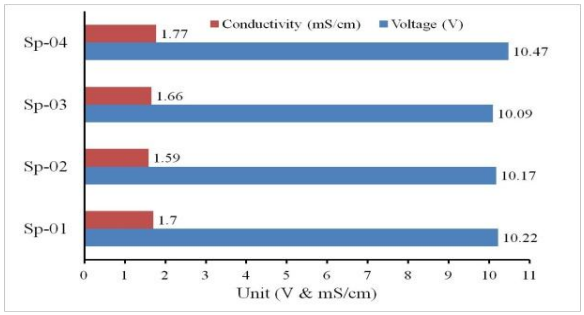

Figure 6: *Voltage and Conductivity Response of NAC100%*

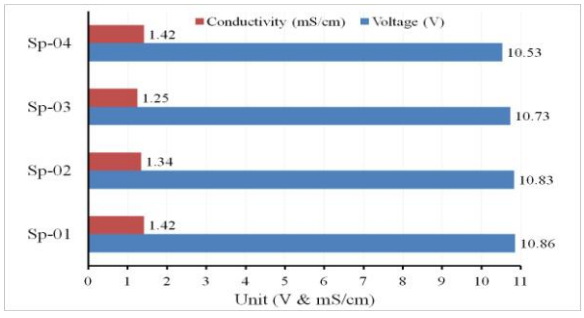

Figure 7: *Voltage and Conductivity Response of RAC30%*

4.2. CC Test Results

Table 4 shows the average value of four specimens and the individual response of each specimen in CC test for both NAC100% and RAC30% are shown in Figures 6 and 7. A higher value was found for NAC100% and the reason for this higher value is unknown. Note that the four measurements do not represent a sufficient statistical base, so more tests are recommended to reduce uncertainty of this outcome. Also rates of diffusion are dependent on temperature, the internal moisture content of concrete, the type of diffusant and the inherent diffusibility of the material. Diffusion into concrete may be complicated by chemical interactions, by partially saturated conditions, by defects such as cracks and voids and by electrochemical effects due to steel corrosion and stray currents. However, from these results it may be concluded that RAC30% shows relatively good durability performance and fulfills the durability requirement for this ingress mechanism.

Good curing and lower water-binder ratios of concrete improves resistance to chloride diffusion. So the ions of hardened concrete cannot move easily which results in lower conductivity values of concrete. It might also be possible to get the same level of conductivity with larger amount of RCA replacement in concrete by increasing cement in concrete mix. Future studies are required to prove this.

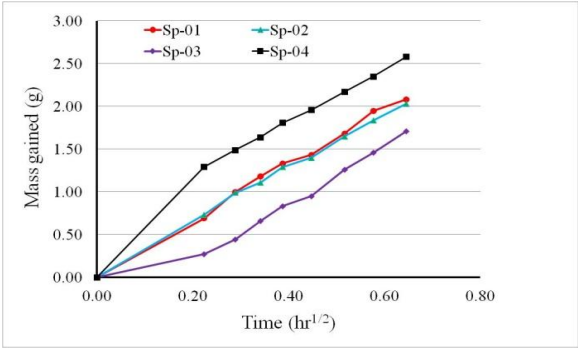

Figure 8: *Mass Gained by NAC100% Specimens with Time*

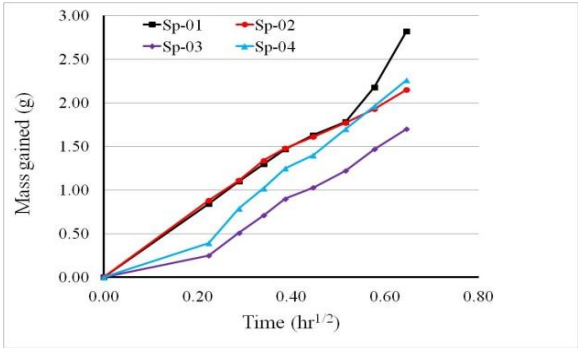

Figure 9: *Mass Gained by RAC30% Specimens with Time*

4.3. WS Test Results

Results of WS tests are also presented in Table 4. Better sorptivity values were found for NAC100%. RAC30% shows about 14% higher sorptivity values than NAC100%. But still RAC30% satisfies the same range requirements as NAC100%. In Figures 8 and 9, it is showing the individual response of

four specimens each from NAC100% and RAC30%. It can be seen that three specimens from NAC100% show mass gains equal to or less than 2 gm. One specimen shows a slightly higher mass gain than 2.5 gm. On the other hand, only one specimen from RAC30% shows a mass gain less than 2 gm. Old mortar in RCA increases the sorptivity of the concrete. Sorptivity values increase with increases of RCA in new concrete. Nevertheless, similar durability index categories were found for both NAC100% and RAC30%.

The sorptivity values can be improved by better curing of concrete, which contributes to the continued formation of hydration products. The gel products block the capillaries and pores inside the concrete, hence reducing the movement of fluids through the hardened concrete [17]. It was also found that the water sorptivity value improves at lower water: cement ratios. This is because the amount of cementitious content increases with decreases in the water: cement ratio. This results in increasing the total products of hydration, thus making the concrete less porous, leading to lower water absorption.

A study [18] on durability of concrete with different cement types shows that concrete durability can be improved by adding fly ash, slag and silica fume. With NA in concrete at 28 days, 10% silica fume shows the possible value of chloride conductivity is 0.39 where the OPC shows the value of 1.35, 30% fly ash shows the value 0.875 and 50% slag replacement in concrete shows the value of 0.4375. Therefore more experimental study is required to prove whether RCA in concrete shows the similar trend of improving durability with slag, fly ash and silica fume.

5. Conclusion and Recommendation

It was the aim of this research to establish the suitability for using RCA30% in structural concrete. On the basis of the experimental tests carried out in this research, it is possible to conclude that the RCA used in this study is of a high quality and there are no any significant differences in the mechanical behavior and durability performance when compared with NA for the same strength class of concrete.

Similar durability performance was found in both NAC100% and RAC30%. RAC30% shows 14% higher sorptivity values, but the range is still within the durability limit of concrete. Higher chloride conductivity was shown for NAC100%. Presence of unseen defects in the specimen may be the reason of this lower performance and a larger statistical base experiment should be used to confirm these results.

Better curing and a higher amount of binder in concrete improves the durability index values. It may be possible to obtain the same durability performance of concrete with certain amount of RCA replacement by adding more binder in comparison to the binder content of conventional concrete, or by use of suitable cement replacement materials. Nevertheless, here a direct comparison of approximately the same mixes was made in order to isolate the role of the RCA in durability. This led to a similar durability performance compared with NAC, and both concrete fall in the same durability category.

It has been shown that RCA30% has similar resistance to ingress by oxygen, water and chlorides. However, some sources of RCA can contain chloride, and should be a concern when such RCA is used in reinforced concrete.

Additional research is continually needed because there are always questions that remain unanswered in the engineering field. Whether the test procedures and specifications for NA are feasible for RCA and whether some of them eliminate the use of RCA without addressing the performance of the material as well as some environmental issues, need to be fully answered and

accepted in order to eliminate the need to retest and re-evaluate every time RCA is used. Of course, performance-based specifications would be beneficial when using both RCA and NA in any major concrete structures.

References

[1] Vyncke J. 2000: *Use of Recycled Materials as Aggregates in the Construction Industry*, Network Management. Belgian Building Research Institute.

[2] U.S. Army Report, 2004: *Reuse of Concrete Materials from Building Demolition*. Public Works Technical Bulletin, 200-1-27.

[3] Obla K., et al., 2007: *Crushed Returned Concrete as Aggregates for New Concrete*. Final Report, RMA Research and Education Foundation Project 05-13. NRMCA Research Laboratory, Branchville College Park MD.

[4] Dhir R.K., et al., 2007: *Performance Related Approach to Use of Recycled Aggregates*, WRAP Aggregate Research Programme, Project AGG 0074. Waste & Resources Action Programme, Banbury, Oxon, UK.

[5] Olorunsogo et al. *Performance of Recycled Aggregate Concrete Monitored by Durability Indexes*. Cement and Concrete Research. 2002. 32 (2) 179–185.

[6] Gomez M.V. *Shrinkage of Concrete with Replacement of Aggregate with Recycled Concrete Aggregate*. ACI Spec. Publ. 2002. 209; 475-496.

[7] Poon et al. *Effect of Microstructure of ITZ on Compressive Strength of Concrete Prepared with Recycled Aggregates*. Construction and Building Materials. 2004. 18 (6) 461-468.

[8] Byung et al., 2004: *Chloride Diffusion and Corrosion Initiation Time of Reinforced Concrete Structures.* In Proceedings of the International Workshop on Microstructure and Durability to Predict Service Life of Concrete Structures, Sapporo, Japan.

[9] Feldman et al. *Investigation of the Rapid Chloride Permeability Test*. ACI Mater J. 1994. 91 (2) 246–55.

[10] Neville et al., 1987: *Concrete Technology*. Addison-Wesley Longman, UK.

[11] Alexander et al., 1999*: Rapid Chloride Conductivity Testing of Concrete, Research Monograph* No. 2, Collaborative Research by Universities of Cape Town and Witwatersrand, 35.

[12] Alexander et al., 1999: *Rapid Chloride Conductivity Testing of Concrete, Research Monograph* No. 3, Collaborative Research by Universities of Cape Town and Witwatersrand, 35.

[13] Alexander et al., 1999: *Guide to the Use of Durability Indexes for Achieving Durability in Concrete Structures*, Research Monograph No. 2, Department of Civil Engineering, University of Cape Town, 35.

[14] Paul S.C., 2011: *Mechanical Behaviour and Durability Performance of Concrete Containing Recycled Concrete Aggregate*, Department of Civil Engineering, MSc Thesis, The University of Stellenbosch, South Africa. http://scholar.sun.ac.za.

[15] Paul S.C., et al., 2012: *Strength of Recycled Concrete Aggregate for Structural Uses.* In Proceeding of ICCRRR Conference, Concrete Repair, Rehabilitation and Retrofitting III, Cape Town, RSA, 1340-1346.

[16] Paul S.C., et al. *Mechanical and Durability Properties of Recycled Concrete Aggregate for Normal Strength Structural Concrete*. International Journal Sustainable Construction Engineering and Technology. 2013. 1 (4) 89-103.

[17] Benjamin K., 2004: *Performance of Concrete Made with Commercially Produced Recycled Coarse and Fine Aggregate in Cape Peninsula*. Master's Thesis, University of Cape Town.

[18] Mackechnie J.R., 2001: *Predictions of Reinforced Concrete Durability in the Marine Environment*, Department of Civil Engineering, University of Cape Town.

Cloud Publications
International Journal of Advanced Civil Engineering and Architecture Research
2013, Volume 2, Issue 1, pp. 65-71, Article ID Tech-168

Research Article

Open Access

Image Based 3D Modeling of Campus (Department of Civil Engineering, IIT Roorkee, Uttarakhand, India) by Using SketchUp

Surendra Pal Singh[1], Kamal Jain[1] and V. Ravibabu Mandla[2]

[1]Geomatics Engineering Section, Department of Civil Engineering, Indian Institute of Technology, Roorkee, Uttarakhand, India
[2]Schools of Mechanical and Building Sciences, Vellore Institute of Technology (VIT) University, Vellore, Tamilnadu, India

Correspondence should be addressed to Surendra Pal Singh, surendra.geomatics@gmail.com

Publication Date: 28 September 2013

Article Link: http://technical.cloud-journals.com/index.php/IJACEAR/article/view/Tech-168

Abstract Virtual 3D modeling is a very important and hot topic for researchers of Geomatics. For all over the world, so many educational institutes are available with its own campus. Campus is the land on which Institute; College or University buildings are situated. In the modern digital era, the demand of 3D Campus is increasing. Virtual 3D model of campus gives a good and photo-realistic appearance. In Geomatics market, So many image based techniques are available for 3D modeling. Photogrammetry and Laser scanning are the main Geomatics techniques. But due to many drawbacks in these techniques, a new approach is possible to make virtual 3D Campus. Time and Cost main key issue for this. In this paper, we are giving a simple and cheapest solution to create virtual 3D campus of any educational institute. This 3D campus model can be exported in various other formats for various applications. These 3D models can be exported to Google Earth. These 3D campus models can also be published on the website of that Institute or University. In this study, we used simple digital images and very cost effective software. This paper will describe the introduction, methodology, advantages, drawbacks and limitations of this method. In this study, we used the study area, Campus of Department of Civil Engineering, Indian Institute of Technology, Roorkee (Uttarakhand), India.
Keywords *Geomatics, Virtual Campus, 3D Modeling*

1. Introduction

Virtual 3D modeling is a very important and hot topic for researchers of Geomatics. 3D city models have evolved to important tools for urban decision processes and information system especially in planning, simulation, networks, and navigation (Markus and Jurgen, 2008). Educational Institute or University has its own campus. Campus is also an important indicator for the quality of Educational Institute. Campus is a land of College, Institute or University, on which the buildings are situated.

Usually campus includes the academic and non-academic buildings. In the modern digital era, the demand of 3D Campus is increasing. Virtual 3D model of campus gives a good and photo-realistic appearance. In Geomatics techniques, so many image based techniques are available for 3D building modeling. Each 3D modeling methods and techniques have some advantage and also some limitations (Singh *et al*., 2013). Photogrammetry and Laser scanning are the main Geomatics techniques. In case of satellite and aerial images, the availability of the data could be a problem due to weather conditions or restrictions on flights (Fabio and Rizzi, 2010).

Close Range Photogrammetry is also a good tool to create Virtual 3D model of Campus (M.Shashi and Kamal Jain, 2007; Singh *et al*., 2012), But due to many drawbacks in these techniques, a new approach is possible to make virtual 3D Campus. Cost and Time are main key issues for this. In this paper, we are giving a simple and cheapest solution to create virtual 3D campus of any educational institute. This 3D campus model can be exported in various other formats for various applications. This method and techniques will be very useful for the owner of College, Institute or University. By using this method they can make a virtual model of campus. These 3D campus models can also be published on the website of that Institute or University. The 3D Campus models can be used for simulation and analysis from visualization and animation (Emem, 2002b).

In this study, we used simple digital images and very cost effective SketchUp software. So the need of this kind of study is very important and useful for 3D modeling community.

2. Study Area

In this study, we used the area of Department of Civil Engineering, Indian Institute of Technology-Roorkee, Roorkee, (Uttarakhand) India. This department is the oldest and largest in India. It was Roorkee Civil Engineering College and established in November 25, 1847. In 1954, it renamed as Thomason College of Civil Engineering. It was University of Roorkee from 1948-2001. From 2001, it becomes seventh IIT as Indian Institute of Technology-Roorkee.

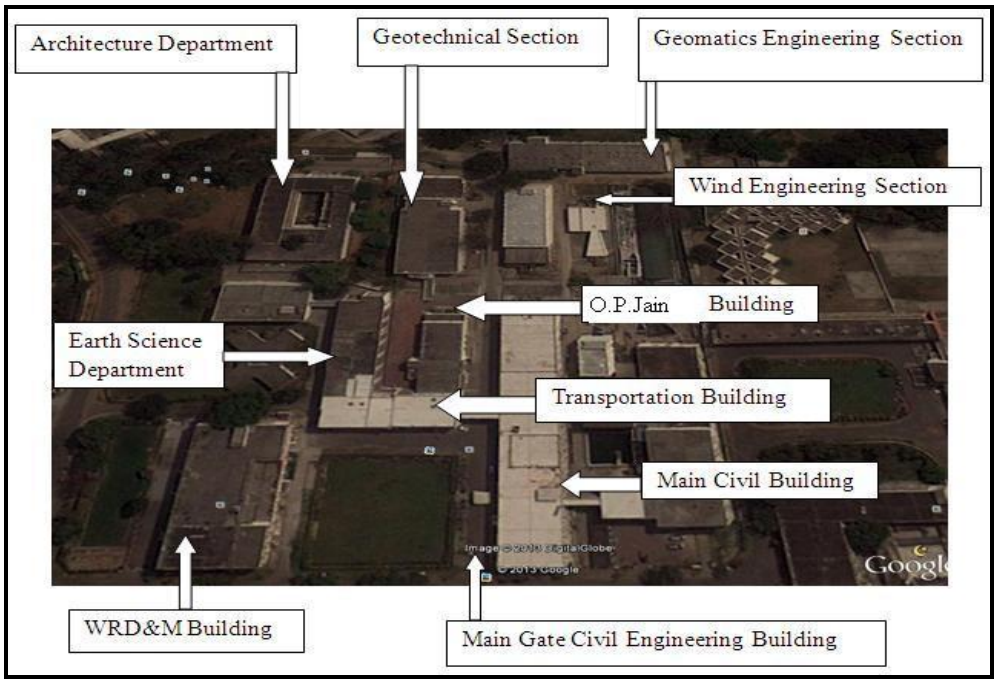

Figure 1: *Department of Civil Engineering, IIT-Roorkee, India*
(**Source**: Google Earth, June, 2013)

The Civil Engineering Department surrounding by Department of Architecture, Department of Water Resources Development and Management (WRD&M), and has the following main sections and buildings: Geomatics Section Building, Geotechnical Section Building (having CAD Lab and Research Scholar Wing), Lecture Hall building (having Newton room and Reyleigh rooms), Wind Engineering Section, O.P. Jain auditorium building, Transportation building, Main Civil building, and Hydraulics building. The location of Departments of Civil Engineering is showing in Figure 1.

In this study, we make the 3D model of Department of Civil Engineering, Indian Institute of Technology, Roorkee, India. We make this department by using SketchUp; an image based 3D modeling software. Images are taken from a Sony Cyber-shot DSC HX7V digital camera.

3. Image Based Modeling by Using SketchUp

Earlier, SketchUp was the product of Google, now it is product of Trimble. It is a 3D modeling software. It works on the sketch-based modeling approach. It supports 2D and 3D model export functions among other features.

In recently, its latest commercial version is SketchUp Pro 2013, (earlier it was SketchUp Pro 8), a free version is also available with name as SketchUp make, that integrates with Google Earth. The model can be exported to Google's "3D Warehouse", to share these 3D models to anybody. These models are useful for the various ranges of applications such as Architectural, Civil Engineering, Mechanical, and Film & Game industry.

The SketchUp (free version) have the capability to export the models in .kmz, while the SketchUp Pro version can export these models to .3ds, .wrl, .xsi, .dwg, .dwf, .fbx, and .obj file formats.

4. Main Features of SketchUp

Following are the main features in SketchUp:

a) We can draw, modify, measure, rotate, scale and move geometry.
b) We can add and use accurate dimensions of buildings.
c) Interiors of building can also be seen in slice view.
d) We can add pre-made texture and can also add new texture.
e) We can add pre-made element of a city like tree, car, doors, window and people or we can also add new elements of city.
f) Walk through model also possible, and we can produce a movie of that area also.
g) It can take 2D images in .JPG, .PNG, .TIF, .TGA, .BMP formats.
h) It can import 3D model from .SKP (from SketchUp), Google Earth Terrain, .3Ds, .DEM.
i) We can make and export the animation and walk-through as MOV or AVI files.
j) We can make Geo-located models and placed them in Google Earth.
k) We can export a Google earth file directly in KMZ format.
l) We can also create add-on programs using the Ruby programming language.

5. Methodology

Firstly, we select the desired location of an area from Google Earth for 3D Modeling. Then we sketch the model and extrude the model. At the last, we give the texture from images. Overall method can be shown in given fellow diagram:

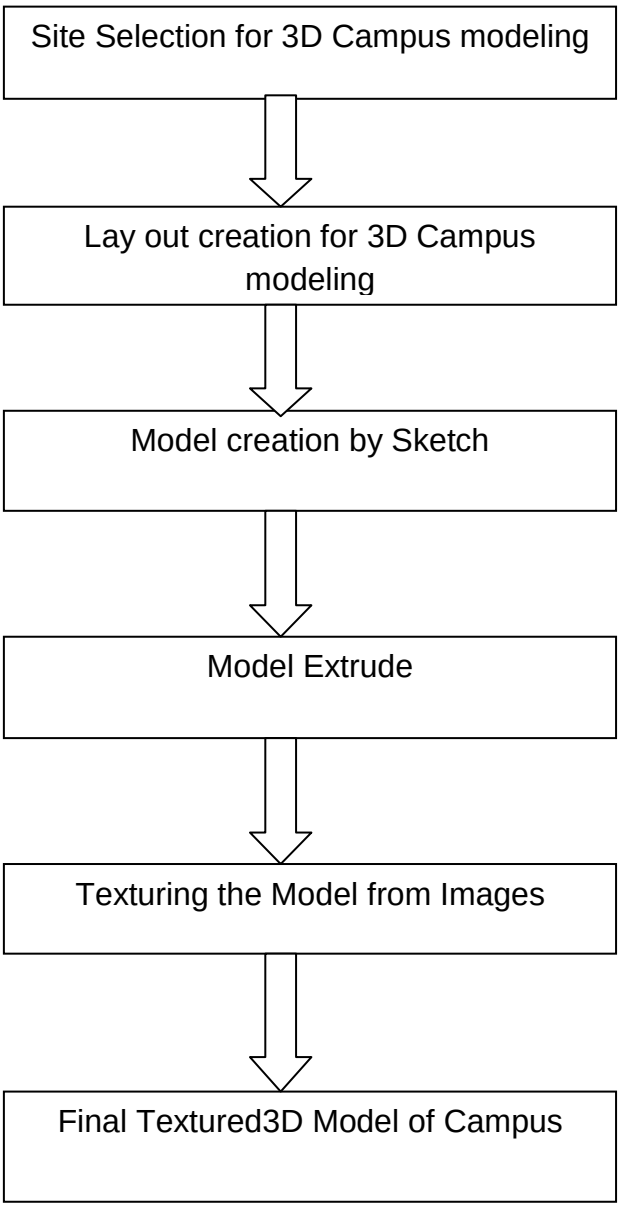

Figure 2: *Flow Diagram of Methodology*

In the First step, we select and choose the desired campus of Department of Civil Engineering, Indian Institute of Technology, Roorkee, India, an educational institute from Google Earth. After this, export this campus area in SketchUp. Then we choose and select the desired Buildings of institute. For Department of Civil Engineering, we choose the Transportation section Building, Civil Engineering main gate and main building, O.P. Jain Auditorium building, Geotechnical building, Lecture hall building, Geomatics Section building. We also make the surrounding department of near Civil Engineering Department such as Department of Water Resources & Management (WRD&M), Department of Earth Science, and Department of Architecture.

In Figure 3, and Figure 4, showing the final textured 3D model of Department of Civil Engineering, IIT-Roorkee, by using SketchUp software.

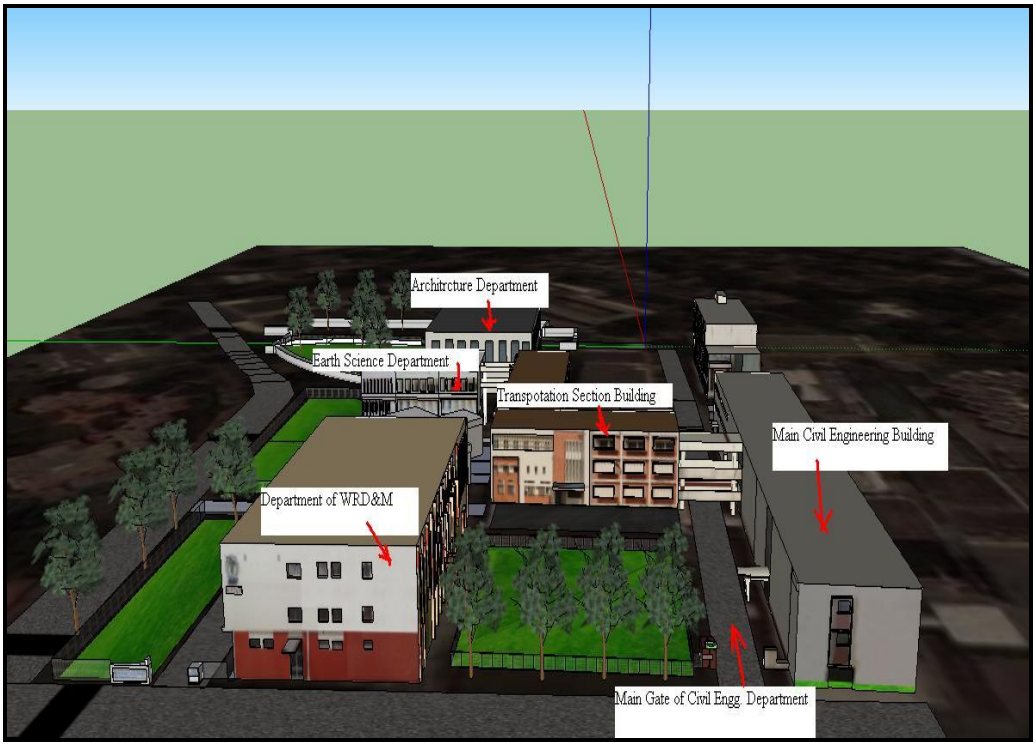

Figure 3: *3D model of Civil Engineering Department, IIT-Roorkee (India) by using SketchUp*

Figure 4: *Another View of 3D model of Department of Civil Engineering, IIT-Roorkee, India*

6. Main Advantages

Following are the main advantages of this SketchUp Software:

- This software is very simple and easy to use.
- Less trained person can also make the 3D model by using this software.
- It is very cost effective solution to create 3D City model.
- Dimensions of buildings can also be added.
- External city elements can also be added.

7. Limitations

Following are the main limitation for this method:

- Its textured quality is not very much advanced.
- The quality of model is not also very high level.
- Its accuracy depends on external dimension measurements.
- The quality of external city elements (like Tree, Bus) is also not good.
- Roof texture is also not accurate.

8. Results and Discussion

With the help of this work, we obtained a 3D model of campus i.e. Department of Civil Engineering, Indian Institute of Technology, Roorkee, India. This model is very basic and textured model. Street texture and Road texture is showing very well but roof texture is not correct. It is due to the unavailability of roof images from camera. In this 3D model other city elements such as Tree and Car (Vehicles) are also not showing properly. Texturing and modeling is not very easy for these elements.

This model has good 3D visualization and useful for 3D simulation and modeling of IIT-Roorkee campus. This model can be exported in various formats for various applications like Multimedia. This 3D model is also useful for Navigation. It can be published on website of Institute.

9. Conclusion

Normally, 3D modeling of any campus is very important. Various techniques and methods are available for 3D campus modeling. Each 3D modeling methods and techniques have some advantage and also some limitations. Some techniques are very costly and not very easy to make the 3D Campus. Satellite and aerial images is not easily available due to weather conditions or restrictions on flights. Satellite Images and Aerial Images are very costly and not easy to obtain for a simple institute. Normal and simple institute cannot afford these costly techniques. So this 3D modeling method gives a very low cost and effective solution for Virtual 3D modeling for a campus or university or institute.

Dimensional analysis is also possible in this method. We can find measured input values of the dimensions of buildings. It is very easy to use and also gives good photo-realistic look. Texture quality depends on camera quality. High resolution gives better textured model.

The main aim of this paper was to provide a very simple and cost effective method for 3D modeling user community to create Virtual 3D model of a Campus or Institute or University. The 3D Campus models can be published on website of Institute or University to attract the visitors for simulation and analysis from visualization and animation.

References

Emem O., 2002b: *3-D Modelling: Design and Application*. MSc Thesis, Yildiz Technological University, Istanbul.

Fabio Remondino and Alessandro Rizzi. *Reality-based 3D Documentation of Natural and Cultural Heritage Sites- Techniques, Problems, and Examples.* Appl Geomat. 2010. 2; 85-100.

Markus Jobst and Jürgen Dollner, 2008: *3D City Model Visualization with Cartography-Oriented Design.* REAL CORP 2008 Proceedings/Tagungsband, Vienna.

M. Shashi and Jain Kamal. *Use of Photogrammetry in 3D modeling and Visualization of Building*, ARPN Journal of Engineering and Applied Science. 2007. 2 (2) 1819-6608.

Singh Surendra Pal, Mandla V. Ravibabu and Jain Kamal, 2012: *3-D Building Modeling from Close Range Photogrammetry*. Geomatrix'12: International Conference on Geo-spatial Technologies and Applications, CSRE, Indian Institute of Technology, Bombay (IITB), India.

Singh Surendra Pal, Mandla V. Ravibabu, and Jain Kamal, 2013: *Virtual 3D City Modeling: Techniques and Applications.* International Archives of the Photogrammetry, Remote Sensing and Spatial Information Sciences, Volume XL-2/W2, ISPRS 8th 3D Geo Info Conference & WG II/2 Workshop, Istanbul, Turkey.

SketchUp, cited 2013; Trimble.

Google Earth, cited 2013; Google.

Cloud Publications
International Journal of Advanced Civil Engineering and Architecture Research
2014, Volume 3, Issue 1, pp. 72-80, Article ID Tech-261
ISSN 2348-5124

Research Report | Open Access

Design of System for Controlling, Scheduling and Monitoring of Construction Project using System Software

Ramadevi P.V.

Department of Construction Engineering and Management, Meenakshi Sundararajan Engineering College, Chennai, Tamilnadu, India

Correspondence should be addressed to Ramadevi P.V., devi1011chlm@gmail.com

Publication Date: 23 May 2014

Article Link: http://technical.cloud-journals.com/index.php/IJACEAR/article/view/Tech-261

Abstract Construction monitoring, controlling and scheduling is one of the important tool in a construction project. Every construction project involve with a lot of activities which need to be planned, monitored, controlled and scheduled properly to ensure the completion of the project. These project management techniques of planning, scheduling and controlling are used to complete the project within the stipulated time, scope, quality and cost. These techniques can be applied to all types of projects. Resource allocation and levelling are among the top challenges in project management, due to the complexity of projects. The main objective of this project is to optimize the resource schedule of construction project activities in order to minimize the total duration of the project, maximization of net present value, or minimization of average tardiness subjected to both precedence and resources constraints using an optimization technique called Ant Colony Optimizing Algorithm (ACO). This work describes an algorithm approach to Resource Constraint Project Scheduling Problems (RCPSP) in construction industry. The study on the optimization technique that is genetic algorithm and its terminology, operator, parameter used is clearly depicted. The modern approach of using ant colony algorithm technique to solve the Resource Constraint Project Scheduling Problems (RCPSP) problem for a construction project with constraints and to find the best optimal solution by overcoming the drawbacks in other optimization technique. The algorithm adapts to dynamic factors such as changes to the project plan or disturbances in the schedule execution. The ACO procedure then searches for an optimum set of tasks and priorities that produce shorter project duration and better-levelled resource profiles.
Keywords *Project Management; Scheduling of Works; Management of Work Task*

1. Introduction

Construction is a whole wide developed industry at present scenario with new innovation and inspiring technology. Construction is a process where many aspect ratios should be considering from design aspect to environment aspect. To execute the work as per the schedule guidelines proper work

assessment and management is required. Construction project management plays a vital work where it satisfies the client requirement. For the success in construction industries good management is required to be following from the execution work to the resource allocation. Project management can deal with both critical path method and Project Evaluation and Review Technique for project planning process which helps to allocate the duration of individual activity.

2. Objective

The objective of the project is to use optimized resource with constraint in cost. Ant Colony Optimizing Algorithm is the main source for optimizing the scheduled duration and resource cost. The major objective of this management is to concentrates on time, cost and quality. To which Comparison study on primavera, easy plan software and ant colony optimizing technique on basis on both aspect of duration and resources cost.

3. Methodology

In order to optimally utilize resources in a resource constrained project the concept of Ant Colony Optimization Algorithm is to be used. Figure 1 show the steps involved in the process. A computer model that solves Resource-constrained scheduling problems in construction projects and by fixed duration of time by implementing the following steps:

a) Carrying out a survey on the previous research that is related to the different approaches to schedule resource-constrained problems;
b) Studying the ACO approach in order to apply it in the current study;
c) Developing a computer model to optimize the process of scheduling projects under a given resource-constraints using ACO technique;
d) Comparison of the conventional technique with Ant Colony Optimization Algorithm with the chosen the real time project.

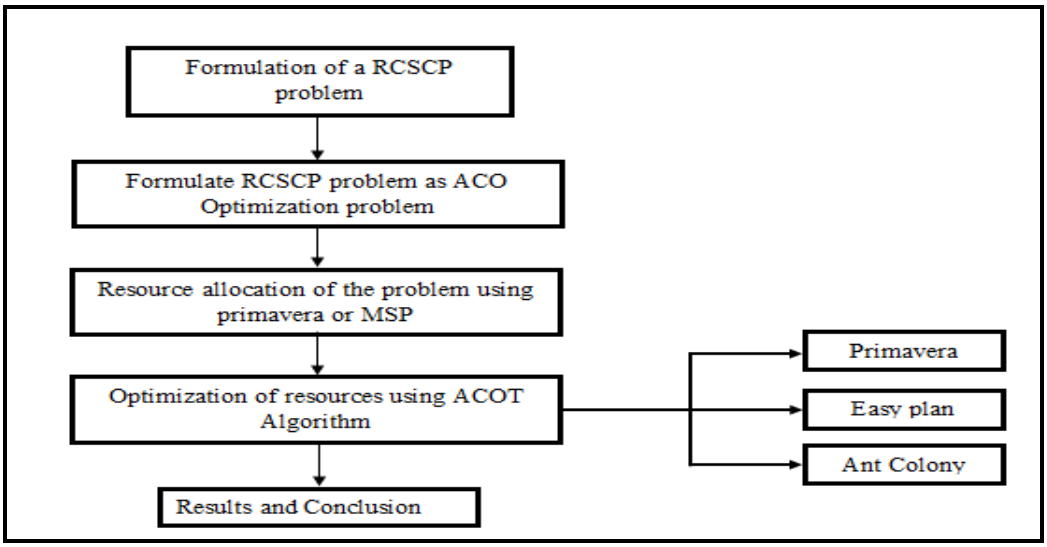

Figure 1: *Methodology*

4. Basic Outline of Ant Colony Optimizing Algorithms

Figure 2 shows the various steps involved in Ant colony optimizing Algorithm process.

A typical implementation of genetic algorithm

1) **[Start]** Generate random time for analysis.
(Suitable solutions for the problem).

2) **[New population]** Create a new population (time) by repeating following steps until the new population is complete.

3) **[Selection]** Select two timing according to their fitness (the better fitness, the bigger chance to be selected). The idea is to choose better timing.

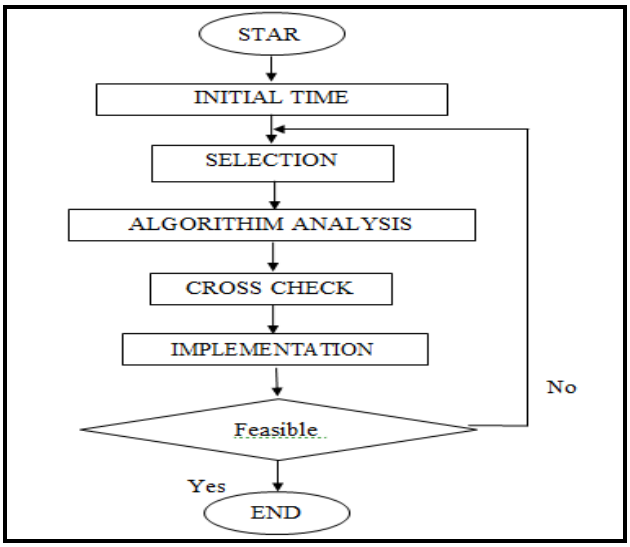

Figure 2: *Steps Involved in Ant Colony Optimizing*

4) **[Crosscheck]** with a crossover probability cross over the time to form a new offspring (time).

5) **[Accepting]** Place new assumption in a new time duration.

6) **[Replace]** Use new generated duration for a further run of algorithm.

7) **[Test]** If the end condition is satisfied, stops, and returns the best solution in current population (time/duration), and

8) **[Loop]** Go to step No. 2.

5. Design of Scheduling System

Every project has unique technique and implementation techniques basis on their requirement accordingly the duration are assumed there are implemented in primavera software as listed below.

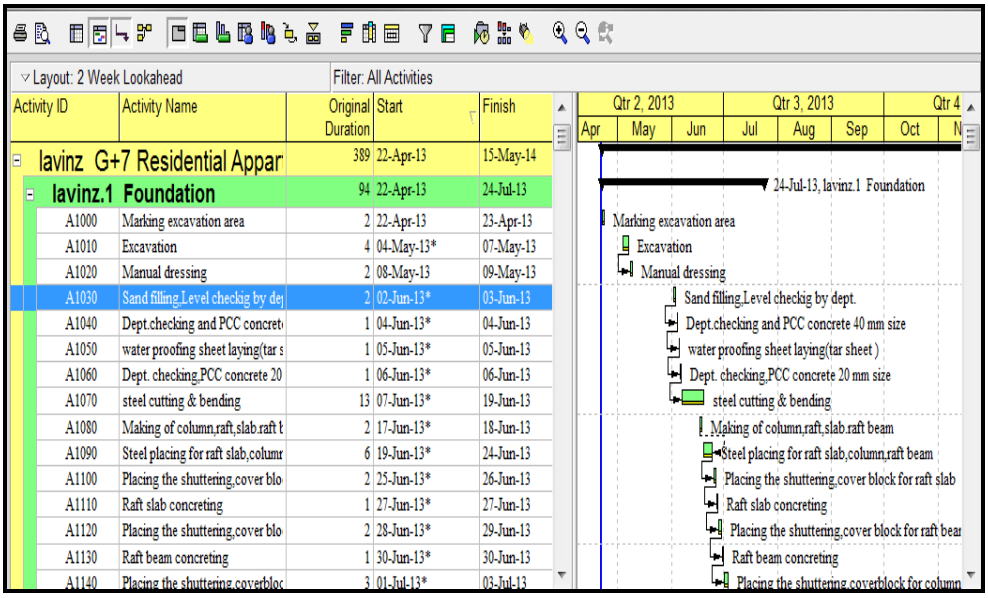

Figure 3: *Primavera Scheduling*

6. Syntax: Algorithm for Scheduling/Duration

Procedure ACO ()

```
While (termination criterion not satisfied)
        schedule activities
        ants generation and activity();
        end schedule activities
end while
end procedure
procedure ants generation and activity()
        while (available resources)

        schedule the creation of a new ant();
        new active ant();
end while
end procedure
procedure new active ant() ant lifecycle
        initialize ant();
        M= update ant memory();
        while (current state = target state)
        A = read local ant-routing table;
        P = compute transition probabilities (A; M; problem constraints);
        next state = apply ant decision policy(P; problem constraints);
        move to next state(next state);
if (step-by-step pheromone update)
        deposit pheromone on the visited arc();
        update ant-routing table();
end if
        M= update internal state();
end while
```

```
        if (online delayed pheromone update)
        evaluate solution();
        deposit pheromone on all visited arcs();
        update ant-routing table();
end if
end procedure
```

Table 1: *Rescheduling Duration*

S. No.	Activity	Predecessors	Duration	Rescheduling using ant optimizing	Manual estimation
1	**5th floor**	**Independent activity**	**24 days**	**17**	**-**
2	column	Independent activity	7 days	4	6
3	floor beam and roof slab	2	17 days	14	15
4	staircase	Independent activity	9 days	6	8
5	OTS	Independent activity	8 days	4	7
6	4th floor brick work	Independent activity	8 days	6	6 1/2
7	**6th floor**	**1**	**30 days**	**36**	-
8	Column	Independent activity	9 days	5	7
9	Floor beam & roof slab	8	19 days	14	17
10	Staircase	Independent activity	8 days	6	7
11	OTS	Independent activity	9 days	4	7
12	5th floor brick work	Independent activity	11 days	7	9
13	**7th floor**	**7**	**24 days**	**34**	-
14	Column	Independent activity	7 days	4	6
15	Floor beam & roof slab	Independent activity	18 days	13	16
16	Staircase	Independent activity	11 days	7	9
17	OTS	Independent activity	9 days	4	8
18	6th floor brick work	Independent activity	9 days	6	7
19	8th floor brick work & weathering course	13	4 days	2	3
20	Plumbing	Independent activity	45 days	36	42
21	Doors and Windows fixing	Independent activity	50 days	42	46
22	Internal plastering	Independent	58 days	49	52
23	External plastering	22	25 days	21	23 ½
24	water tank & balcony work	Independent activity	20 days	14	16
25	Finishing	Independent activity	31 days	20	26

7. Resource Algorithms

Resource allocation for the delay work is been analyzed by using ant colony optimizing algorithm and the values are listed in Table

Input: Activity

Output: Optimal allocation of Resources

For i= n to m (Resources size) do
Assume value = x (generate valid solution)
End
Curr alloc = min (assume value)
For i = n to m (Resources size) do
If i < 15% of manual estimation
Cost perc =15% (increase)
Else
If i < 25% of manual estimation
Cost perc =30 % (increase)
Else
If i < 40% of manual estimation
Cost perc =50 % (increase)
Else
End

Table 2: *Resources Allocation*

S. No.	Activity	Description	Duration (days)	Required Resources/day		
				R1	R2	R3
1		**5th floor**				
2	A	column	4	4	16	3
3	B	floor beam and roof slab	14	6	17	5
4	C	staircase	6	2	5	2
5	D	OTS	4	2	6	
6	E	4th floor brick work	6	4	11	
7		**6th floor**				
8	F	Column	5	4	15	3
9	G	Floor beam & roof slab	14	6	15	5
10	H	Staircase	6	2	6	2
11	I	OTS	4	2	6	
12	J	5th floor brick work	7	4	13	
13		**7th floor**				
14	K	Column	4	4	15	3
15	L	Floor beam & roof slab	13	6	16	5
16	M	Staircase	7	2	7	2
17	N	OTS	4	2	6	
18	O	6th floor brick work	6	4	11	
19	P	8th floor brick work & weathering course	2		10	
20	Q	Plumbing	36		14	
21	R	Doors and Windows fixing	42	4	15	
22	S	Internal plastering	49		16	

23	T	External plastering	21	14
24	U	water tank & balcony work	14	15
25	V	Finishing	20	15

8. Easy Plan

Easy Plan is program for Integrated Project Management. A simple but powerful spreadsheet program for integrated project management.

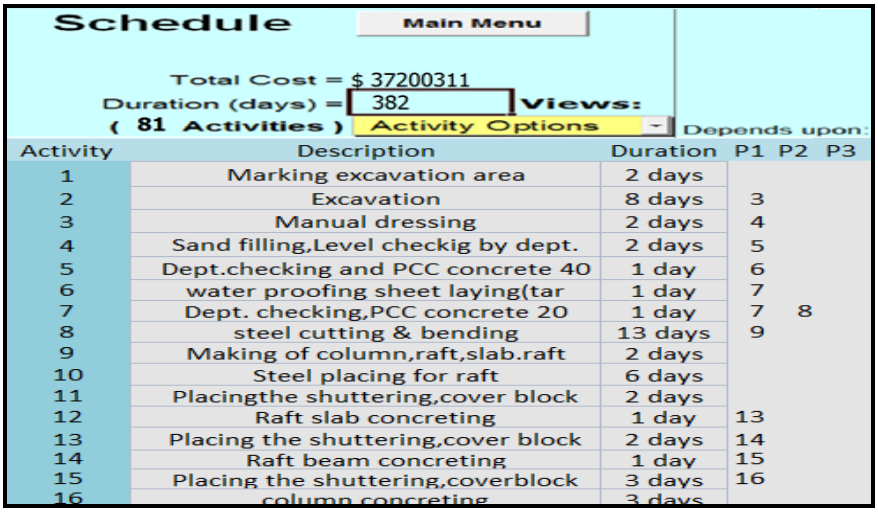

Figure 4: *Easy Plan Solution*

The converging result obtained was **T = 382 days** using Easy Plan.

9. Resource Limit

Resource limit for the whole project and actual usage of resources are listed below,

Table 3: *Resource Limit for Sample Problem*

Resource	Limit		Actual usage (Nos)
	Min (Nos)	Max (Nos)	
R1	50	65	58
R2	280	310	294
R3	60	75	67

10. Start Date and Duration Limit

Activity start date and code is mentioned and duration range is also given below,

Table 4: *Duration Limit and Start Date Sample Problem*

Activity	Min. Range(days)	Duration (days)	Max. Range(days)
column	4	4	6
floor beam and roof slab	14	14	15
staircase	6	6	8
OTS	4	4	7

4th floor brick work	6	6	6 1/2
Column	5	5	7
Floor beam & roof slab	14	14	17
Staircase	6	6	7
OTS	4	4	7
5th floor brick work	7	7	9
Column	4	4	6
Floor beam & roof slab	13	13	16
Staircase	7	7	9
OTS	4	4	8
6th floor brick work	6	6	7
8th floor brick work	2	2	3
Plumbing	36	36	42
Doors and Windows	42	42	46
Internal plastering	49	49	52
External plastering	21	21	23 ½
water tank	14	14	16
Finishing	20	20	26

Optimised duration obtained in Ant colony optimizing = **379 days.**

11. Comparison of Results

Implementation of all the activities, duration and resources in Primavera, Easy Plan, and Ant Colony Technique obtains the following results,

Table 5: *Comparison of Results*

	Primavera	Easy Plan	Ant colony
Optimized duration, (days)	389	382	379
R1, (Nos)	175	145	140
Cost, (Rs)	122000	115000	108000
R2, (Nos)	360	300	294
Cost, (Rs)	244000	210000	197600
R3, (Nos)	165	135	125
Cost, (Rs)	113000	110000	99000
Net Project Cost, (Rs)	**479000**	**435000**	**404600**

13. Discussion

- Studies should be done to enlarge the type of relationships between activities that the program can solve other than finish to start relationships.
- In practical projects, the activity does not necessary has a constant rate of resources over his total duration. Actual resource usage must be taken in consideration in future researches.
- Should integrate the efforts toward an integrated program for optimizing scheduling that optimize time, resources, costs and other measurements of project management performance.

14. Conclusions

Ant Colony Optimizing algorithms are conceptually simple and well-suited to problems with multi constraint problem. Although the basic ideas are straightforward, there is actually a great deal of work to implement algorithms on real problems with large search spaces. An implementation of the ACO

developed model for resource-constrained project scheduling has resulted in optimized output with reduced cost. A real time project is solved using this optimization software shows that best converging result can be obtained by fixing the time as constant.

References

CADD Center Training Services Pvt. Ltd., 2004: Primavera Reference Guide.

Garold D., Oberlender, 2000: *Project Management for Engineering and Construction.* McGraw Hill Publishing, New Delhi.

Chitkara, K.K., 2001: *Construction Project Management.* Tata McGraw Hill Publishing, New Delhi.

Cloud Publications
International Journal of Advanced Civil Engineering and Architecture Research
2014, Volume 3, Issue 1, pp. 81-88, Article ID Tech-327
ISSN 2348-5124

Research Article | Open Access

FHWA Model for Predicting Traffic Jam Noise in Varanasi City India

Kanakabandi Shalini and Brind Kumar

Department of Civil Engineering, Indian Institute of Technology (BHU), Varanasi, U.P., India

Correspondence should be addressed to Kanakabandi Shalini, kskanakabandishalini@gmail.com

Publication Date: 22 December 2014

Article Link: http://technical.cloud-journals.com/index.php/IJACEAR/article/view/Tech-327

Abstract Industrial and transport activities are the two major sources of noise pollution in any city. Most of the cities in India are facing serious noise pollution problems due to the concentration of motor vehicles and human population within the limited urban areas. Varanasi is the spiritual capital of India on the banks of the Ganga in Uttar Pradesh has an area of 1,550. Km^2. The population of Varanasi city as per census 2011 is 1,201,815. Main source of noise was vehicular traffic. A study has been performed in Varanasi city to assess the noise levels at selected locations with heavy traffic. Equivalent noise levels were measured at ten different traffic jam locations. From the data it was found that noise levels at all selected locations were much higher (70–90 dB(A)) than the prescribed limits. Federal Highway Administration Agency (FHWA) model was used to predict noise levels and the calculated noise levels were compared with the observed levels for checking the suitability of this model. It was observed that the results obtained by FHWA model were very close to the observed noise levels.

Keywords *Noise Pollution; Heavy Traffic; FHWA Model; Ambient Noise Levels*

1. Introduction

In the context of urbanization process, the road traffic noise is increased due to the increasing urban transport demand and leads to destroy the quality of life of people. With deteriorating level of mass transport services and increased use of personalized motor vehicles, vehicular noise pollution is assuming serious dimensions in most of the cities in view of its associated health hazards [1]. Vehicular noise pollution is increasing at an alarming rate in cities with an increase in urbanization. Road traffic noise mainly caused due to a rapid increase in population, unplanned urbanization and the development of transportation projects without environmental impact assessment [2].

The main source of road traffic noise is motor vehicles. Motor vehicles noise is created by mainly from horn, friction between tyre and roadway, engine, and exhaust system of vehicles. Patil and Nagarale (2013) reported that India is exceeding the permissible noise limits in major cities. Increasing the vehicle population is directly proportional to noise pollution and associated health effects and can cause both short term as well as long term psychological and physiological disorders like hearing

impairment, hypertension, and ischemic heart disease, annoyance, and sleep disturbance. Disturbances created by noise may cause hypertension, headache, allergy, asthma, emotional breakdown, insomnia, hypertension, gastrointestinal problems, heart diseases, high blood pressure [1; 2; 3].

Shukla et al. (2009) reported that noise levels in India cities have reached very high levels i.e., 76–80 dB(A). Due to a lack of enforcement and poor legislation, the traffic management technologies have been failed. Motor vehicles, which are significant part of this urban environment, and produce more than 55% of the total noise in our environment [2].

Koushki et al. (1993) monitored traffic noise at 42 locations in 13 districts in Riyadh, Saudi Arabia. They found the perceived impact of noise on their welfare and health and maximum mean district equivalent noise levels by road type were presented. They found that extent and degree of annoyance with traffic noise varied with the change in the functional classification of urban roadway. Reported that traffic noise caused headaches, and nearly one in four stated nervousness as a result of exposure to noise, only in 10 indicated awareness concerning the loss of hearing from long term exposure to traffic noise. Annoyance levels with traffic noise also increased with a change in the functional classification of roadways.

Koushki et al. (1999) presented the measurements of traffic noise at the edge of traffic lanes and at distances equivalent to residence locations, and traffic flow variables for nine freeway/ arterial/collector roadway locations in Kuwait. They reported that 50% of the time during the daily peak periods the noise from roadway traffic ranged between 67 and 87 dB(A), at the local street; between 71 and 92 dB(A), at the arterial roadway, and between 83 and 94 dB(A) at the freeway section. The L50 noise levels were 69, 74, and 76 dB(A) at the local, arterial, and freeway sections, respectively. Li et al. (2002) studied the traffic noise levels in the roads of the Beijing city, China. They found that traffic flow conditions on the main city roads in Beijing are significant, exceeding national standards by 5.2 dB(A).

Morrilas et al. (2002) carried out noise studies in Caceres, Spain and found out that noise levels were quite high with 90% of values higher than 65 dB(A) and the results were in coincidence with the results of other researchers. Pandya et al. (2003) states that road transportation plays a major role in the economic and social development of a country. They proposed a method to reduce the noise levels; one approach is to utilize education, persuasion and the tools of public relations to emphasize the need to control unreasonably loud, disturbing or unnecessary noise. Another approach is to controlling the impact of traffic noise on communities is to reduce the noise at the source by designing quieter vehicles and quieter road surfaces.

Phan et al. (2008) collected data on community response to road traffic noise, from the cities. Hanoi and Ho Chi Minh, in order to investigate the characteristics of road traffic noise and to establish dose-response relationships for road traffic noise in Ho Chi Minh's. They reported that road traffic noise in Hanoi and Ho Chi Minh City was characterized by a large number of motorbikes emitting frequent horn sounds. Pathak et al. (2008) to evaluate the noise pollution problem in the Varanasi city and its effect on the exposed people. They reported that most of the sampling sites were badly affected with traffic noise as these noise levels were higher then compared to the standards of the Central Pollution Control Board.

Road traffic noise has become serious problems to many authorities. Anti-noise laws, major highway control regulations, ordinances, and other governmental laws that concern environmental noise cannot be decreased without a priori empirical considerations. Therefore, it is the needed to prevent noise before it reaches a dangerous level.

In this paper attempt has been made to study the noise levels due to traffic in selected areas of Varanasi city and to predict noise levels using Federal Highway Administration Agency (FHWA) model and compared the calculated valued with observed levels for checking the suitability of this model.

2. Back Ground of Varanasi City

Varanasi is one of the oldest cities in continuous habitation in the world, with a history dating back to more than 3000 years. It is a major religious, cultural and educational centre of India. Varanasi town lies between the 25°15'N to 25°22' N latitudes and 82°57'E to 83°01'E longitudes. The river Ganga only here flows in a south-to-north direction, having the world famous Ghats on the left bank of the river. The environment of the town is tropical with temperature ranging from 5°C in winter to 45°C in summer. The mean annual rainfall lies between 680 mm to 1500 mm with a large proportion of its occurring during the months of July to September. Varanasi heavily populated city. According to 2011 census Varanasi has a population of 1,201,815. Its population growth rate over the decade 2001 to 2011 was 17.32%. Increase in living standards due to exponential economic growth the number of vehicles has also having the significant contribution in vehicular traffic there by leading to noise pollution. Varanasi is unable to support the exponentially growing traffic because its ancient buildings and old roads have stood since ages. Traffic congestion is a common scene in the entire city [11].

3. Methodology

A progressive development in predicting the traffic noise levels has made from past decades. Most of the early work concentrated on forecasting noise level from freely flowing traffic. These studies has been used to calculate noise emanating from the highway and a similar type of a new road carrying traffic travelling at moderate and high speed.

Traffic noise prediction models are used in the design of highways and other roads and sometimes in the assessment of existing or envisaged changes in traffic noise conditions. These models are generally needed to predict sound pressure levels, specified in terms of L_{eq}, L_{10}, etc. The prediction models represent national responses to the noise pollution concerns, and also from the current interest in environmental matters generally [12].

FHWA (Federal Highway Administration Agency) Model

FHWA (Federal Highway Administration Agency) model, like several other traffic noise prediction models, arrived at a prediction noise levels through a series of adjustment to a reference sound level. In FHWA model, the reference level is the energy mean emission level. Adjustment are then made to the reference energy mean emission level to account for traffic flows, for varying distance from the roadway, for finite length roadways, and for shielding.

$$L_{eq} = L_o + \Delta Li$$

Where: L_o – basic noise level of a stream of vehicles; ΔLi – adjustment applied.

FHWA model calculations were depend on a series of adjustments to the reference sound level measured through field measurements. L_{eq} in this paper was calculated using the following formula [13].

$$L_{eq}(h)_i = (L_o)E_i + 10\,log\left(\frac{N_i D_o}{S_i}\right) + 10\log\left[\frac{D_o}{R_n} - \frac{D_o}{R_f}\right] - 30$$

Where

$L_{eq}(h)_i$ = is the hourlly equivalent sound level of the ith class of vehicle

$(L_o)E_i$ = is the reference energy mean emission level of ith class of vehicle

N_i = is the no of vehicles in the ith class passing a specified point during some specified time

D_o= is the refernce distance at which the emission levels are measured. In FHWA model, D_o is 15 meters

S_i = is the average speed of ith class vehicle and is measured in kilometers/ hour

T = is the time period over which the equivalent sound level computed

R_n = is the distance in meters between the centerline of the near end of the roadway segment and the observer

R_f = is the distance in meters between the centerline of the far end of the roadway segment and the observer

Limitations on FHWA model:

1) In this model, vehicles are classified into three categories namely light commercial vehicles, medium trucks and heavy trucks.
2) Adjustments are applied for the calculation of hourly Leq.
3) Reference distance for measurement is taken as 15 meters from the centre of the near site lane and the actual distance of measurement is recorded.
4) No separate lane concept for acceleration or de-acceleration is considered [2].

4. Field Studies

Noise levels were measured at different locations in order to study the impacts on the environment with a possibility of a further expansion of the Varanasi city. Ambient noise levels were measured at different locations selected on the basis of traffic jams. Details of study locations in the Varanasi city covered during the survey are shown in Table 1.

Table 1: *Details of Study Locations*

Location	Location
Ravidas Gate	Cantt.
Rathyatra	Manduadi
Godowalia	Maidagin
Girijaghar	Andhra Pool
Saajan	Maldahiya

Keeping in view the objective of the study, a field data was collected. Geometric parameters like road width, the number of lanes, and lane width were measured. Longitudinal section parameter like the distance of a receptor point from the intersection was measured.

Classified traffic speed: The classified traffic speed was measured at each of the selected locations. The classified traffic speed study was carried out for the same duration as the noise level study and the traffic volume study. The speed was calculated using this formula.

$$q = KV_s$$

Where q = the average volume of vehicles passing a point during a specified period of time (vehicles/hour)

K = the average density or number of vehicles occupying a unit length of roadway at a given instant (vehicles/ km)
V_s = space mean speed of vehicles (kmph)

Ambient noise level: Ambient noise levels for the selected locations were collected using the noise level meter. Ambient noise pollution data was collected continuously for a period of 10 min at all identified locations.

Traffic volume: As the directional classified traffic volume is the basic data requirement of this study, traffic volume studies were carried out at all locations identified for the detailed study. At all selected locations, traffic volume studies were conducted continuously for a period of 10 min.

Here Passenger Car Equivalent (PCE) was used to convert a mixed vehicle traffic stream into an equivalent traffic stream. Srivastava *et al*., (2003) had suggested an equation for determining the passenger car noise equivalence factor (PNCE).

Passenger Car Equivalent (PCE): Traffic volumes at all locations have been presented, both in the form of total vehicles per hour as well as converted into PCEs and expressed in terms of equivalent passenger car units [14]. Traffic volume count in PCE is given in Table 2.

Table 2: *PCE values of Different Vehicles at Ten Intersections*

Intersection	Cycle	Motor cycle	Auto	Rickshaw	Car	Bus	Truck	Others
Andhra pool	0.0401	1.5738	2.8894	0.0613	1	5.5970	7.2023	3.9812
Ravidas gate	0.0455	1.6304	3.0915	0.0649	1	4.8895	8.5354	3.8012
Godowalia	0.0451	1.2596	2.6384	0.0216	1	4.0033	6.6112	2.1345
Girijaghar	0.0444	1.3665	3.0846	0.0636	1	3.4543	7.1045	3.1645
Saajan	0.0409	1.4600	2.9469	0.0563	1	6.0217	8.1529	2.2901
Cantt	0.0395	1.2338	2.9589	0.0600	1	6.4929	7.3494	3.6314
Manduadi	0.0415	1.7703	3.2862	0.0607	1	6.6127	8.2684	5.4983
Maidagin	0.0406	1.7079	3.0898	0.0630	1	7.2991	8.3930	3.0957
Maldahiya	0.0416	1.0935	2.8218	0.0626	1	5.5184	7.4051	2.3987
Rathyatra	0.0393	1.1620	2.8232	0.0655	1	5.4187	7.0447	4.4632

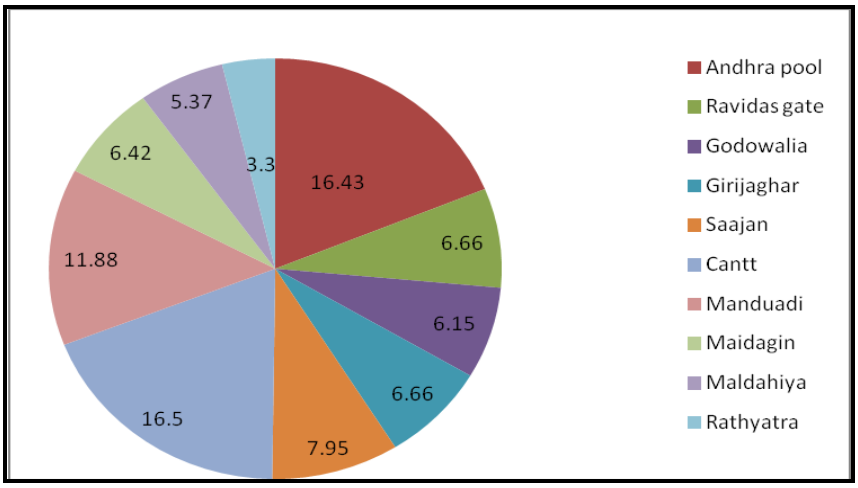

Figure 1: *Percentage of Heavy Vehicles at Different Intersections*

5. Analysis, Results and Discussion

From the observed data, we were calculated the traffic volume, speed of the vehicles, and Leq values at each location. The Leq obtained for near and far lanes were combined to get the final hourly Leq values for each location the calculation of which has been compared with the observed Leq values of each location. Leq values for different locations were tabulated in Table 3.

Table 3: *Leq Values for Different Locations Observed and Calculated*

S. No	Location	Leq Observed	Leq Calculated
1	Andhra pool towards Cantt 1	87	87.29269
2	Andhra pool towards Cantt 2	100	99.72478
3	Ravidas Gate 1	79	79.89382
4	Ravidas Gate 2	81	84.29473
5	Ravidas Gate 3	80.5	82.11419
6	Godowalia towards Bata Show Room 1	82	79.85732
7	Godowalia towards Bata Show Room 2	85	84.39069
8	Godowalia towards Titan Show Room	85	83.90565
9	Godowalia	83	82.23308
10	Girijaghar towards HP Petrol Bunk 1	86	80.02736
11	Girijaghar towards HP Petrol Bunk 2	86.5	84.26301
12	Girijaghar towards Dinshwas	86	81.21241
13	Girijaghar towards Ganga Opadi Kedhur	87	86.83675
14	Saajan towards Sigra 1	86	87.64154
15	Saajan towards Sigra 2	86	86.4983
16	Saajan towards Sigra 3	86	82.80811
17	Saajan towards Sigra 4	85	82.40663
18	Saajan towards IP Mall	91	92.68291
19	Saajan towards Sigra 5	92	90.00023
20	Cantt towards Lahartara	86	84.77389
21	Cantt towards Andhra Pool	85.5	84.84456
22	Cantt towards Lahartara 2	89.5	85.34415
23	Cantt towards Nadesar 1	92	90.98418
24	Cantt towards Lahurabir	84.5	81.33911
25	Cantt towards Nadesar 2	90	90.22529
26	Cantt towards fly over	90	89.43825
27	Manduadi 1	87	87.18489
28	Manduadi 2	87	88.22607
29	Maidagin towards Kabir Chaurah 1	87	81.53178
30	Maidagin towards Kabir Chaurah 2	93	94.17099
31	Maldahiya towards Teliyabaag 1	81.5	80.65819
32	Maldahiya towards Teliyabaag 2	93	91.89976
33	Rathyatra	87	85.90245

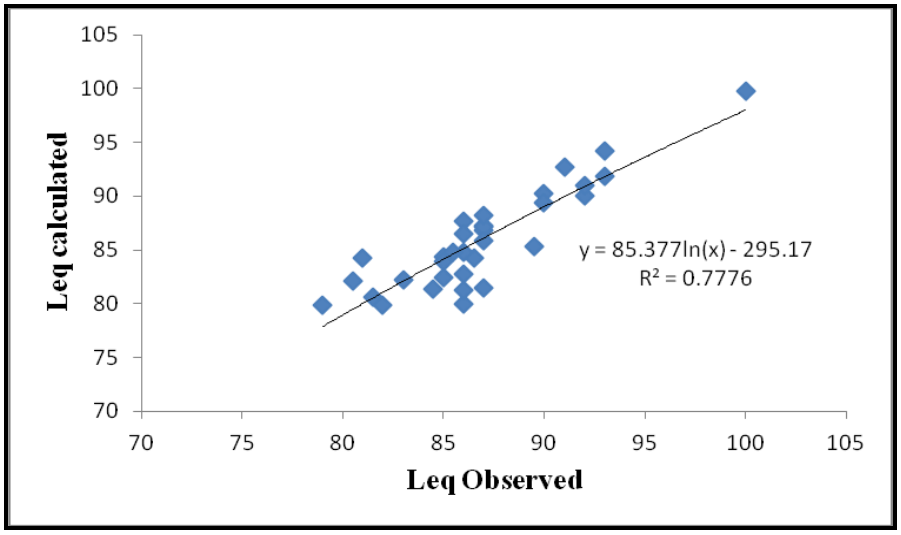

Figure 2: *Correlation Plot between Observed and Predicted Leq Values*

5. Conclusions

Leq values predicted from FHWA model were almost same to observed Leq values.

The developed noise prediction model is

$$\text{Predicted } Leq \text{ noise level value} = 85.3 \ln(\text{Observed Leq noise level value}) - 295.1$$

Hence, it can be concluded that FHWA model may be used for predicting noise pollution levels in Varanasi city. Vehicles, in fact, are forced to reduce their speed because of congestions, traffic jams and safety distance, resulting in a lower than expected equivalent level.

References

[1] Tanvir, S., and Rahman, M.M., 2011: *Development of Interrupted Flow Traffic Noise Prediction Model for Dhaka City.* 4th Annual Paper Meet and 1st Civil Engineering Congress, December 22-24, Dhaka, Bangladesh.

[2] Shukla, A.K., Jain, S.S., Parida, M., and Srivastava, J.B. *Performance of FHWA Model for Predicting Traffic Noise: A Case Study of Metropolitan City, Lucknow (India).* Transport. 2009. 24 (3) 234-240.

[3] Patil, V.K., and Nagarale, P.T. *Modeling of Road Traffic Noise in Selected Areas of Nashik City.* International Journal of Advanced Technology in Civil Engineering. 2013. 2 (1) 108-111.

[4] Koushki, P.A., Cohn, L.F., and Felimban, A.A. *Urban Traffic Noise in Riyadh, Saudi Arabia: Perceptions and Attitudes.* Journal of Transportation Engineering. 1993. 119 (5) 751-762.

[5] Koushki, P.A., Al-Saleh, O., and Ali, S.Y. *Traffic Noise in Kuwait: Profiles and Modeling Residents' Perceptions.* Journal of Urban Planning and Development. 1999. 125 (3) 101-109.

[6] Li, B., Tao, S., and Dawson, R.W. *Evaluation and Analysis of Traffic Noise from the Main Urban Roads in Beijing.* Applied Acoustics. 2002. 63 (10) 1137-1142.

[7] Barrigon Morillas, J.M., Gomez Escobar, V., Mendez Sierra, J.A., Vílchez Gómez, R., and Trujillo Carmona, J. *An Environmental Noise Study in the City of Cáceres, Spain.* Applied Acoustics. 2002. 63 (10) 1061-1070.

[8] Pandya, G.H. *Assessment of Traffic Noise and Its Impact on the Community.* International Journal of Environmental Studies. 2003. 60 (6) 595-602.

[9] Phan, H.Y.T., Yano, T., Phan, H.A.T., Nishimura, T., Sato, T., Hashimoto, Y., and Lan, N.T., 2008: *Social Survey on Community Response to Road Traffic Noise in Hanoi and Ho Chi Minh City.* Proceedings of ICBEN.

[10] Pathak, V., and Tripathi, B.D. *Evaluation of Traffic Noise Pollution and Attitudes of Exposed Individuals in Working Place.* Atmospheric Environment. 2008. 42 (16) 3892-3898.

[11] Kumar, P., and Tomar, V. *Monitoring of Traffic and Its Impact on Environment Using Geospatial Technology.* Journal of Ecosystem & Ecography. 2013. 3 (2) 123-127.

[12] Steele, C. *A Critical Review of Some Traffic Noise Prediction Models.* Applied Acoustics. 2001. 62 (3) 271-287.

[13] Barry, T.M., and Reagan, J.A., 1978: FHWA Highway Traffic Noise Prediction Model (No. FHWA-RD-77-108 Final Rpt.).

[14] Srivastava, J.B., Lal Pandey, B.B., and Kumar, B. *A Conceptual Approach for Determination of Passenger Car Noise Equivalence (PNCE) Factors for Indian Hill Highways.* Highway Bulletin Research, Indian Road Congress. 2003. 68; 145-156.

Cloud Publications
International Journal of Advanced Civil Engineering and Architecture Research
2018, Volume 4, Issue 1, pp. 89-99
ISSN 2348-5124, Crossref: 10.23953/cloud.ijacear.391

Research Article

Assessment of Dynamic Groundwater Reserve of Kamarup District Lower Assam, India

A. Bhuvaneswari Devi[1], Archana M. Nair[2]

[1]Research Scholar, Department of Civil Engineering, IIT Guwahati, 781001, India
[2]Assistant Professor, Department of Civil Engineering, IIT Guwahati, 781001, India

Correspondence should be addressed to A. Bhuvaneswari Devi, *bhuvi27@iitg.ac.in*

Publication Date: 7 December 2018

DOI: https://doi.org/10.23953/cloud.ijacear.391

Abstract Despite sufficient rainfall, a large portion of the northeast region of India suffers from water scarcity especially during dry seasons when groundwater acts as a significant source of water supply. Consequently, a proper assessment of groundwater condition at a district/block level is very much essential to adopt sustainable water management practices. Additionally, climate change and cross-border water disputes generate new challenges in the water management of Northeast India. In this study, an attempt has been made to present groundwater scenario of Kamarup district in lower Assam as a case study representing North-East India. For this purpose, we used the available temporal groundwater-level data derived from observation wells at five sites namely Agyathuri, Azara, Bamunigaon, Khara and Rangia located in the Kamrup district (lower Assam) of north-east India. The dynamic groundwater reserve (DGWR) has been estimated for the period from 1996 to 2006 using groundwater level data from these five sites along with monthly rainfall data and published pumping test data. This will help to analyze the groundwater dynamics of the study area. In order to cross check the obtained results, we used terrestrial water storage changes (TWS) derived from GRACE (Gravity Recovery and Climate Experiment) satellite data. TWS is a satellite-based monthly mean liquid water equivalent thickness with one degree spatial and monthly temporal resolution available from 2002. Terrestrial water storage includes the soil moisture, surface water equivalent and groundwater anomaly based on satellite observations of earth gravity field from the (GRACE). In the present study, TWS data was analyzed for over a period of 5 years from 2002 to 2006. The results of the study indicate that the maximum groundwater fluctuation was in the range of 0.84 to 3.48 m and minimum between -5.07 to -1.47m. Over the entire study area, we observed a decrease in dynamic groundwater reserves. From the trend analysis, it is obvious that there is an increasing trend of groundwater level at Khara, Rangia and Bumungiaon site and a decreasing trend at Agyathuri and Azara site. Further, the DGWR results showed that two sites (Agyathuri and Azara) were continuously subjected to stress from 1999 onwards. We observed that the DGWR and TWS are showing a comparable negative trend in the dynamic groundwater storage capacity for the study period. In the year 2004 the recorded TWS and estimated average_DGWR are relatively high during the study period. Thus, the results of this study provide a clear picture of spatial and temporal variations of dynamic groundwater resources in the study area, based on which important recommendations can

be made for managing the scarce groundwater resources of the study area in a sustainable manner to address future challenges.
Keywords *Groundwater reserve; Specific yield; Terrestrial water storage*

1. Introduction

The demand for fresh water is on an exponential increase due to the rapid growth of the population augmented by the subsequent increase in urbanization, industrialization as well as irrigation needs from agricultural sector. It was estimated that around 2.5 billion people worldwide depends purely on groundwater resources to satisfy their basic daily water needs (UNESCO, 2012). A global assessment on the groundwater consumption shows that countries such as India, China, Nepal, Bangladesh, and Pakistan are using nearly half the world's total groundwater resources (WWRD, 2015). Over exploitation of groundwater is a dominant concern for India as well as in many other parts of the world (Mutao et al., 2015). Moreover, the recharge process of the aquifer is impacted by the change in climate pattern and land use changes. Consequently, the conservation and management of groundwater resources is getting more attention from the scientific community. Likewise, the concept of conservation and management of groundwater resources have a noticeable role in adapting sustainable development. Therefore, an understanding of groundwater recharge process and assessment of groundwater recharge quantity is very essential. Numerous methods are available to quantify and monitor groundwater recharge that can be categorized as physical, chemical, analytical and numerical methods (Ahmadi et al., 2013 & Park 2012). Recent advancement in satellite based remote sensing techniques has led to the development of GRACE (Gravity Recovery and Climate Experiment) satellite which is widely used to evaluate the temporal changes in global ground water storage (Chinnaswami et al., 2015 & Richey et al., 2015).

In the present study an attempt has been made to understand the groundwater resource scenario of Kamrup district of lower Assam as a representation of the scenario of North East. Dynamic Groundwater Reserve (DGWR) of the study area was calculated with the available groundwater data from CGWB (Central Groundwater Board) using the guidelines provided by GWREC (1997). The method is found to be an effective method in calculating the status of groundwater in a region (Murasingh et al., 2015). Terrestrial water storage from GRACE data is found to be valuable in analyzing the regional trends in the groundwater as well as surface water scenario of North East region. In the present study, DGWR is validated with respect to the trends in precipitation as well as regional trends emerging from the analysis of terrestrial water storage.

The study area falls in the in the Survey of India Toposheet No. 78 W and No. 78 O and bounded by North longitude 25°42'03'' and 26° 50' 10'' and East latitude 91° 00' 01'' and 92° 10' 04''. The Kamrup district covers an area around 4,345 square kilometers and can be classified physiographical into three units namely the hilly region in the south, the alluvial plain in the central and western part and the swampy areas along Brahmaputra plains. The climate of the area has been classified as the sub-tropical humid climate with heavy rainfall, hot summer, and high humidity. The mean maximum and minimum temperatures recorded in the area are 12 to 38℃. The average annual rainfall of the area is about 1752 mm as per IMD records. The average number of rainy days in the district is 97 days in years. Based on variation in proportions of sand, silt, clay and organic material the soil group in the district are grouped into three broad categories district are grouped into three broad categories.

2. Methodology

Dynamic Groundwater Reserve (DGWR) of the study area was calculated for Kamrup district using well data available from CGWB (Central Groundwater Board) using the guidelines provided by GWREC (1997). Dynamic groundwater reserve is the optimum amount of water which an aquifer can

store or release at the maximum consumption. In this method, the groundwater storage or release is related to the hydraulic property of aquifer media (specific yield) and water level fluctuations. The following equation gives the Dynamic Groundwater Reserves:

$$DGWR = S_y(h_{pre} - h_{post}) - - - - - - - - - - - (1)$$

Where

Sy = Specific yield of aquifer media
h_{pre} = Depth to water level during pre-monsoon season of next year (L)
h_{post} = Depth to water level during the post-monsoon season of the current year (L)

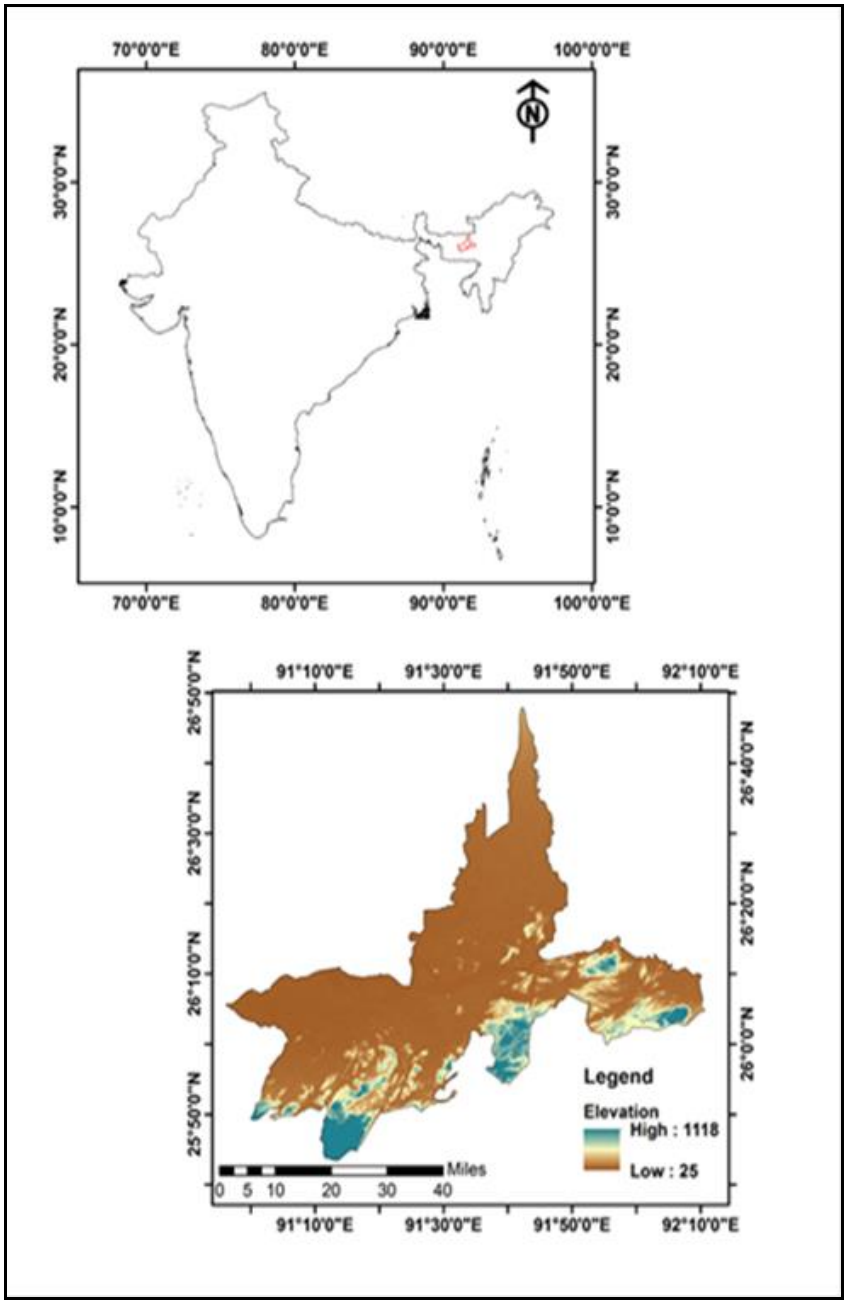

Figure 1: *Study area map*

Where depth to water level data (mbgl) were collected from Central Groundwater Board, India website. The CGWB, observes the groundwater level for entire India using a network of monitoring wells. For this purpose, CGWB measures water level depth four times in a year, in the month of January, April, August and November. This temporal variation in the depth of water level represents the seasonal variations in water level. In the present paper we discuss the analysis carried out for 10 years of water level data recorded by CGWB. The other major parameter used in the DGWR is specific yield, which is one of the major hydraulic property of an aquifer. The specific yield is estimated by CGWB based on in situ aquifer test and textural characteristics of soil sediments in the study area. The specific yield is a fraction of constant value for an area based on the textural characteristic of aquifer material (GWREC, 1997). The specific yield value used in the analysis is given in Table 1. The outline of the methodology adopted in this study is depicted in the flowchart (Figure 2).

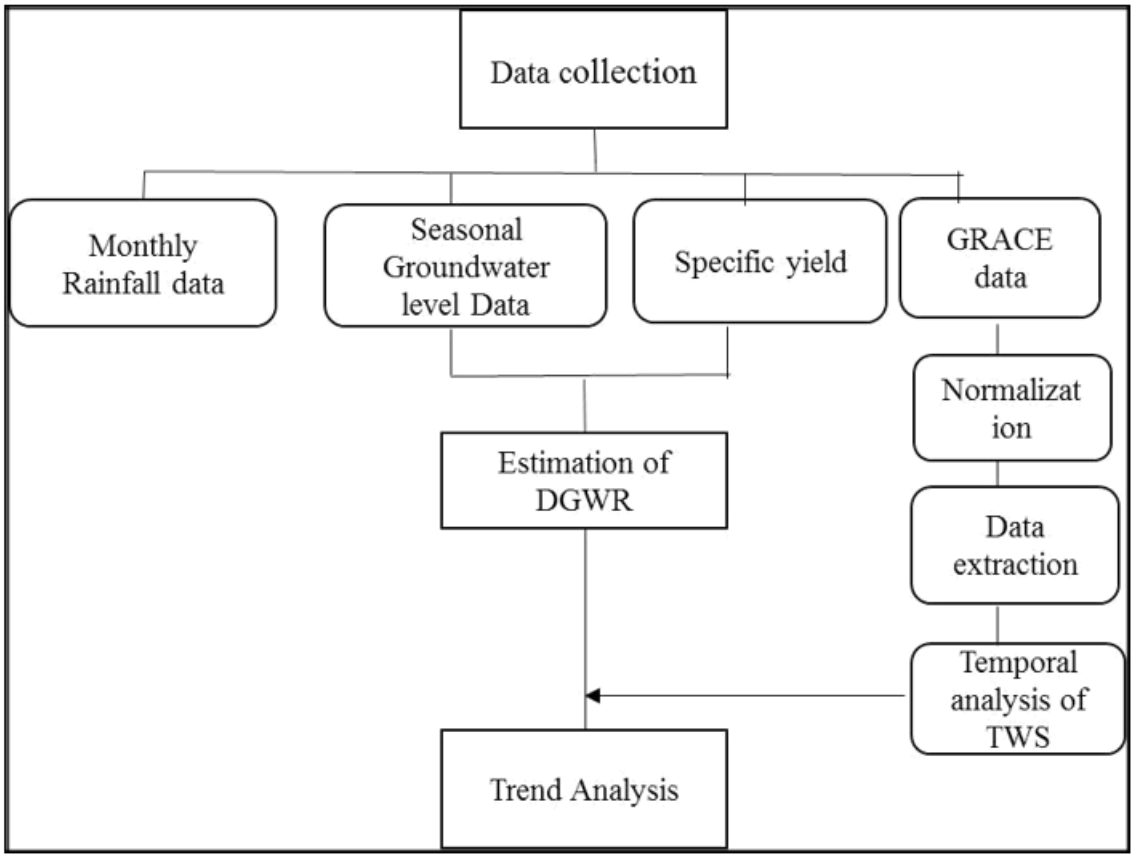

Figure 2: *Flowchart of methodology adopted in the present study*

Table 1: *Specific yield of geological formations based on the well locations (GWREC 1999)*

S. No	Site name	Geological formation	Specific yield
1	Hajo (Agyathuri)	Alluvium	0.2
2	Chandrapur	Alluvium	0.2
3	Chhaygaon (Bamunigaon)	Hard rock	0.04
4	Boko (Khara)	Alluvium	0.2
5	Palasbari (Azara)	Hard rock	0.04
6	Rangia	Alluvium	0.2

Terrestrial water storage (TWS) is one of the end products of satellite-based gravity measurement popularly known as GRACE, which continuously sample the variation in the Earth's Gravity field. GRACE mission was launched by US and German space agencies (NASA and DLR) in 2002. The spatial resolution of GRACE data is 1° by 1°with monthly temporal resolution. The TWS, or liquid water equivalent is a major component of the global hydrological cycle. In the present study, we used GRACE data to extract the TWS data for the entire region of North East, which includes the Kamrup district of lower Assam. For the analysis purpose, we considered only four years of TWS data that overlap the groundwater depth data available from CGWB. TWS change reflects natural variability in climate and is controlled through a series of processes and feedback mechanisms. The seasonal variation of TWS for the study area is illustrated in Figure 3.

The other parameters used in this study are monthly rainfall data. The rainfall data for the study area was obtained from Indian Metrology Department, Pune. For the analysis purpose, 10 years of rainfall data was considered. We considered the entire year in seasonal context as Monsoon I, Monsoon II, Post monsoon, and pre-monsoon in accordance with CGWC (1997). The seasonal variation of rainfall for a period of 10 years over the study area is illustrated in Figure 4.

3. Results and Discussion

In the present study, we identified five well locations for the study area from the network of wells monitored by CGWB. Depth to groundwater levels was analysed for these five sites of Kamrup district in lower Assam namely, Agyathuri, Azara, Bamunigaon, Khara and Rangia for a period of ten years from 1996 to 2006. Rainfall data of the study area for the same period was considered and the total rainfall for the entire year was separated in a seasonal context as Monsoon I, Monsoon II, Post monsoon, and Pre-monsoon. The average trend in the rainfall pattern shown an increasing trend with the highest rainfall contribution in the monsoon I season followed by pre-monsoon. In 2004, though the total rainfall shows an average trend, the area received the lowest rainfall in Monsoon I but highest rainfall in pre-monsoon period. The analysis of TWS from 2002 to 2006 shows that TWS is the highest during the monsoon I of 2004. This could be due to the fact that the groundwater recharge was maximum in 2004 as that year received the highest amount of rainfall during pre-monsoon.

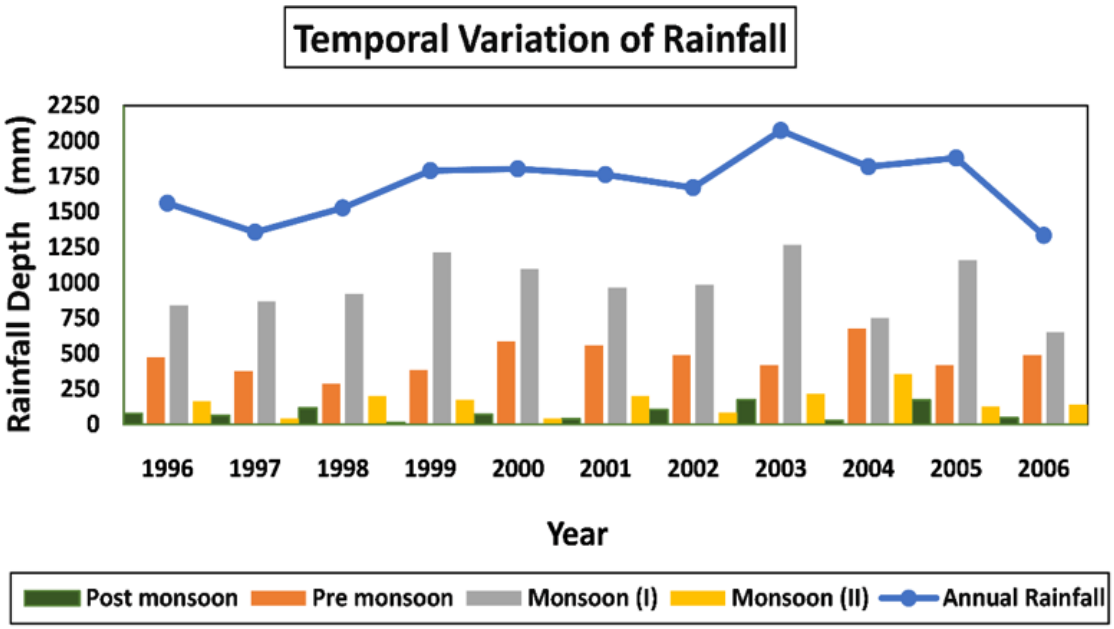

Figure 3: *Temporal variation of rainfall*

For the five well locations namely, Agyathuri, Azara, Bamunigaon, Khara and Rangia, the pre-monsoon depth to groundwater level ranges from 10.97 to 0.19 (mbgl) and the post-monsoon depth to groundwater level ranges from 10.15 to 0.35 m. Season-wise depth to groundwater level and seasonal fluctuations are tabulated in Table 2.

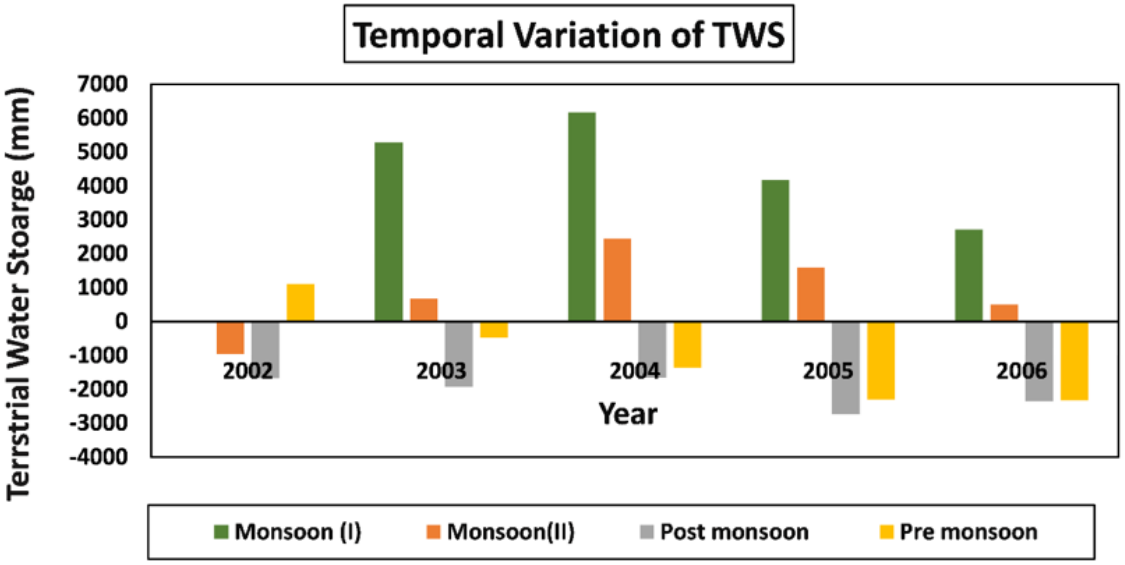

Figure 4: *Temporal variation of TWS*

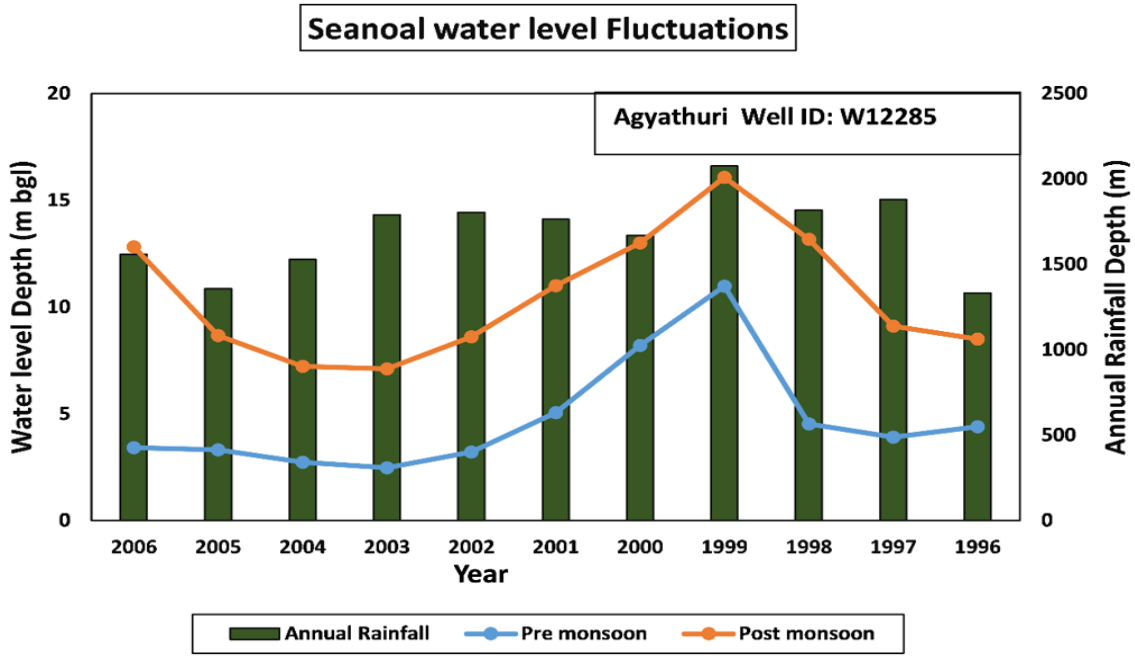

Figure 5: *Seasonal water level variations at Agyathuri*

Table 2: *Range of water level fluctuations at different sites*

Well id	Site name	The range of Level (mbgl)	Groundwater	Seasonal fluctuations	
		Pre-monsoon	Post monsoon	Maximum	Minimum
W12285	Agyathuri	10.97-2.47	10.15-4.1	3.48	-5.07
W12293	Azara	5.77-1.22	5.79-2.31	1.22	-2.97
W12275	Bamunigaon	4.96-1.97	4.4-3.6	0.84	-1.97
W12289	Khara	3.79-0.42	3.55-0.35	1.95	-1.47
W12300	Rangia	10.97-2.47	10.15-4.1	2.85	-2.47

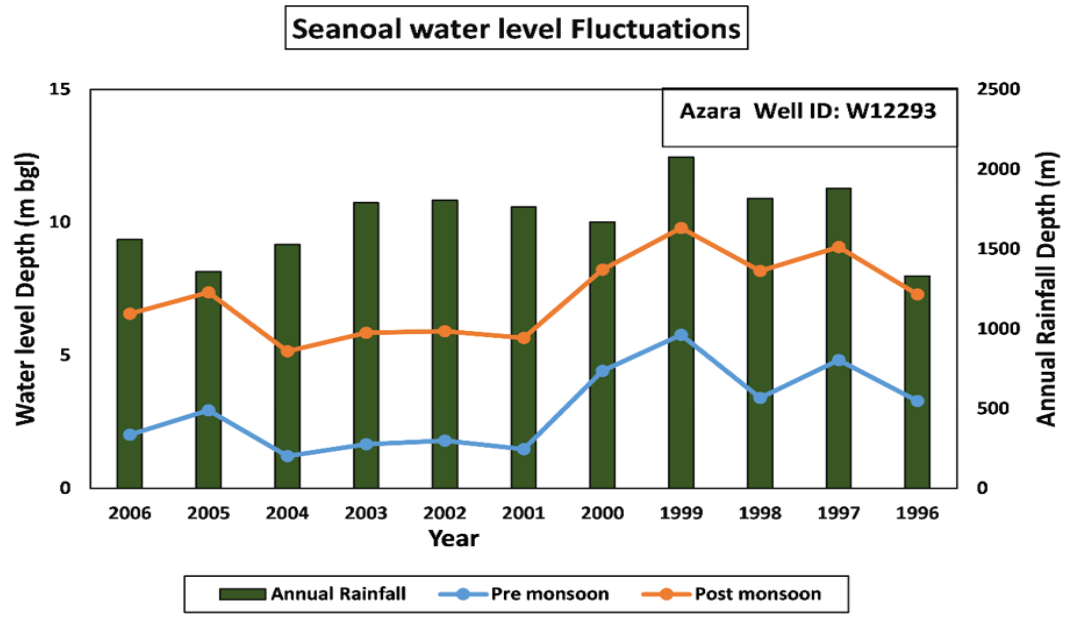

Figure 6: *Seasonal water level variations at Azara*

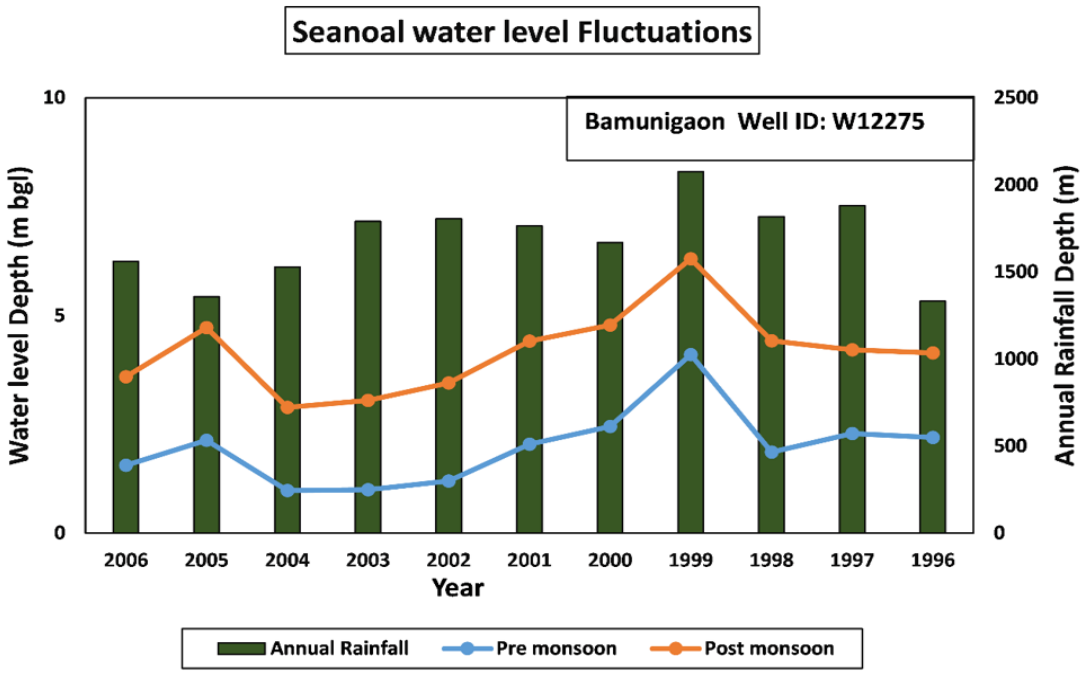

Figure 7: *Seasonal water level variations at Bumunigaon*

Moreover, the trends at all five sites were examined for the period from 1996 to 2006. At Agyathuri the water level was showing a declined trend from 2002 onwards both in the pre-monsoon and the post-monsoon seasons as shown in Figure 4. Azara site exhibit a change in the trend with a decreasing (year 1999-2001) and increasing trend (2004 to 2006) as shown in Figure 5. The groundwater level trend at Bamunigaon (Figure 6) site was more are less similar to the Azara. Figure 7 and Figure 8 shows a declining water level trend at Boko and Rangia. We observed that at all five sites the water level declination commenced from 2002 onwards even though the rainfall was higher than the previous years.

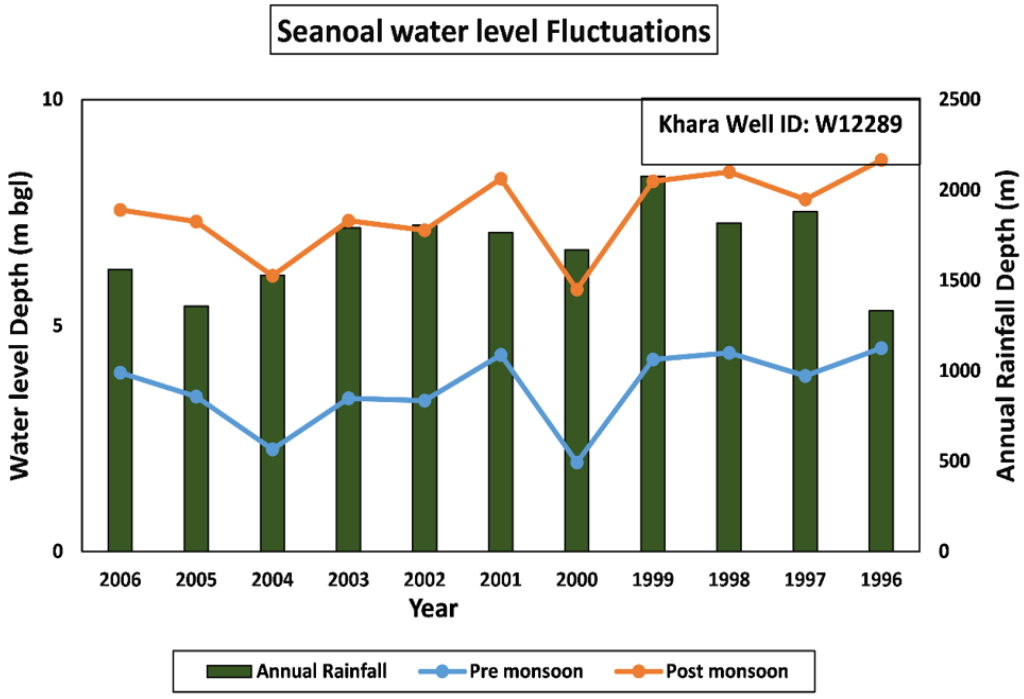

Figure 8: *Seasonal water level variations at Khara*

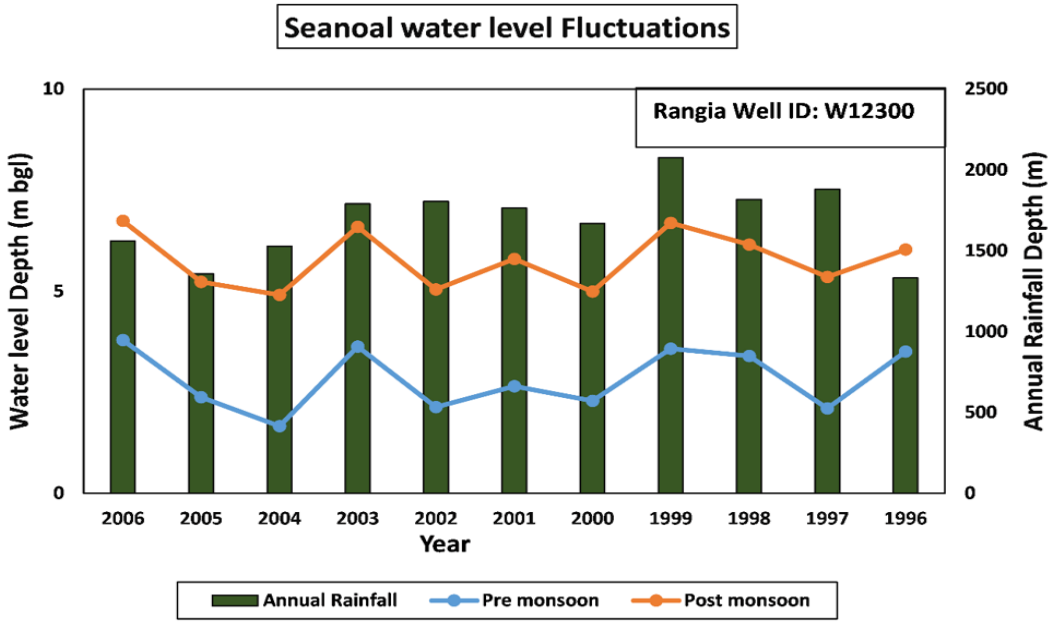

Figure 9: *Seasonal water level variations at Rangia*

Dynamic Groundwater Reserves

Dynamic groundwater reserve (DGWR) is the potential amount of water, which can be released or stored in an aquifer. In the present study we estimated the DGWR for ten years (1996-2006) from each well using the post and pre-monsoon water level data. Figure 9 illustrates the change in DGWR for a period of ten years. From the Figure 9, it is very much obvious that the DGWR is getting lowered with time for all the five locations at an alarming rate.

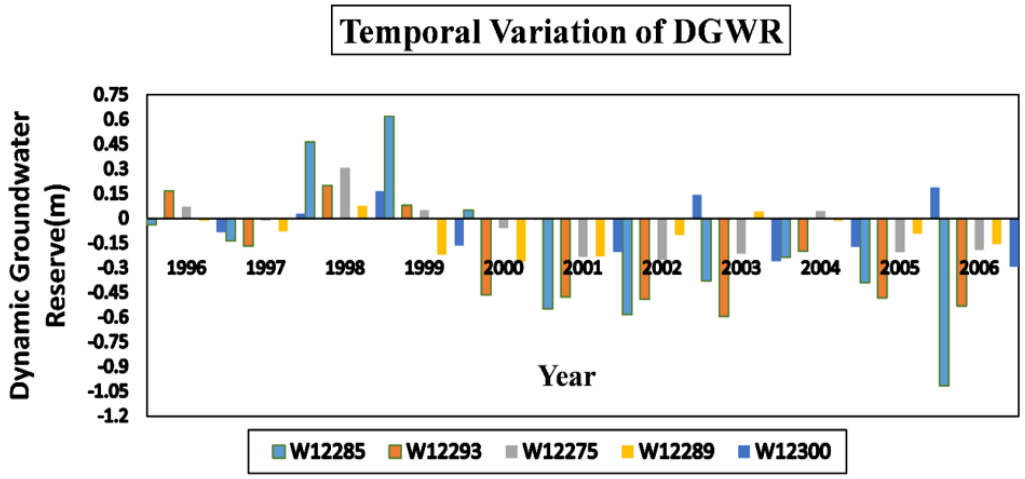

Figure 10: *Dynamic Groundwater Reserve*

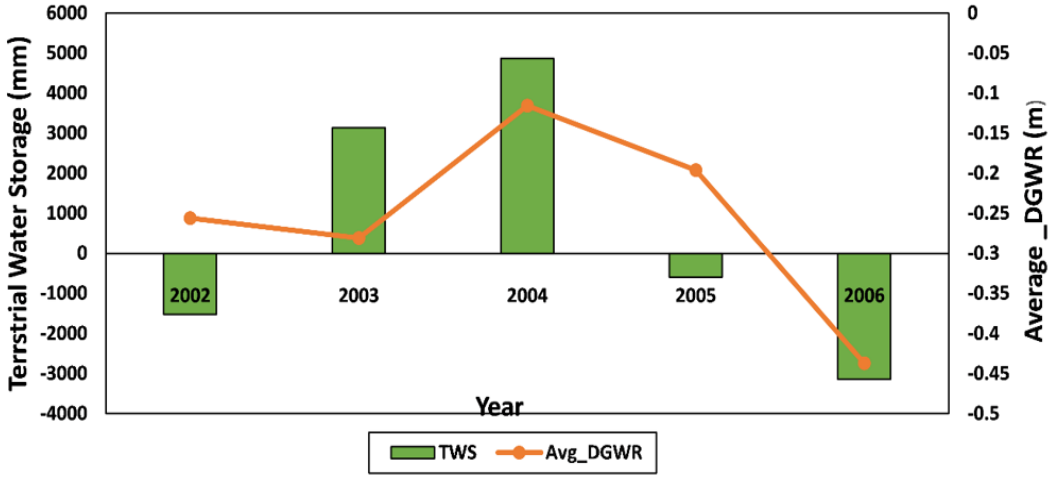

Figure 11: *Comparison of Dynamic Groundwater Reserve with TWS*

For the entire analysis, in 1998 and 1999 at few locations the DGWR was positive but with time the reserves are showing a gradual depletion. From the trend analysis, it is clearly indicating that at Agyathuri (Well ID: W12285) the DGWR are under more critical situation compared to other locations. At Bamunigaon (Well ID: W12275), there is consistency in results that are also under stress. At Rangia (Well ID: 12300) in the years 2002 and 2005 the DGWR was positive and in the remaining years the reserves are showing a negative trend. At Khara (Well ID: W12289) the trend is rising towards positive situation from 2002 onwards. At Azara (Well ID: W12293) location each year the reserves show distinct variations and those are negative in nature. Overall from results, we observed that availability of groundwater is in critical condition and further extraction of groundwater may lead to

a severe groundwater crisis in the district. An average value of DGWR was calculated for five years from 2002 to 2006 to do a comparative analysis with respect to TWS since TWS is on a regional scale. In the present study it was observed that the average DGWR computed for the five well sites for each year is showing a consistent trend with respect to TWS. The result is very much indicative of a decreasing trend in the groundwater reserves.

The DGWR and TWS trends are following the same pattern. In the year 2004, the recorded TWS and estimated average DGWR are relatively high. The results indicating that the DGWR and TWS are showing a comparable negative trend in the dynamic groundwater storage capacity for the study area.

4. Conclusion

In the present study, an attempt was made to know the groundwater scenario of Kamrup district of lower Assam district. The basis of this study is dynamic groundwater reserve at five sites of the study area for a period of 1996 -2006. The following things are observed during the study period.

- The maximum groundwater fluctuation was in the range of 0.84 to 3.48 m and minimum between -5.07 to -1.47m.
- From the trend analysis, it is obvious that there is an increasing trend of groundwater level at Khara, Rangia and Bumungiaon site and a decreasing trend at Agyathuri and Azara site.
- The two sites (Agyathuri and Azara) were continuously subjected to stress from 1999 onwards.
- The DGWR and TWS are showing a comparable negative trend in the dynamic groundwater storage capacity.
- Overall, we observe a decrease in dynamic groundwater reserves.

Thus, the results of this study provide a clear picture of spatial and temporal variations of dynamic groundwater resources in the study area based on which important recommendations can be made for managing the scarce groundwater resources of the study area. Such studies can motivate the policymakers and experts to formulate and implement effective, appropriate and sustainable response strategies to minimize the undesirable effects on groundwater.

Acknowledgement

We wish to thank the Central Ground Water Board, New Delhi, and Indian Meteorological Department Pune for providing water level and rainfall data for Kamrup District. We thankful to Indian Institute of Technology Guwahati for providing facilities during the study. The constructive comments of the reviewers and the editors are also gratefully acknowledged.

References

Ahmadi, T., Ziaei, A.N., Davary K. and Izadi, A.A. 2013. Estimation of groundwater recharge using various methods in Neishaboor Plain, Iran. *Journal of Groundwater Modeling and Management under Uncertainty*. International Groundwater Symposium, At Kuwait Institute for Scientific Research, Kuwait.

CGWB. 2013. Ground water information booklet of Kamrup & Kamrup Metro District, Assam.

Chinnasamy, P., Maheshwari, B. and Prathapar, S. 2015. Understanding groundwater storage changes and recharge in Rajasthan, India through remote sensing. *Journal of Water* 7, pp.5547-5565.

GWREC. 1997. Ground Water Estimation Methodology - 1997, Ground Water Estimation Committee (GWREC). Ministry of Water Resources, Government of India, New Delhi. Available from: *https://blogs.egu.eu/network/water-underground/2017/03/20/wtf-of-the-wtf-method*.

Murasingh, S., Wable, P. and Jha, M.K. 2015. *Groundwater scenario in South Tripura District of North-East India*. International Conference on Hydraulics, Water Resources and River Engineering, IIT Roorkee, Uttarakhand, India.

Mutao, H. and Yong, T. 2015. *Prediction of groundwater level for sustainable water management in an arid basin using data-driven models*. International Conference on Sustainable Energy and Environmental Engineering.

Park, E. 2012. Delineation of recharge rate from a hybrid water table fluctuation method. *Journal of Water Resources Research,* 48, pp.1-6

Richey, A.S., Thomas, B.F. and Rodell, M. 2015. Quantifying renewable groundwater stress with GRACE. *Journal of Water Resources Research*, pp.5217-5238.

Cloud Publications
International Journal of Advanced Civil Engineering and Architecture Research
2019, Volume 5, Issue 1, pp. 100-113
ISSN 2348-5124, Crossref: 10.23953/cloud.ijacear.421

Research Article

Spatial Strategies for Crowd Management in Haridwar, India

Sindhuja Kasthala[1], Binoy B.V.[2], Harshit S. Lakra[3]

[1]Research Scholar, Climate Studies, IIT Bombay, Mumbai, Maharashtra, India.
[2]Research Scholar, Department of Architecture and Planning, NIT Calicut, Kozhikode, Kerala, India.
[3]Assistant Professor, Department of Architecture and Planning, IIT Roorkee, Roorkee, Uttarakhand, India.

Correspondence should be addressed to Binoy B.V., *binoy9344@gmail.com*

Publication Date: 27 July 2019

DOI: https://doi.org/10.23953/cloud.ijacear.421

Abstract Crowd-related hazards are prevalent in densely populated countries like India where there is increase in the number of visitors to religious gatherings (NDMA, 2014) and the major task of authorities lies in reducing the risk of crowd disasters. The purpose of this work is to spatially analyze the crowd management and emergency preparedness strategies formulated by authorizes for the safe conduction of the *Ardh Kumbh* Mela, 2016 in Haridwar with the help of tools and technologies. In this paper, we examine the potential of using technologies like Remote Sensing and Geographical Information System (GIS) for evaluating and recommending guidelines for crowd management and emergency response. The study was largely dependent on field visits during the 2016 *Ardh Kumbh* Mela and it attempted to capture the merits and demerits of the proposed crowd management strategies such as the major crowd flow routes, infrastructure facilities, critical crowd management and emergency routes to hospitals. Various analyses like crowd capacity analysis, infrastructure scoring, and crowd flow analysis helped to recommend guidelines for Crowd Control Management.
Keywords *Mass gathering; Crowd management; Crowd flow; Kumbh Mela; Emergency response*

1. Introduction

India with its increasing population (Census, 2011) attracts a large number of people to gatherings and pilgrimages such as *Kumbh Melas, Rath Yatra, Thrissur Pooram, Ramzan* and *Durga Puja*. Over the years, several tragedies in mass gatherings caused fatalities and the greatest task lies with effectively managing the crowd and prevent the loss of control over mass (Hanna, 1994). Lack of information about the expected number of people visiting makes it difficult to successfully plan the event and effectively manage the crowd. World Health Organization (2008) defined Mass gatherings as 'more than a specified number of persons (may be as few as 1000, although the available literature refers to gatherings exceeding 25,000 persons) at a specific location for a specific purpose for a defined period of time'.

Haridwar, prominent spiritual and religious city in the state of Uttarakhand, is known for its temples and bathing Ghats. *Ghat* refers to a series of steps leading to a holy body of water, in this case, the river Ganges, which is considered sacred in the Hindu tradition. Pilgrims come from all over the world to take a holy dip in the Ganga at the most revered location of Haridwar, *Har-ki-paudi*. Haridwar is one

of the four venues in the country to host *Kumbh Mela* and *Ardh Kumbh Mela*, once every 12 years and 6 years respectively (Mehrotra, 2015). Mela refers to a cultural or religious fair or a festival and *Kumbh* is 'repetitively described as microcosm of India' (Maclean, 1968). The *Kumbh Mela* is held for about one and a half month with people participating from all over the world and there is no precise method to determine the number of people taking holy dip on an auspicious day. Haridwar is home to various fairs and gatherings throughout the year which makes it vulnerable to crowd-related hazards including but not limited to stampedes, fire, and epidemics (Mohd Arif Shuib, 2013).

Mehrotra (2015) with a team from Harvard University has investigated and documented the large-scale Allahabad *Kumbh Mela* of 2013 with the participation of approximately 34 million, monitored from its preparation stage to the actual celebrations. He spoke about the construction activities carried out in the city in terms of its scale and complexity and documented the most interesting elements of the process such as the functionary temporary structures and bridges, housing, transport, and emergency services. Alongside addressing the complex construction and destruction of the city given the scale of the city and compressed timeframes the team also identified and addressed many complex issues related to but not limited to crowd and resource management.

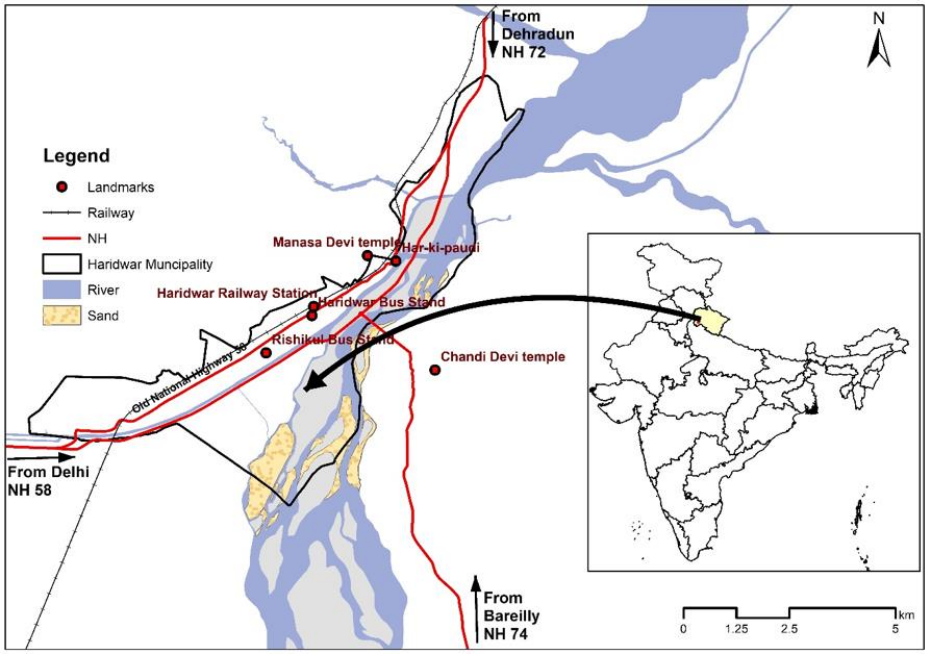

Figure 1: *Study area map*

Bihar State Disaster Management Authority (2013) studied the details of operational planning of Allahabad *Kumbh Mela* and captured the best practices that could be adopted by other states and countries all over the world for planning any mass gatherings. National Remote Sensing Centre (ISRO) & Uttarakhand Space Application Centre (2011) combinedly developed a methodology for estimating pilgrims present in *Kumbh* area on an auspicious day in 2010 Haridwar *Kumbh Mela*. The integrated data from space-based remote sensing technology and ground-based data for estimating the number of pilgrims. Various works (Mehrotra, 2015; NDMA, 2014; Sindhuja, 2015; Jeffrey Tubbs, 2007; Rani, 2017; Sultan, 2015; M Devi Anju, 2016; Hanna, 1994; BSDMA, 2013) abetted to understand the management of mass gatherings and derived useful recommendations for event organizing and safe crowd management.

This article is an attempt to evaluate the crowd control and management strategies, and emergency response strategies formulated by authorities during a mass gathering in Haridwar. With the help of

field observations, GIS and Remote Sensing technologies we have spatially analyzed the strategies laid by government authorizes during 2016 *Ardh Kumbh Mela*. Documentation and evaluation of strategies implemented during any gathering will help the authorities to learn from the past and effectively plan the upcoming gatherings. Various analyses like the crowd capacity analysis and crowd flow analysis were conducted and the suggestions were used in formulating the preparedness measures. The paper aimed at constructing certain guidelines for better crowd control and management in the case of Haridwar.

Study Area

The study area, Haridwar municipality (**Error! Reference source not found.**), lies between 78°50'E - 78°11'E longitude and 29°54'N - 29°59'N longitude encompassing a geographical area of 23.7 km^2. The *Kumbh Mela* area outspreads the municipality to an approximate area of 130 km^2. Haridwar with a current population of 0.2 million and mean floating population of 0.16 million attracts an annual average of 8 million tourists (Appraisal of City Development Plan, Haridwar, 2007). The growth rate of the floating population was estimated to be 2.5% per annum which is slightly above the national average of 2% per annum. The city which is home to spiritual societies and ashrams is attracting a large number of people with its industrial development as well. The unparalleled influx of visitors during *Kumbh Mela* creates tremendous pressure on the infrastructure facilities and natural resources.

Indian National Trust for Art and Cultural Heritage (INTACH) undertook 'Cultural Resource Mapping of Haridwar District' and listed 164 cultural resources in Haridwar which included temples, ashrams, Ghats, sacred waterbodies, rituals and other. *Har-ki-paudi* is one of the holiest places on earth for Hindus, the ancient ghat is of prime importance and a registered society carries out its maintenance activities and *Ganga Aarti* in the evenings. Notable Ghats in Haridwar besides *Har-ki-paudi* are *Gau ghat, Astipravah ghat,* Malviyadweep, Subash ghat, and *VIP ghat*, which are only a few in many.

The city has restricted physical expansion due to hills and reserved forests to the North-west and south-east, and the river which flows from North-east to the south (City Development Plan: Haridwar. Revised Under Jawaharlal Nehru National Urban Renewal Mission (JNNURM), 2007). The development is linear along the main corridor of the city confining within the municipal boundary. The old areas witness high-density unplanned development without proper infrastructure and road hierarchy. Lack of sufficient parking areas, narrow roads, unplanned commercial establishments in ghat areas, traffic junctions etc. are causing severe traffic problems and danger to pedestrian movement.

Whole new temporary city mushrooms along the river bed during *Kumbh Mela* to facilitate the tourists coming from all over India and other parts of the world. The authorities are often challenged to provide basic facilities for the tourists including but not limited to shelter, roads, electricity, sanitation, and hospitals, thus establishing a "temporary city". The Mela area extends from Haridwar to Rishikesh and has been divided into 31 sectors and those in and around Haridwar are shown in **Error! Reference source not found.**. Most of the sector areas are on the floodplains while a few are in the open lands of the industrial and residential neighbourhood. The residential tents will be provided to the pilgrims in the sector areas, but the availability and accessibility of these amenities are often questionable.

The most important and busy route of Haridwar is the Haridwar main road (old NH) which goes through the municipal area connecting principal areas like Railway station and bus stand. From the main road the traffic flows to *Har-ki-paudi* through *Upper-road* and *Lower-road*. In Haridwar the primary bus terminal which is located opposite to the railway station will be closed during mela periods as the surrounding areas will be pedestrianized. Instead of that, the *Rishkul ground* which is closer to

the national highway will be used as an alternative bus terminal to cater the increasing demand. A new transportation plan will be executed during mass gatherings, often developed by city police under the supervision of the commissioner.

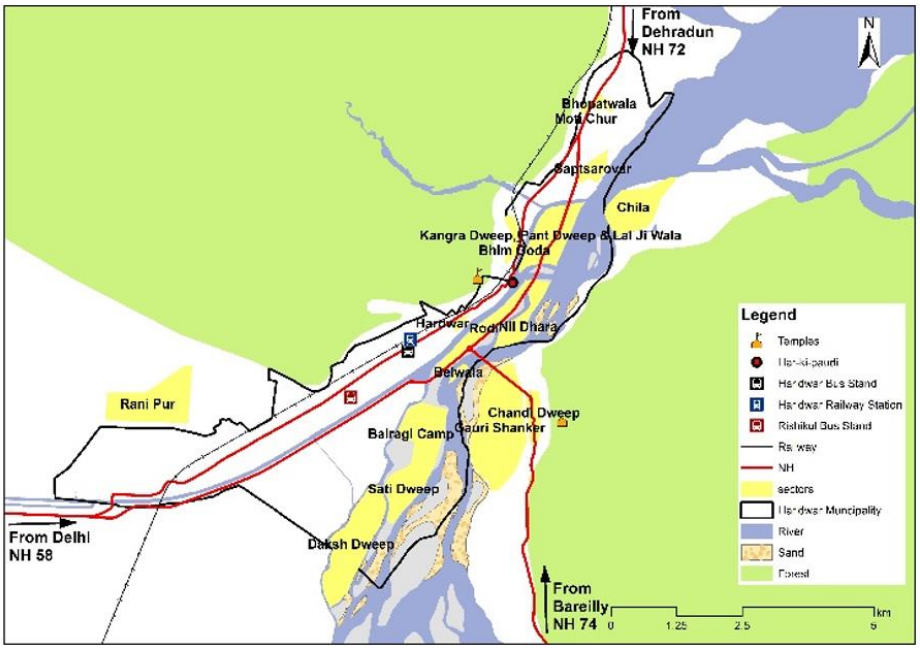

Figure 2: *Kumbh mela sector map*

2. Methodology

The study comprises two main components, field study and spatial analysis in the digital environment. Most of the primary data collection was carried out during the Haridwar *Ardh Kumbh Mela*, 2016. The primary data was collected through field visits, reconnaissance survey, questionnaire, interviews, photographs, and satellite imagery. Interviews were conducted with Mela officials and other prominent people for understanding the measures taken during the event. An observational study was undertaken to identify the existing infrastructure facilities which include structural, transport, security & information and amenities & utilities. The checklist further extends to understand the movement of the crowd and its behavior by identifying crowd triggers and interrupters in an area. Infrastructure scoring was carried out to understand the positive and negative influence of infrastructure facilities on crowd movement.

The secondary data includes information from *Ardh Kumbh mela* (2016) media Centre, user manuals, books, and newspapers. Scanned map of the municipal boundary was obtained from City Development Plan (CDP), which was georeferenced and digitized in GIS to produce the vector boundary of the study area Attribute data collection was conducted through extracting information from various sources such as google maps, field surveys, and CDP. Multispectral Sentinal Satellite images of the 10-meter resolution obtained from USGS for the year 2016 were found to be useful in the preparation of GIS base layers due to its medium resolution. Adequate help was taken from Google Satellite images and ArcGIS Online imagery since both are very high-resolution imagery. Various thematic layers such as Waterbody, Forest, Bridges, Roads, Parking areas and flood plains are digitized from Satellite imagery. Google Imagery and ArcGIS imagery helped in identifying and correcting the missing features in the maps and Web Mapping Services (WMS) like Google Maps, Wikimapia and Bhuvan helped in identifying the landmarks including but not limited to Major Temples, Ghats, Hospitals and Fire stations. The locations of landmarks obtained from online sources are

converted into GIS points and stored as layers in the GIS database which are later verified during filed visits. Thematic maps such as sector map, Parking map, and crowd flow map are prepared with the help of field data, satellite images and city development plan (CDP).

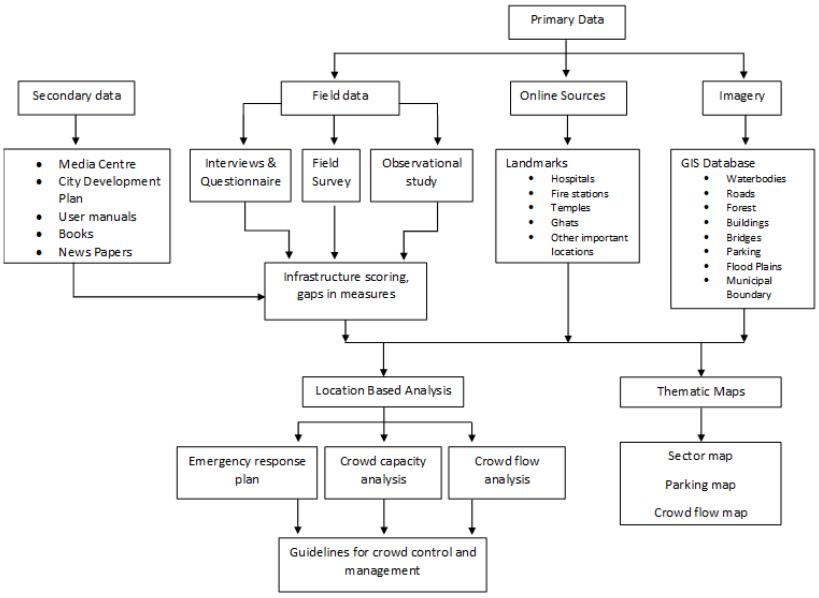

Figure 3: *Methodology flow chart*

Spatial analysis of the data was carried out to analyse the strategies laid by authorities and to eventually derive certain guidelines for crowd control and management. The crowd flow in and out of the city was studied in detail and areas with critical crowd movement were identified. The crowd capacity analysis carried out in *Har-ki-paudi* area can act as a major preparedness measure for crowd control. The crowd carrying area of *Har-ki-paudi* was calculated using GIS to compute maximum crowd capacity of the area. After spatially representing the emergency response plan laid out by authorities in *Ardh Kumbh* 2016, the appropriateness of the emergency response strategies was checked and emergency response routes to hospitals and fire stations were identified. Based on the analyses we have framed the lessons learned from the *Ardh Kumbh Mela* 2016 and the guidelines for crowd control and management are proposed.

3. Results and Discussion

Even though the 2016 *Ardh Kumbh mela* is a success in any measure, the city of Haridwar can further improve in view of upcoming *Kumbh melas* and other gatherings. Adequate field studies during *Ardh Kumbh mela* combined with GIS spatial analysis provided a sight of the issues faced during mass-gatherings in Haridwar. The findings of the study are organized into 4 key segments for further discussion: inferences from field observations, infrastructure scoring, crowd flow analysis, crowd capacity analysis, and emergency response plan.

3.1. Inferences from Field Observations

Field studies showed the lack of awareness regarding the main procession routes and alternative routes and hence causing irregular movement of people in all directions in the surrounding roads. The people coming from *Rishkul* Bus stand and Railway station areas were supposed to take a turn and walk through the Rodi Belwala sectors to eventually reach *Har-ki-paudi*; instead, many people took

the upper road and lower road to reach *Har-ki-paudi* which was solely for the people coming back from *Har-ki-paudi.*

The absence of adequate parking areas which led to unplanned on-street parking along the main road hindered the movement of crowd and vehicles. The road outside the railway station got congested because of the on-road parking of rickshaws and taxis. Due to improper execution of guidelines vehicles are parked even near railway station which should be vehicle free during *mela* days. Pedestrianized upper and lower roads faced encroachment by street hawkers, one of the main causes of crowd congestion. During normal days, the mixture of pedestrian and vehicular traffic along the Ghats due to lack of proper regulations creates safety issues for the people. The absence of designated parking areas near the Ghats results in hectic parking and obstructs the pedestrian flow.

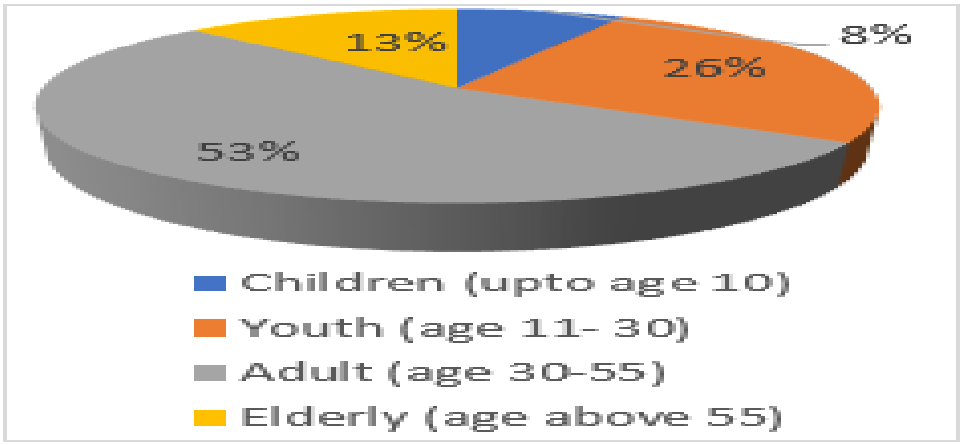

Figure 4: *Age profile of the visitors (Raheja, 2015)*

	Structural	Transport	Information and Security	Amenities and Utilities	Crowd Triggers	Crowd Interuptions
Bus Stand	0.6	-0.2	1	0.67	-0.5	-0.67
Railway Station	0.7	-0.29	1	0.89	-0.67	-0.67
Shiv-murthi Junction	0.5	-0.75	1	0.87	-1	-0.83
Mela Office	0.83	1	0.9	0.7	-0.83	-0.33
Kangra Dweep	1	0	1	1	-0.16	-0.33
Rodi Belwala	0.7	-0.29	1	0.89	-0.67	-0.67

Figure 5: *Infrastructure scoring*

Diversity in visitor's age, gender, abilities and group size in combination with their movement pose unique issues. The ghat areas are not easily accessible by elderly and persons with disabilities. The demographic profile of the pilgrims visiting the Ghats over a year reflects a higher percentage of elderly with a good number of children and women in **Error! Reference source not found.**. Nearly 50% of the tourists are women and 21% of the total visitors constitute children (up to age 10) and elderly (Raheja, 2015). The ghat of *Har-ki-paudi* was observed to be at an elevation difference of 6-9 meters which is accessible by stairs and there is no provision of ramps or elevators for the elderly.

3.2. Infrastructure Scoring

Infrastructure scoring is given for selected nodal points by using infrastructure checklist which broadly has been categorized into structural, transport, security & information and amenities & utilities. The observational study conducted identified the strengths and weakness of the existing infrastructure facilities. The checklist further extents to understand the movement of the crowd and its behavior by identifying the crowd triggers and interrupters in the area. The study nodes are identified based on the complex crowd flow patterns and congregations. The observational survey required for the infrastructure checklist was carried out during *Ardh Kumbh Mela*, 2016 with the purpose of including the temporary amenities and structures in the checklist. The categories and subcategories in the checklist are defined based on the Causes and Triggers for Crowd Disasters listed by NDMA in the National Guide on Crowd Management (NDMA, 2014). For example, railings, barricades, lighting, temporary structures, staircases, and ramps come under the category of structural. Based on the existence or non-existence of an infrastructure element and its positive or negative influence on the crowd movement, the scores are given (Table 1).

Table 1: *Criteria for the provision of scores for elements in infrastructure scoring*

Criteria	Provision Score
Existence of an infrastructure element (positive influence)	1
Existence of an infrastructure element (Negative influence)	-1
Non-existence of an infrastructure element (positive influence)	-1
Non-existence of an infrastructure element (negative influence)	1
Non-relevant infrastructure for the location	0

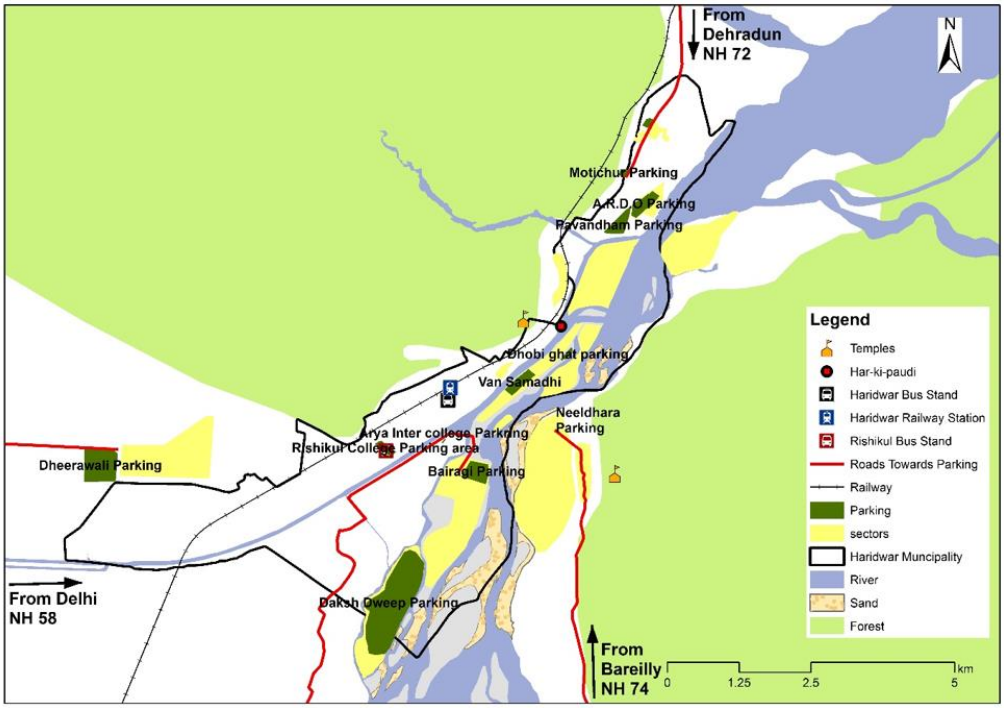

Figure 6: *Major parking areas*

For example, lighting is needed for proper crowd movement and the absence of the same can hinder crowd flow and trigger a crowd disaster. Therefore, under the criteria ‘existence of an infrastructure

element (positive influence) the score will become '1' and for the absence of lighting the score will be given as '-1' under criteria 'Non-existence of an infrastructure element (positive influence)'.
The scores of all elements/ subcategories are averaged to get the overall score of each category (**Error! Reference source not found.**). The analysis carried out in excel identified the strengths and weaknesses of infrastructure at various locations. Based on the analysis, most of the places have excellent structural facilities with *Mela* office (0.83) in the top and Shivmurthi junction (0.5) at the bottom. Likewise, the other elements- information & security and amenities & utilities also showed positive results. Transport showed negative results due to the presence of on-street parking and encroachments on footpaths. The categories- crowd disaster triggers and Crowd movement interrupters, showed negative values which showed the magnitude of triggers and interrupters in those areas. The Focus should be laid on reducing the triggers and interrupters for safe crowd management in a mass gathering.

3.3. Crowd Flow Analysis

The mapping of people's primary activities in *ghat* combined with their secondary activities such as vending, and parking helped in defining crowd flow patterns. This section discusses crowd flow pattern at the city level and crowd flow in *Har-ki-paudi* area at a detailed level.

The proportions of the traffic flow into the city of Haridwar as given by the authorities are 55% from NH 58 (from *Delhi, Meerut, and Muzaffarnagar*), 25% from NH 74 (*Saharanpur* direction) and 15% from NH 72 (*Dehradun* direction). The major parking areas that are used to accommodate the traffic flow during the *mela* days for both government and private vehicles are shown in **Error! Reference source not found.** along with major routes that carry traffic into the city. The major parking areas even though located far away from the *Har-ki-paudi* area are very easily accessible from residential sectors.

The major crowd flow routes during mass gatherings in Haridwar were identified and represented in **Error! Reference source not found.**. The crowd flow in and out of *Har-ki-paudi* during *Kumbh Mela* days is majorly through three directions: through *Rodi Belwala*, through *Neeldhara*, and through *Kangradweep*. People coming from Jwalapur-commercial area, Khankal-old town area and old National Highway go to *Har-ki-paudi* through *Rodi Belwala* sector direction. The crowd from NH72 pass through *Kangradweep* to reach *Har-ki-paudi*. All the crowd coming from *Neeldhara* and *Rodi Belwala* directions reach *Har-ki-paudi* traveling through the temporary bridges. Four new temporary bridges are constructed during every mass gathering as an alternative to the narrow roads to *Har-ki-paudi.*

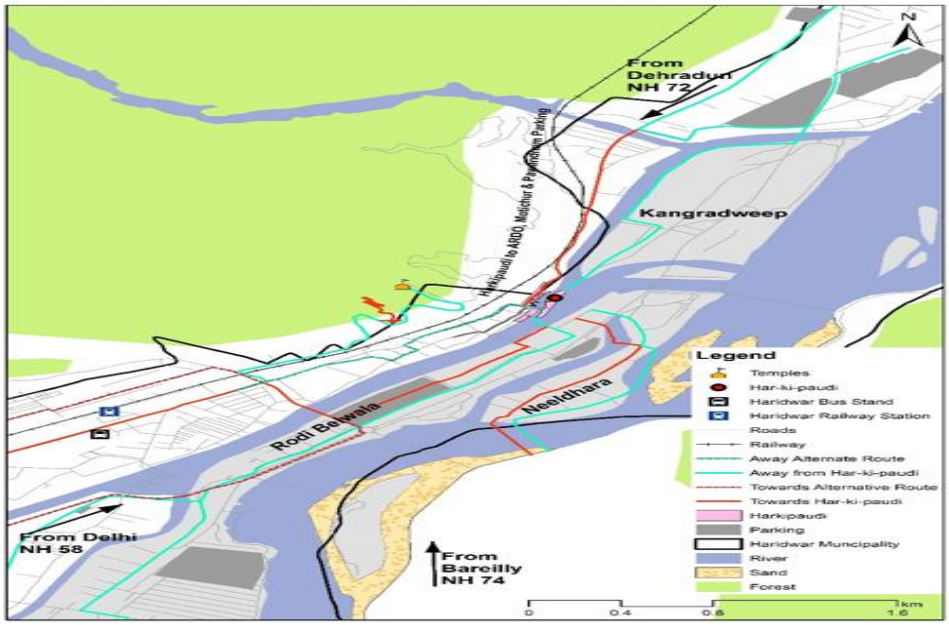

Figure 7: *Crowd flow in and around Har-ki-paudi area*

Har-ki-paudi is connected to the other side of the river with four temporary bridges besides one permanent bridge during mass gatherings and the crowd flow in *Har-ki-paudi ghat* area is shown in **Error! Reference source not found.**. Among the four temporary bridges connecting the *Har-ki-paudi* with sector areas, three carry the crowd towards *Har-ki-paudi* while the other carries the crowd outside towards *Neeldhara*. The crowd should flow out of *Har-ki-paudi* through seven exits out of which five open to upper road and one open to lower road. Crowd flow into *Har-ki-paudi* is through five ways: two permanent bridges and three temporary bridges. *Har-ki-paudi* is located at a lower elevation from the abutting road and is accessed through staircases.

The field study identified certain crowd flow issues as well as the elements acting as triggers for crowd hazards. Several puja stalls on the ghat steps which are beside the temple complex are interrupting the crowd flow and increasing the crowd density. One temporary bridge which has a direct opening to ghat steps has the possibility to exponentially increase the crowd density. Lack of emergency entries and exits from *Har-ki-paudi* is one major issue. Controlled entries and exits should be implemented to reduce the risk of crowd congestion in the area.

3.4. Crowd Capacity Analysis

Har-ki-paudi, the prominent ghat, needs to accommodate the increasing demand from pilgrims. The maximum allowable number of tourists in the *Har-ki-paudi* area is not determined specifically whereas implementation of any strategy should be based on the expected crowd size. The estimates as per *mela* authorities during the interviews about the maximum crowd capacity of *Har-ki-paudi* area was lacking authenticity and are merely rough approximations. Determining the crowd capacity of the available area helps authorities in controlling and regulating the crowd more effectively.

For crowd capacity analysis, detailed mapping of *Har-ki-paudi* area was carried out to demarcate areas with crowd movement (**Error! Reference source not found.**). By excluding immovable features such as temples, clock tower and stalls the remaining area was calculated in GIS. The probable crowd carrying area was calculated to be 15,120 m^2 of levelled ghat surface, 620 m^2 wet/slippery surface and 1159 m^2 of steps in *Har-ki-paudi* ghat.

The maximum density that can be allowed in case of rainy and slippery conditions is only 2 p/m^2 (persons per square meter) (Oberhagemann, 2012). For static (immobile) crowds, 5 p/m^2 is the maximum allowable limit and even allowing 6 p/m^2 is high risk as per Still (2014). As per a report by Oberhagemann (2012) the densities of 5-6 p/m^2 must not be exceeded for static crowds. For dynamic (moving) crowds the acceptable limit is 1.5 p/m^2 and the critical limit is reached at 2 p/m^2 (Oberhagemann, 2012).

Crowd capacity of *Har-ki-paudi* was calculated for two different scenarios using maximum allowable crowd densities. The first scenario considered the ghat area to have the static crowd, which is the case during occasions like Ganga Aarti or other special worships. The second scenario assumed typical ghat activities and considered the crowd to be dynamic. The crowd capacity gives the maximum number of persons that can be accommodated in the area at any given time.

The maximum number of individuals that can take a dip in *Har-ki-paudi* area depends on ghat length and is calculated based on the approach employed by Mehrotra (2015). The length of the ghat was calculated to be approximate 1100m. Taking 0.5m as an average width of the human body nearly 2200 individuals can line up side by side. Thus, 6600 individuals can be accommodated if people stack up in 3 layers. Taking into consideration that people take holy dips for 14 hours, i.e., from 5 a.m. to 7 p.m. and if a devotee takes an average time 5 min for a holy dip then nearly 1,108,800 individuals can take a dip in *Har-ki-paudi* area. Considering 24 hours of time, if specials arrangements are made, nearly 1,900,800 people can take holy dips in *Har-ki-paudi* area. Taking the fact that nearly 17 million (USAC & NRSC, 2011) took baths on Shani-Snan day on April 14, 2010, *Kumbh Mela*, all the tourists cannot visit and take a dip in *Har-ki-paudi* without increasing the risk of the area.

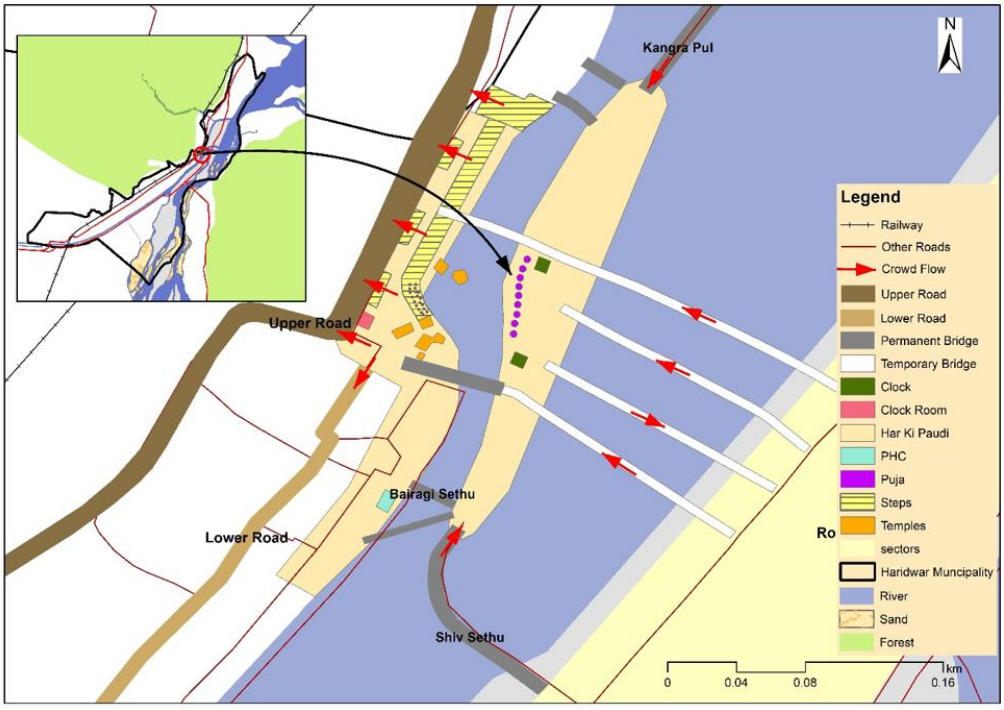

Figure 8: *Har-ki-paudi crowd flow map along with direction of crowd flow*

Table 2: *Crowd Capacity of Har-ki-paudi area*

Scenario	Crowd count in static and dynamic crowd zones (in persons)	Crowd

	Leveled ghat area- 15,120 m^2	Slippery area- 620 m^2 (Critical limit - 2 p/m^2)	Ghat steps area- 1159 m^2 (Critical limit - 2 p/m^2)	capacity (persons)
Scenario 1 (Static crowd)	15120*5=75,600 (Critical limit- 5 p/m2)	620*2=1,240	1159*2=2,318	79,158
Scenario 2 (Dynamic crowd)	15120*2=30,240 (Critical limit- 2 p/m^2)	620*2=1,240	1159*2=2,318	33,798

3.5. Emergency Response Plan

Field visits aided in the identification of certain emergency plans premeditated by the authorities that will be laid down if the inflow increases suddenly. In case of emergencies like a stampede in *Har-ki-paudi* or if the crowd capacity exceeds the limit, the crowd will be held in holding areas. As it was discussed earlier that crowd flow towards *Har-ki-paudi* in three directions, the holdings areas were concentrated in those areas (**Error! Reference source not found.**). Based on the expected crowd of an event, the authorities will modify the capacity of holding areas. Even after utilizing holding areas, if the authorities fail to control the density in *Har-ki-paudi*, then people in holding areas will be directed towards nearby Ghats but not to *Har-ki-paudi*. Besides the use of holding areas, other emergency plans include directing the crowd to take longer routes from bus stand area to reach *Har-ki-paudi* (Figure 8). The last stage of the emergency plan will be implemented when it is impossible to allow more people into Haridwar. In such case, both public and private vehicles will be stopped from entering Haridwar. The trains will be diverted to nearby railway stations avoiding people to reach Haridwar.

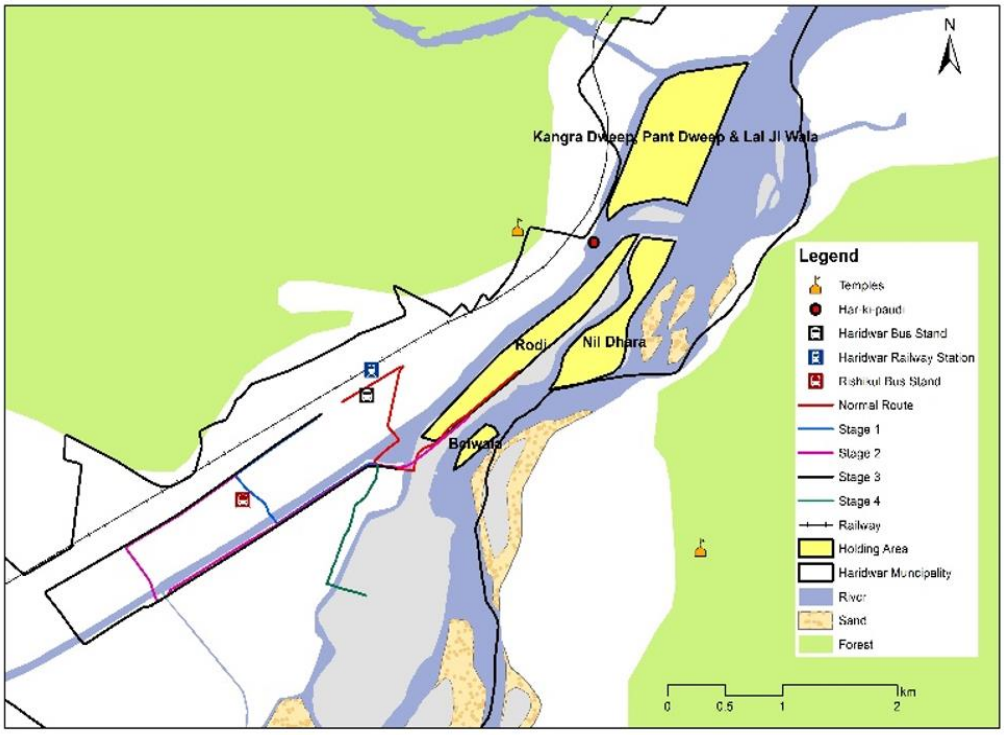

Figure 9: *Map showing Emergency plans such as holding areas and alternative routes*

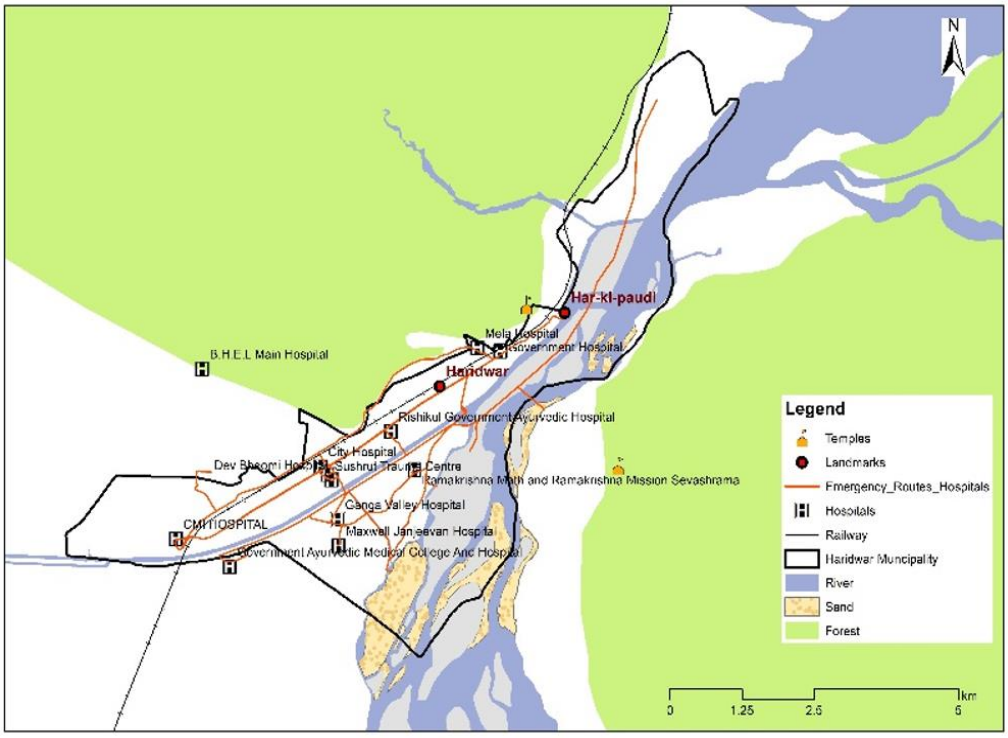

Figure 10: *Emergency routes to major hospitals*

To identify emergency vehicle routes to hospitals we have mapped major hospitals falling in the municipality area, with the help of field visits and WebGIS. Emergency routes to those hospitals from major Ghats and sector areas were identified using network analysis in GIS (**Error! Reference source not found.**). The analysis does not include the numerous first aid centers and clinics that mushroom during *Kumbh Mela* and the temporary fire stations that come up in and around the residential sectors. The proximity of Mela Hospital and Government Hospital makes them the immediate respondents for emergencies in *Har-ki-paudi*. In the worst-case scenario, waterbody (Ganga River) will act as a better alternative route to a hospital for emergency response. For effective emergency response, authorities should recognize the importance of emergency routes and provide these lanes with necessary services.

4. Conclusion and Future Scope

Mass Gatherings have the potential to create a strain on the infrastructure and living of the city. Many challenges were faced by event organizers, resource planners, emergency services and other departments to provide a safe gathering during 2016 *Ardh Kumbh*. Analysis of Crowd control and Emergency response strategies implemented during *Ardh Kumbh* indicate the need for detailed planning of evacuation procedures, dynamic crowd control, and preparedness measures. This study was intended to provide backing for authorities to efficiently organize and manage upcoming mass-gatherings.

Weaknesses of the city are determined by mapping the essential facilities and infrastructure with the help of Remote Sensing Images. Infrastructure scoring identified the strengths and weakness of existing infrastructure elements leading to the identification of crowd interrupters and triggers. Crowd flow analysis in the pilgrim zone helped to derive the possible crowd control issues which can aid the authorities to prepare better for emergencies. Crowd capacity of *Har-ki-paudi* provides authorities with crucial information regarding the maximum allowable limit to avoid disastrous events. Due to fluctuations in the expected crowd count and dynamic nature of the crowd, the task of successfully

managing the mammoth gatherings can only be achieved with constant efforts from both governments and local bodies.

Spatial analysis of the data mostly obtained from detailed field studies during *Ardh Kumbh Mela*-2016 helped in formulating guidelines for disaster risk reduction in Haridwar considering its vulnerability towards crowd disasters. Taking into consideration the massiveness and complexity of *Kumbh Mela* some guidelines are recommended apart from the above discussions:

Local bodies and the public should be educated regarding emergency routes and evacuation plans and their participation should be encouraged. Counting the number of pilgrims precisely using modern techniques such as sensors should be employed to monitor crowd count at any given point of time. This will aid in regulating the number of people and hence reducing unlikely events. Also, uncontrolled entries and exits in and around *Har-ki-paudi* area need to be strictly regulated. Another major issue which needs immediate attention is the lack of recreational and open spaces in Haridwar, which leads to increase in density of *Har-ki-paudi* and surrounding commercial areas which can be tackled by developing more recreational facilities. Construction of open-air auditorium and other recreational facilities in *Pant Dweep* which hosts cultural events during *melas*s will attract more people towards that area. Increasing tree cover and other shaded seating areas in *Har-ki-paudi* will improve the comfort of pilgrims during hot sun. Provision of temporary seating arrangements will reduce the number of people seated on the ground at random locations. Strategies should be employed to enhance the natural beauty of Rodi Belwala sector thereby stimulating the crowd to take bath in those Ghats. The *Har-ki-paudi* ghat which is at 6-9-meter elevation difference needs the provision of ramps and elevators in the view of providing Universal accessibility for elderly and differently abled. The recommendations can be considered when planning for mass gatherings events.

References

BSDMA. 2013. *Mass Gathering Event Management. A Case Study of MahaKumbh, 2013, Allahabad.* Bihar State Disaster Management Authority, Patna.

Census, 2011. *2011 Census Population Data*. Retrieved from: *https://www.census2011.co.in/census/city/458-thrissur.html.*

City Development Plan, Haridwar. 2007. *Revised Under Jawaharlal Nehru National Urban Renewal Mission (JNNURM).* Urban Development Department, Government of Uttarakhand.

Hanna, J.A. 1994. *Emergency Preparedness Guidelines For Mass, Crowd-Intensive Events.* Office of Critical Infrastructure Protection and Emergency Preparedness, Minister of Public Works and Government Services, Government of Canada.

Jeffrey Tubbs, B.M. 2007. *Egress Design Solutions: A Guide to Evacuation and Crowd Management Planning.* John Wiley & Sons.

M Devi Anju, P.P. 2016. An appraisal of tourism infrastructure and analysis of tourist influx in Haridwar City, Uttarakhand. *International Journal of Research in Social Sciences*, pp.528-538.

Maclean, K. 1968. *Pilgrimage and Power: The Kumbh Mela in Allahabad, 1765-1954.* Oxford University Press, New York.

Mohd Arif Shuib, S.A. 2013. *Assessing psychosocial elements of crowds during hajj: scale construction and content validation*. *N*ational seminar on hajj best practices on crowd and health during hajj, Penang.

NDMA. 2014. *Managing Crowd at Events and Venues of Mass Gathering. A Guide for State Government, Local Authorities, Administrators and Organizers.* National Disaster Management Athority (NDMA), Government of India.

Oberhagemann, D.D. 2012. *Static and Dynamic Crowd Densities at Major Public Events.* Technical-scientific advisory board (TWD): German Fire Protection Association.

Raheja, G., Kiran, S., Sharma, U., Garg, R. and Ramachandra, A. 2015. Universal design strategies for inclusive riverfront development in India. 14th International Conference on Mobility and Transport for Elderly and Disabled persons, TRANSED, July 2015, Lisbon.

Mehrotra, R. 2015. *Kumbh Mela: Mapping the Ephemeral Mega City.* Academia Verlag Gmbh.

Rani, D.A. 2017. The Soft Crowd Management "Special reference to Kumbh - Haridwar". *Journal of Computer Engineering*, pp.99-102.

Sindhuja, H.L. 2015. Mass religious gatherings and disaster preparedness: a planning perspective. *Institute of Town Planners, India Journal*, p.13.

Still, G.K. 2014. *Introduction to Crowd Science.* CRC Press.

Still, G.K. 2018. Visualising crowd density. Retrieved from: *http://www.gkstill.com/Support/crowd-density/CrowdDensity-2.html.*

Sultan, M.I. 2015. Tourism, economy and environmental problems of a religious town : a case study on Haridwar, Uttarakhand, India. *International Journal of Humanities and Social Science Invention*, pp.09-15.

USAC and NRSC. 2011. *Estimating population of pilgrims in the Haridar Kumbh Mela 2010 on the Pramukh Shani Snan: Using high resolution Indian satellite data and ground based information.* National Remote Sensing Centre (ISRO) & Uttarakhand Space Application Centre (U-SAC), Dehradun.

WHO. 2008. *Communicable disease alert and response for mass gatherings.* World Health Organization Press, Geneva.